

Biocatalytic Oxyfunctionalisation of Butane in Bubble Column Reactors

**Vom Promotionsausschuss der
Technischen Universität Hamburg
zur Erlangung des akademischen Grades**

**Doktor-Ingenieur (Dr.-Ing.)
genehmigte Dissertation**

von
Sven Frederic Perz

aus
Hamburg

2022

Vorsitzender: Prof. Dr.-Ing. Michael Schlüter

1. Gutachter: Prof. Dr. rer. nat. Andreas Liese

2. Gutachter: Prof. Dr.-Ing. Ralf Pörtner

Tag der mündlichen Prüfung: 17.12.2021

DOI: <https://doi.org/10.15480/882.4213>

<https://orcid.org/0000-0003-4106-9576>

Creative Commons License Agreement

The text is licensed under the Creative Commons Attribution 4.0 (CC BY NC 4.0) license unless otherwise noted. This means that it may be reproduced, distributed and made publicly available provided that the author, the source of the text and the above-mentioned license are always mentioned. The exact wording of the license can be accessed at <https://creativecommons.org/licenses/by-nc/4.0/legalcode>

Acknowledgements

I would like to thank Prof. Andreas Liese for the great opportunity of doing my doctorate in his group. I am very grateful for the support throughout the three years of the thesis and the trust he placed in me with this “explosive” topic. I’m happy that I could become part of the ITB-Family!

Further, I would like to thank the other members of examination commission, Prof. Michael Schlüter (chair) and Prof. Ralf Pörtner (second examiner), for their time in evaluation of my thesis and the examination.

In the end a doctoral thesis is never the work of a single person, but many people contribute directly or indirectly. Therefore, I like to thank the following:

The cooperation partners of the two projects I was involved. For one I would like to thank Evonik Industries/the Creavis for the financial and intellectual support during our project, in name: Felix Nissen, Hans-Georg Jörg Hennemann, Oliver Thum, Bastian Grund, Susanne Leuchs and Simone Sieberz.

On the other, more academic, side, I want to thank the “BUPOx”-Team, for the journey from poster to cooperation to paper and project proposal. Many thanks to Prof. Frank Hollman for supplying the huge amount of enzyme, Prof. Dirk Holtmann for his overall support and special thanks to Sebastian, for all the preparation and the exiting time together in the lab.

Excellent partners are great, but the home base is at least as important. And the ITB is one of the best home bases one can think of. The basis for this is the permanent staff at ITB. I want to thank all of you: Starting with my group leader Paul, who gave me the space to work independently. Thi Lien, Maren, Uta and Anna for helping with all the little things without a lab would not be working. For the organizational support from the secretariat, I would like to thank Ulrike, Miranda and særlig Franziska. Sistnevnte også for litt norsk ved instituttet!

Besides the permanent staff the non-permanent staff contributed greatly to a good working atmosphere with lively discussion during the coffee break or the small engineering challenges I was given. I want to thank all the colleagues for this. There are too many to mention all but you all make the ITB great.

During my time at the ITB I have supervised seven Biological Technical Assistants (BTA) interns. Each BTA candidate has contributed with four months of experimental work and therefore I want to thank Caro, R. Marie, Johan, Anna-Lena, Jennifer S., Miriam, Lena and my three students: Mayla, Philipp, Akhila (All written in chronological order.)

Some special thanks for my time at the ITB go to Gerrit, Claudia, Robert, Jannis and Daniela. Thank you all for your scientific (and non-scientific) contributions and discussions.

In addition to the scientific environment, I would also like to thank my friends (the “VTler” and “SBler”) and especially my family. Thank you for standing by me throughout my academic career, in good and in bad times, and to help me to paint life more colourful.

Last but definitely not least Jennifer: Guardian angel from madness, but maybe sometimes also the cause of it. Thank you for all the fruitful discussion, the support on countless situations and being with me on this journey.

Frederic Perz

Abstract

The potential of butane and other short chain alkanes, as an abundant and cheap raw material, is so far not fully exploited in the chemical industry. Instead of burning (e.g. for heat and transportation) or utilising harsh reaction conditions biocatalysis offers an alternative approach. Thereby, one of the dream reactions of organic chemistry, the selective oxyfunctionalisation, can be realised. In this thesis the biocatalytic oxyfunctionalisation of butane with three biocatalysts was investigated. For this purpose, two whole cells systems and one soluble enzyme approach were employed in a 0.2 L and 2 L bubble column reactor.

The first investigated biocatalytic system was a whole cell approach, in which a modified *E. coli* W3110 strain heterologously expresses the membrane bound AlkBGT system. Utilizing these bacteria, the hydroxylation of butane to butanol and subsequent oxidation to butyric acid was investigated as a model system. Besides the examination of the biocatalysts activity, a process window was generated. For this, the impact of different process parameters on the mass transport limited reaction were studied using the Design of Experiment method. The analysed parameters were gassing rate, overpressure, and butane content in the feed gas.

The second whole cell system combined the AlkBGT system with the Ato system, the latter allowing the metabolism of butyric acid. Here the growth on butane and its derivatives, butanol and butyric acid, as sole carbon source was examined.

Lastly the unspecific peroxygenase (UPO) was applied as free enzyme to catalyse the hydroxylation of butane to 2-butanol in a 0.2 L bubble column reactor. Thereby demonstrating the first utilisation of this reaction system outside the analytical scale. Kinetic parameters for the hydroxylation of butane to 2-butanol were determined under process relevant conditions. Additionally, kinetic parameters for the over oxidation of 2-butanol to butanone were estimated. In the end, the process was scaled up to the 2 L scale and an *in situ* product removal was integrated.

Table of Content

Abstract.....	V
Table of Content	VII
List of Figures.....	XI
List of Tables	XIV
List of Abbreviations.....	XVI
List of Symbols, Units and Indices	XVIII
1 Introduction.....	1
1.1 (Oxy-)functionalisation of Alkanes	2
1.2 Mass Transport and Mass Balance	4
1.2.1 Influencing Mass Transfer.....	7
1.3 Burnable Gases and Safety	9
2 Aim and Objective	12
3 Materials, Reactors and Methods.....	13
3.1 Materials	13
3.1.1 Biocatalysts	13
3.2 Experimental Setup	15
3.2.1 Gas Mixing Station.....	15
3.2.2 Reactors.....	16
3.3 Experimental Procedure.....	21
3.3.1 Bacteria Cultivation	21
3.3.2 Bubble Column Experiments	24
3.3.3 Thermovessel Experiments: UPO Process Curve Analysis	27

Table of Content

3.4 Analytics.....	28
3.4.1 GC Analytics	28
3.4.2 Glucose	29
3.4.3 ABTS Assay	29
4 Gas Mixing Station	31
4.1 Introduction	31
4.2 Design.....	31
5 Whole Cell Catalysed Oxidation of Butane to Butyric Acid.....	35
5.1 Introduction and Fundamentals	35
5.1.1 Whole Cell Biocatalysis.....	36
5.1.2 AlkBGT System	36
5.1.3 Design of Experiment	38
5.2 Activity test	40
5.2.1 Induction Period	41
5.2.2 Freezing of Cells	42
5.2.3 Glucose Demand	43
5.3 Single Parameter Studies	45
5.3.1 Butane	45
5.3.2 Gassing Rate.....	46
5.4 Multivariable Process Analysis by DoE	48
5.4.1 Design Space	48
5.4.2 DoE Response: Volumetric Productivity	50
5.4.3 DoE Response: Yield of Butyric Acid on Butane	52
5.4.4 Combined DoE Response: Process Window.....	54
5.5 Mass Transport Vectors.....	56
5.6 Interim Summary	59
6 Utilisation of Butane as Energy- and Carbon-Source.....	60

6.1	Introduction and Fundamentals	60
6.1.1	Ato-Enzyme System.....	61
6.1.2	Bacterial Cell Growth.....	62
6.2	Cultivation on Butane Derivatives	65
6.3	Cultivation with Butane.....	67
6.3.1	Discussion of Cultivations with Butane	72
6.4	Interim Summary	74
7	Butane Hydroxylation by Unspecific Peroxygenase	75
7.1	Introduction and Fundamentals	75
7.1.1	Unspecific Peroxygenase	76
7.1.2	Enzyme Kinetic	78
7.2	Proof of Principle	81
7.3	Kinetic Characterisation of rAaeUPO	83
7.3.1	Kinetic for the Hydroxylation of Butane to 2-Butanol	83
7.3.2	Kinetics for the Oxidation of 2-Butanol to Butanone.....	91
7.3.3	Discussion of Kinetic Investigations	94
7.4	Investigation of the Stability and TN of rAaeUPO	97
7.5	Application of UPO for Synthesis.....	100
7.5.1	0.2 L Bubble Column Reactor	100
7.5.2	Scale up with <i>in situ</i> Product Removal	102
7.5.3	Comparison of the UPO Application	106
7.6	Interim Summary	110
8	Discussion and Outlook.....	111
8.1	Whole Cell Catalysed Oxidation of Butane to Butyric Acid	111
8.2	Utilisation of Butane as Energy- and Carbon-Source	116
8.3	Butane hydroxylation by Unspecific Peroxygenase.....	117
8.4	Comparison.....	122

9 Summary	125
10 References	126
11 Appendix.....	138
11.1 Composition of Stocks	138
11.1.1 HCD media salt mix.....	138
11.1.2 Trace elements solution.....	138
11.1.3HCD Feed	139
11.1.4 M9 media.....	139
11.2 Design of Experiment	140
11.2.1 Experimental Conditions and Results	140
11.2.2 DoE Modell: Volumetric Productivity.....	141
11.2.3 DoE Modell: Yield	142
11.3 Matlab scripts	143
11.3.1Butane single substrate kinetic	143
11.3.2 Two-substrate kinetic	143
11.3.3 Process curve analysis.....	144
11.4 Laboratory Protocols	147
11.4.1 Fermentation.....	147
11.4.2 Bubble column experiments.....	148
11.4.3 Cultivation of the alkBGT/ato strain.....	149
11.5 Chromatograms	150
11.6 Engineering drawing	151

List of Figures

Figure 1.1: Schematic illustration of the two-film theory and further mass transport to the biocatalyst (here a whole cell).	5
Figure 1.2: Ternary plot of butane, nitrogen, and oxygen.	10
Figure 3.1: a) P&ID and b) picture of the gas mixing station.	15
Figure 3.2: Experimental setup with the STR/Fermenter (left), the 2 L (middle) and 0.2 L (right) bubble column reactor inside the fume hood.	16
Figure 3.3: General P&ID for the three reactor systems with all available utilities, here shown for a bubble column setup.....	18
Figure 3.4: P&ID for the 0.2 L bubble column reactor with external pumping loop.	20
Figure 3.5: 2 L bubble column reactor setup with external extraction column (0.2 L)	20
Figure 4.1: Simplified P&ID of the GMS for an arbitrary mixing of butane and air.	32
Figure 5.1: Schematic view of the alkBGT system expressed in <i>E. coli</i>	37
Figure 5.2: Graphical illustration for different three factor design.	39
Figure 5.3: QP for the formation of butyric acid and associated activity at varying ODs.	41
Figure 5.4: Influence of the induction time on the activity of alkBGT.	42
Figure 5.5: Impact of cell freezing on the alkBGT activity.	42
Figure 5.6: alkBGT activity in dependency of the specific glucose feed rate and glucose factor.....	43
Figure 5.7: Product-substrate ration for butyric acid and glucose during the investigation of the glucose demand.	44
Figure 5.8: QP (a)) and dissolved oxygen concentration (b)) for varying butane content in the feed gas.....	46
Figure 5.9: Comparison of the QP for different spargers and feed gas supply.	47
Figure 5.10: Response surface plots for the QP depending on gassing rate and butane content at a) 100 mbar(g) and b) 500 mbar(g), as well as QP depending on pressure and butane content at 1.5 L min^{-1}	50

Figure 5.11: Parameter interaction for gassing rate with pressure	51
Figure 5.12: Response surface plots for the yield	53
Figure 5.13: Process windows for the oxidation of butane by the alkBGT system heterologously expressed in <i>E. coli</i>	55
Figure 5.14: Increase in <i>QP</i> for different mass transfer vectors, compared to a control without vectors.	56
Figure 5.15: <i>QP</i> increase conditions a) 300 mbar and 1.5 L min ⁻¹ , b) 400 mbar and 1.4 L min ⁻¹	58
Figure 6.1: Schematic view of the changes, compared to chapter 5, to the applied <i>E. coli</i>	61
Figure 6.2: Overview of the ato and fad system.....	62
Figure 6.3: Phases of bacterial growth.	63
Figure 6.4: Concentration profiles during the initial activation of the cells with a) butanol and b) butyric acid as starting substrate.....	66
Figure 6.5: Measured growth rates depending on the initial substrate concentration for a) butanol and b) butyric acid.	66
Figure 6.6: Parallel cultivation in 50 mL STR	68
Figure 6.7: Control experiment for the dual substrate cultivation. OD in bubble column reactor and shaking flask with butyric acid as single substrate.	69
Figure 6.8: Cultivation in a bubble column (with butane) and shaking flask (without butane).	70
Figure 7.1: Simplified reaction mechanism of the UPO adapted from Hofrichter and Ullrich [81], including the catalase reaction and malfunction adapted from Karich et al. [83].	77
Figure 7.2: Reaction schema for the UPO catalyses hydroxylation of butane to 2-butanol using hydrogen peroxide as cosubstrate.....	78
Figure 7.3: a) Schematic reaction progress of a simple enzymatic catalysed reaction. b) Visualisation of the dependency between reaction rate and substrate concentration for a simple Michaelis-Menten-Equation.....	79
Figure 7.4: rAaeUPO catalysed butane oxidation with stepwise increase of hydrogen peroxide feed rate, 2-butanol concentration and active enzyme concentration.....	81

Figure 7.5: a) QP and H_2O_2 -yield in dependency of the step wise increase in H_2O_2 feed rate, corrected for the volume change. b) TOF in dependency of the enzyme specific H_2O_2 feed rate.....	83
Figure 7.6: Visualisation of the concentrations profiles under constant supply of substrate and irreversible reaction.....	84
Figure 7.7: Measurement results and Michaelis-Menten fit, including 95 % confidence interval, for the hydroxylation of butane by rAaeUPO.....	86
Figure 7.8: QP and corresponding TOF at 150 mbar butane partial pressure and different enzyme concentrations.....	87
Figure 7.9: TOF in dependency of the applied hydrogen peroxide feed rate and residual amount of active enzyme after 1 hour.....	88
Figure 7.10: Experimental data and fitted kinetic for the two substrate kinetic of the rAaeUPO catalysed hydroxylation of butane.....	89
Figure 7.11: Measured (single data points) and simulated (lines) concentration for 2-butanol (blue), butanone (red) and active enzyme (green).	92
Figure 7.12: Enzyme deactivation rate during process curve analysis for 2-butanol starting concentrations of 5 and 10 mM.....	92
Figure 7.13: Enzyme deactivation rates during the kinetic study for the hydroxylation of butane.....	98
Figure 7.14: TN_{app} in dependency of the applied butane partial pressure and H_2O_2 feed rate.....	98
Figure 7.15: rAaeUPO catalysed hydroxylation of butane with a starting enzyme concentration of 2 μM	101
Figure 7.16: rAaeUPO catalysed oxidation of butane with a starting enzyme concentration of 10 μM	101
Figure 7.17: rAaeUPO catalysed oxidation of butane in 2 L scale with ISPR.	104
Figure 7.18: rAaeUPO catalysed oxidation of butane in 2 L scale with ISPR. Total amount of performed reactions	105
Figure 7.19: Pictures taken during the rAaeUPO catalysed oxidation of butane in the 0.2 L bubble column reactor	108
Figure 8.1: Comparison of the process windows for the oxidation of butane by the alkBGT system heterologously expressed in <i>E. coli</i> . QP and yield on butane depending on all possible parameter combinations.....	113

List of Tables

Table 3.1: Main features of the three applied reactors.	17
Table 3.2: System specific information for the bacteria cultivation in shaking flasks.	21
Table 3.3: Nutrients for the HCD fermentation. Added after autoclaving.	23
Table 3.4: Overview over the applied conditions for the different reaction systems.	25
Table 3.5: Overview of the extraction system depending on the reaction system and products and/or substrates.....	28
Table 3.6: Pipetting scheme for the ABTS assay. Reactants are prepared in buffer.	29
Table 4.1: Maximum possible flow rate of the MFC installed in the GMS.	33
Table 5.1: Summary of factors and corresponding values.....	49
Table 5.2: Point prediction for QP with applied conditions	52
Table 6.1: Fitted kinetic parameters.....	67
Table 6.2: Summary of the experimental data for the dual substrate cultivation... ..	71
Table 6.3: Amount of fixated butane, the rate of fixation and the OD specific fixation rate for dual substrate cultivations.....	71
Table 7.1: Fitted kinetic parameters for the hydroxylation of butane by rAaeUPO at a constant hydrogen peroxide feed rate of 2.5 mM h^{-1} . Temperature 25°C , Medium of 100 mM KP_i at pH 7.	85
Table 7.2: Fitting results for the two-substrate kinetic of rAaeUPO catalysed hydroxylation of butane; with 95 % confidence interval as total values and percentage.	90
Table 7.3: Results of the parameter fitting for the process curve analysis of the oxidation of 2-butanol to butanone and subsequent reactions.....	93
Table 7.4: Summary of determined kinetic parameter for the organic substrates .	94
Table 7.5: Selectivity for the rAaeUPO catalysed butane oxidation at infinite runtime and no mass transport limitation.	95
Table 7.6: Residual enzyme activity and apparent partition coefficient.....	103
Table 7.7: Summary of average TOF and TN for the three application experiments.	106

Table 7.8: Enzyme deactivation rates during the initial and end phase as well as the average.....	109
Table 7.9: Reactions conditions and corresponding TOFs as calculated based on double substrate Michalis-Menten kinetic and actual measurement. .	109
Table 8.1: Summary of kinetic parameters regarding the organic substrate.....	117
Table 8.2: Summary and comparison of the alkBGT system (in <i>E. coli</i>) and the UPO (as free enzyme).....	122

List of Abbreviations

ATP	Adenosine triphosphate
ABTS	2,2'-azino-bis(3-ethylbenzthiazoline-6-sulfonic acid)
alkB	Membrane bound non-heme diiron alkane-1-hydroxylases
ATEX	ATmosphères EXplosives
BC	Bubble column reactor
BDE	Bond dissociation energies
BMO	Butane monooxygenases
CCD	Central composite design
CCF	Face centred central composite design
DCPK	Dicyclopropyl ketone
DoE	Design of Experiments
<i>E. coli</i>	<i>Escherichia coli</i>
FAD	flavin adenine dinucleotide
GMS	Gas mixing station
HCD	High cell density (fermentation)
IPTG	Isopropyl β -d-1-thiogalactopyranoside
LEL	Lower explosive limits
MFC	Mass flow controller
MFM	Mass flow meter
MTBE	Methyl-tert-butylether
NAD(P)H	Nicotinamide adenine dinucleotide (phosphate)
NTP	Normal temperature and pressure
OD600	Optical density measured at 600 nm
P&ID	Piping and instrumentation diagram
PLC	Programmable logic computer
pMMO	Particulate methane-monooxygenases

rAaeUPO	Recombinant evolved unspecific peroxygenase mutant from <i>Agrocybe aegerita</i>
Re	Reynolds Number
RMSE	Root-mean-square deviation
RSM	Response surface methodology
sMMO	Soluble methane-monoxygenases
SOP	Standard operation procedure
STR	Stirred tank reactor
TCA	Tricarboxylic acid cycle
UEL	Upper explosive limits
UPO	Unspecific peroxygenase

List of Symbols, Units and Indices

Symbols & units:

a	[m ² m ⁻³]	Interfacial area
c	[mmol L ⁻¹]	Concentration
c^*	[mmol L ⁻¹]	Maximum solubility
c_E	[mmol L ⁻¹]	Active enzyme concentration
DO	[%]	Dissolved oxygen
\dot{F}	[L h ⁻¹]	Feed rate (liquids)
$\dot{F}_{Glucose}$	[mL h ⁻¹]	Glucose feed rate
$f_{Glucose}$	[mL h ⁻¹ L ⁻¹ OD ⁻¹]	Glucose factor
H	[mmol L ⁻¹ bar ⁻¹]	Henry constant
k_{cat}	[s ⁻¹]	Catalytic constant
$k_{deact.}$	[μmol h ⁻¹]	Enzyme deactivation rate
k_G	[m h ⁻¹]	Mass transport resistance, gas phase
k_L	[m h ⁻¹]	Mass transport resistance, Liquid phase
k_{LA}	[h ⁻¹]	Volumetric mass transfer coefficient
K_M	[mmol L ⁻¹]	Michaelis-Menten constant
K_s	[mmol L ⁻¹]	Monod constant
n	[mmol]	Amount of substance
\dot{n}	[mmol h ⁻¹]	Molar flow or formation rate
p	[mbar] or [mbar(g)]	Pressure or over pressure (gauge)
$P_{app.}$	[$-$]	Apparent partition coefficient
p_i	[bar ⁻¹]	Partial pressure
\dot{Q}_P	[mol L ⁻¹ h ⁻¹]	Volumetric productivity
q_s	[mol L ⁻¹ h ⁻¹]	Specific substrate uptake rate
r	[mmol L ⁻¹ h ⁻¹]	Reaction rate (general)
t	[h] or [s]	Time
TN	[$-$]	Turnover number
TOF	[s ⁻¹],	Turnover frequency
TR	[mmol L ⁻¹ h ⁻¹]	Transport rate
TTN	[$-$]	Total turnover number
UR	[mol L ⁻¹ h ⁻¹]	Uptake rate

V	[L]	Volume
\dot{V}	[L h ⁻¹]	Gassing/aeration rate
V_M	[L mol ⁻¹]	Molar volume (22.4 L mol ⁻¹ at 0°C)
V_R	L	(working) Reactor volume
VVM	[L L ⁻¹ min ⁻¹]	Volume flow per reactor volume
X	[-] or [%]	Conversion
x_i	[-]	Gas volume fraction of species i
Y_i	[%]	Yield on substance i
$Y_{i/j}$	[mol mol ⁻¹] or [OD mol ⁻¹]	Yield coefficient for substance i regarding substance j
v	[mmol L ⁻¹ s ⁻¹]	Reaction rate (enzymatic)
μ	[h ⁻¹]	Growth rate

Indices:

0	Initial / starting
avg.	Average
app.	Apparent
B-2ol	2-butanol
B-Ac	Butyric acid
B-one	Butanone
BC	Bubble colum
butane	Butane
crit.	Critical (value)
end	At the end / final
i	Replacement character for chemical species
in	Input
max	Maximum
min	minimum
n	Norm
opt	Optimal
out	Output
P	Product
S	Substrate
SF	Shaking flask

1 Introduction

Short chain alkanes, like butane, are an abundant and cheap raw material whose potential for the chemical industry is not yet fully exploited.[1] Instead, they are often burned to generate heat or are used in transportation. In respect to the United Nations sustainability goals this burning should be stopped and the utilisation must be intensified. Not only for today's waste streams of short chain alkanes but also for sustainable produced alkanes, like biogas.

The use of butane and other alkanes in chemical synthesis is restrained by its saturated aliphatic structure, making alkanes thermodynamically strong and kinetically inert.[2] In petrochemistry the high chemical stability is overcome using harsh (temperatures of up to 850°C) and unselective reaction conditions in (steam) cracking, primarily for middle and long chain alkanes. These methods lead to unsaturated hydrocarbons which, after purification, can finally be oxyfunctionalised, e.g. by unspecific oxidations to the corresponding alcohols. In contrast a biocatalytic conversion offers the advantage of a selective oxyfunctionalisation using mild reaction conditions, making one of the dream reactions in organic chemistry [2] come true.

Biocatalysts, irrespective of whether isolated enzymes or microorganisms are used, naturally perform reactions in an aqueous reaction media. One of the key points for a successful process is therefore the mass transport of the rather hydrophobic alkanes to the aqueous reaction media. In this regard bubble columns are a cost-effective reactor type, as they offer a good mixing efficiency at low operating costs. [3] At the same time the simple design offers a maximum of process safety when working with butane or other burnable gases.

In the following subchapters a basic understanding of the theory for this topic is established. First a general introduction into the (biocatalytic) oxyfunctionalisation of alkanes is given. A more detailed introduction to the used biological systems is prepared at the start of each chapter. Besides the (bio-)chemical knowledge, the fundamental principles to mass transport and the impact of the chosen reactor configuration are explained. Afterwards the process safety is discussed.

1.1 (Oxy-)functionalisation of Alkanes

Chemical functionalisation describes the introduction of functional groups into a molecule. A typical example in biocatalysis is the functionalisation of carrier surfaces. In a subsequent reaction these newly formed functional groups can be used to covalently bind enzymes and thereby to immobilise these to the carrier. This example demonstrates the main reason for functionalisation: the possibility to perform directed reactions with an otherwise inert compound. Further catalytic steps can then be used to synthesise a desired compound.

A special case in organic chemistry is the functionalisation of unactivated C-H bonds, as it remains one of the most challenging task in organic synthesis.[4–6] The particular interest of this reaction arises from the insertion of an additional group. While other catalytic steps normally (ex-)change a functional group the C-H functionalisation generates new functional groups to work with.[7] Special interest can be placed on the two extremes: The selective functionalisation of a C-H bond in a late stage of the synthesis of a complex molecule, e.g. a drug candidate [5], or the initial activation of a chemically inert compound, like alkanes [1].

Especially, in the first case, a three dimensionally structured catalysts is needed to orient the substrate and reach high selectivity.[8] As the protein scaffold of enzymes often offers these kinds of structure, some enzymes are capable of performing the C-H activations. Thus have gained tremendous interests in the organic synthesis.[7] This is especially true for the synthesis of biologically active compounds. Here the cost of the catalysts are justified by the high value of the target compound.[9] Specifically the research on the P450 enzyme family in recent years has to be mentioned in this context.[5, 7]

Alkanes on the other hand constitute to one of the largest and cheapest carbon feed stock for organic chemicals.[1, 10] Alkanes are aliphatic hydrocarbons that only consist of C-C and C-H bonds. The high bond dissociation energies (BDE) of around 350 kJ mol⁻¹ and 400-430 kJ mol⁻¹, for C-C and C-H, respectively, results in their chemically stability.[1] The latter is thereby influenced by the structure of the molecule (linear, branched or cyclic) and the position of the bond. Generally, terminal bonds are stronger by ~15 kJ mol⁻¹.[11] For functionalisation these high BDEs have to be overcome. While the aforementioned (steam) cracker offers an unselective process, a “dream reaction” [2] is the selective single insertion of an oxygen molecule into an

alkane yielding the corresponding alcohol. These alcohols are a particularly interesting platform chemicals.[1] As further oxidation leads to desired intermediates, as aldehydes, ketones, esters or carboxylic acid. At the same time a direct use as fuels, solvents or preservatives is possible.

Over the years many catalysts have been investigated, homogeneous as well as heterogeneous ones.[2, 10, 12] While higher alkanes remain a challenge, improvements are made at the oxidation of methane. Still quite harsh reaction conditions are needed.[11] Generally, powerful chemocatalysts suffer especially from the drawback that the oxygenated products are more reactive than the starting alkanes. This causes over oxidation up to the total oxidation of the hydrocarbon to CO₂ and H₂O.[1] In a process the oxidation and over oxidation needs to be balanced, which leads to a non-ideal conversion and selectivity. Additionally, chemo catalysts offer no three-dimensional structure, which leads to reactions directed only by the BDE, possibly further decreasing selectivity. Inspired from biological systems, chemo catalysts with three-dimensional structures are under development for the C-H functionalisation.[11]

On the other hand, many microorganisms have been found, that developed enzymes to selectively activate alkanes. As the original aim of these enzymes was to make the activated hydrocarbons accessible for further metabolism, total oxidation is ruled out for these catalysts. Enzymes that catalyse the insertion of single oxygen atoms in an alkane molecule, effectively performing mono-oxygenation reactions, are alkane hydroxylases.[1] Of these, three major subgroups are differentiated: (1) the monooxygenases (MO), including the soluble and membrane bound/particulate the methane-monooxygenases (sMMO and pMMO) as well as the butane monooxygenases (BMO), (2) membrane bound non-heme diiron alkane-1-hydroxylases (alkB), and (3) the previously mentioned P450 enzymes.[1, 11] In recent years the unspecific peroxygenase (UPO) has gained rising attention as well. A comprehensive overview of these enzymes is given by Bordeaux et al. [11], Soussan et al. [1] and Borrman et al. [13]. The biocatalysts used for the hydroxylation of butane in this work will be described in detail in the corresponding chapters.

Given the comparable low value of the targeted products Bordeaux et al. [11] defined criteria for an ideal catalyst that can be summarised as follows. To be economically feasible the catalyst needs to be produced cheaply and easily, preferable by renewable resources. To further reduce costs, a high stability of the catalyst is needed. At the same

time the C-H functionalisation should be performed selectively at high reaction rates and mild reaction conditions. Which includes avoiding toxic and/or expensive reagents and solvents. Lastly, an atom-economical process with minimal (non-toxic) waste production is desired. For this, molecular oxygen or hydrogen peroxide are the preferred oxidants.

While analysis of the catalysts is often performed in analytical scale, the worth of a catalyst must be demonstrated under process relevant conditions. Therefore, this work aims on the application of the biocatalyst in a preparative reactor scale.

1.2 Mass Transport and Mass Balance

Under normal conditions (normal temperature and pressure (NTP): 20°C and ambient pressure) butane is in a gaseous state. The desired oxyfunctionalisation is performed in the liquid reaction media inside a bioreactor. Therefore, the alkane and, as described above, often oxygen must be transported from the gaseous phase into the aqueous phase. To describe these gas to liquid mass transport phenomena several theories [14] were published. Well known theories are the “two-film” theory by Lewis and Whitman [15], the “penetration” theory by Higbie [16] and the “surface renewal” theory by Danckwerts [17]. While these theories might not perfectly describe all mass transport phenomena, the first vividly illustrates the involved steps, see also Figure 1.1. In the two-film theory a double boundary layer at the interface between gas and liquid is assumed. The gas diffuses from the gas bulk over the boundary layer to the gas liquid interface. At the interface the gas dissolves in the liquid and a concentration (c [mmol]) equal to maximum solubility (c^*) is assumed. Further diffusion brings the dissolved gas into the liquid bulk.

As normally the mass transport resistance is significantly higher in the liquid phase (k_L [m h^{-1}]) than in the gas phase (k_g [m h^{-1}]), the boundary layer of the gas is usually neglected. For a substance i the mass transfer rate per reactor volume (TR [$\text{mmol L}^{-1} \text{h}^{-1}$]) can be mathematically described as follows:

$$TR = k_L a \cdot (c_i^* - c_i) \quad 1$$

In this a [$\text{m}^2 \text{ m}^{-3}$] describes the interfacial area between gas and liquid per volume liquid. As a separate measurement of the k_L and a value is impractical, normally a combined value, the k_{LA} [h^{-1}], is determined for bioreactors [18].

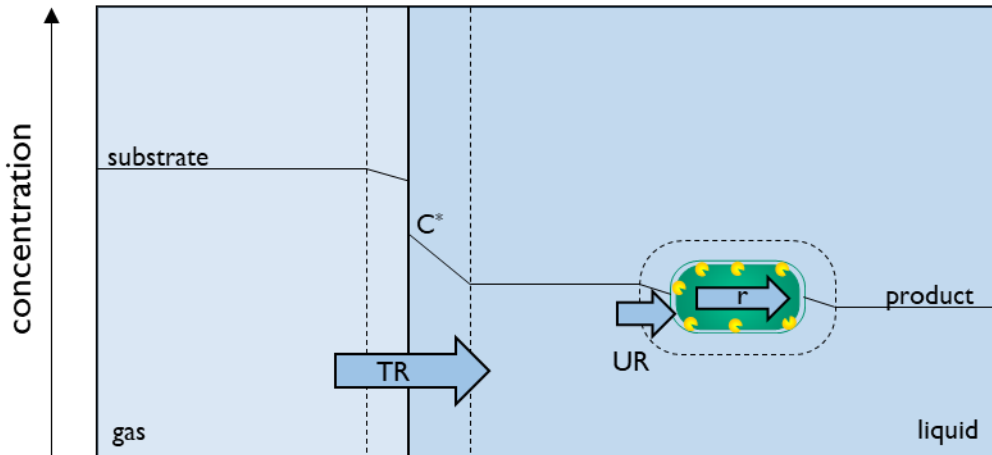


Figure 1.1: Schematic illustration of the two-film theory and further mass transport to the biocatalyst (here a whole cell). Boundary layers indicated by --; TR: transfer rate; UR: uptake rate; r: reaction rate.

The maximum solubility of a gas in a liquid can be approximated by the law of Henry [19]. For this the Henry constant (H [$\text{mmol L}^{-1} \text{ bar}^{-1}$]) and the partial pressure of the substance in the gas phase are used (p_i [bar]), see eq. 2.

$$c_i^* = p_i \cdot H \quad 2$$

By measuring the amount of dissolved substance, e.g., oxygen, the transfer rate can be calculated. When the concentration of the substance cannot be measured, the transfer rates can be determined by mass balance around the bioreactor.

Mass Balance

The general structure of a mass balance equation is given in eq. 3. For simplification a system in steady state is assumed, the change is therefore zero.

$$\underbrace{\frac{dn_i}{dt}}_{\text{change}} = \underbrace{\frac{d(V \cdot c_i)}{dt}}_{\text{input}} = + \underbrace{\dot{n}_{i,in}}_{\text{output}} - \underbrace{\dot{n}_{i,out}}_{\text{reaction}} \pm r \cdot V = 0 \quad 3$$

Depending on the placement of the system boundaries, the transfer rate can be determined by different means. E.g., by balancing around the gas phase inside the reactor. In this case only the feed gas (\dot{V}_{in} [L h⁻¹]) enters the system boundaries. The off gas (\dot{V}_{out} [L h⁻¹]) and the gas that dissolves into the liquid (TR) leave the system. By measuring the amount of gas and composition in the feed and off-gas the TR can be calculated, see eq. 4 & 5. As the TR is a volume specific rate, the working volume of the reactor (V_R [L]) is needed.

$$\frac{dn_i}{dt} = 0 = c_{i,in} \cdot \dot{V}_{in} - (c_{i,out} \cdot \dot{V}_{out} + TR \cdot V_R) \pm 0 \quad 4$$

$$TR \cdot = \frac{c_{i,in} \cdot \dot{V}_{in} - c_{i,out} \cdot \dot{V}_{out}}{V_R} \quad 5$$

At the same time these measurements allow the determination of the conversion (X [%]) of the gas, see eq. 6.

$$X_i = 1 - \frac{c_{i,out} \cdot \dot{V}_{out}}{c_{i,in} \cdot \dot{V}_{in}} \quad 6$$

The liquid media inside the bioreactor can be used as system boundary as well. In this case the gas (the substrate) that enters the system (the TR) is converted by the biocatalyst. When utilising a free enzyme this conversion is described by the reaction rate (r). In whole cell biocatalysis the conversion is often more complex. In many cases the substrate is metabolised and only parts of the mass of the substrate end up in the product. For a clear mass balance, an uptake rate (UR) is defined. The metabolism of butane will be addressed later in this work. For now, no metabolism but a simple conversion of the substrate inside the cell, followed by secretion, is assumed. With this assumption the whole cell and free enzyme can be described together. Therefore, the volumetric productivity (\dot{Q}_P [mmol L⁻¹ h⁻¹]) will be used. The \dot{Q}_P describes the formation rate of the product (P), eq. 7.

$$\frac{dc_P}{dt} = \dot{Q}_P \quad 7$$

For the previously mentioned steady state assumption the mass balance (eq. 3) for the liquid phase inside the bioreactor can be described as follows:

$$0 = TR - 0 - \dot{Q}_P \quad 8$$

$$TR = \dot{Q}_P \quad 9$$

Using this dependency, the \dot{Q}_P could be used for the calculation of the conversion of the gaseous substrate. But as not necessarily all reactions are detected, the yield is used. The yield (Y_i [%]) describes the amount of product per supplied substrate. In the semi-continuous bubble column reactor this is the molar product formation rate (\dot{n}_P [mol h⁻¹]) divided by the molar gassing rate of the substrate (\dot{n}_S [mol h⁻¹]).

$$Y_i = \frac{\dot{n}_P}{\dot{n}_S} = \frac{\dot{Q}_P \cdot V_R}{x_{S,in} \cdot \frac{\dot{V}_{in}}{V_M}} \quad 10$$

Here the \dot{n}_P is the product of the \dot{Q}_P and the reactor volume (V_R [L]). The \dot{n}_S can be described using the gassing rate (\dot{V}_{in} [L h⁻¹]), the substrate content in the gas ($x_{S,in}$) and the molar volume ($V_M \approx 22.4$ L mol⁻¹ at 0 °C).

Mass Transport - and Biological Limitation

Besides others factors, the \dot{Q}_P is depending on the substrate concentration and the amount of biocatalyst (cells or enzymes, $c_{catalyst}$) present in the system. When this is combined with the definition of the TR in eq. 1, eq. 9 can be converted as follows:

$$k_l a \cdot (c_i^* - c_i) = f(c_i, c_{catalyst}, \dots) \quad 11$$

Assuming all other parameters were kept constant, a steady state substrate concentration is reached, which is depending on the amount of applied catalyst. With increasing catalyst concentration, the \dot{Q}_P increases, and the steady state substrate concentration decreases. Until reaching a substrate concentration of zero, the system can be defined as biologically limited. At a substrate concentration of zero, the TR reaches its maximum. A further addition of catalyst does not increase the \dot{Q}_P . The system is mass transport limited.

1.2.1 Influencing Mass Transfer

As stated above, the maximum transfer rate (TR_{max}) is reached when the concentration of the substance in the liquid bulk equals zero, eq. 12.

$$TR_{max} = k_L a \cdot c_i^*$$

12

To further increase the mass transfer either the k_{LA} or the solubility of the substance need to be increased. The possibilities for this can generally be categorized in three types: (1) the reactor design and configuration, (2) the reaction conditions or (3) additives.

Reactor Design

As stated before, the k_{LA} is usually determined specifically for every bioreactor. This is done, as it is strongly influenced by the type of reactor and additional instalments. The main factor is the gassing and dispersion of the gaseous phase. In a stirred tank reactor, the gas is dispersed by the stirrer, while in a bubble column reactor the gas might enter through a perforated plate without additional dispersion. Besides the main features of a reactor, additional instalments, like flow breakers or riser and down-comer, influence the overall k_{LA} of a reactor. For a detailed description of the different reactor types see also [20]. In this work a bubble column reactor is used, as it offers good k_{LA} values while keeping experiments very safe, see next chapter.

Reaction conditions

Besides the reactor design, the reaction conditions have a huge impact on the TR. A change in reaction conditions can impact the k_{LA} as well as the maximum solubility or both at the same time. For example, a change in gassing rate influences the k_{LA} by changing the interfacial area. Pressure, or rather partial pressure, on the other hand impacts the maximum solubility, as shown by the law of Henry in eq. 2. The impact of pressure on the k_{LA} on the other hand is neglectable under usually applied pressures [21]. Temperature can, depending on the system impact the k_{LA} as well as the maximum solubility. Generally, the former is increasing, while the latter is decreasing at increasing temperatures. These effects can cancel each other as shown by Vogelaar et al. [22].

The reaction media has an impact as well. Changing viscosity or buffer salt concentrations impact the hydrodynamics or gas solubility, respectively.

Additives & Mass Transfer Vectors

While buffer salts or special reaction media are often needed for the biocatalyst to function properly, further components can be added to the reactor that are not

necessary for the reaction. This includes additives like anti-foam agents or mass transfer vectors.

Anti-foam agents are used to decrease foam formation and prevent over foaming of a reactor. This is generally done by reducing the surface tension of the reaction media. While this reduces also the bubble size, thereby increasing the interfacial area, excessive amounts can decrease the TR.[23, 24]

In general, all substances which positively influence mass transport can be called mass transfer vectors. Their physical properties and working principles differ significantly. The vectors can be liquid (with no or low solubility in water), solid or even soluble in the aqueous phase [25, 26]. The possible involved mechanisms, e.g. “shuttle effect”, “permeability effect” and “bubble covering”, are subject of current research [27–30] and differ between the separate vectors.

1.3 Burnable Gases and Safety

Butane, as all small chain alkane, is a burnable gas. Additionally, it can form explosive mixtures with air, or more precise, with oxygen. Figure 1.2 shows the ternary plot for the possible mixtures of butane, oxygen, and nitrogen. The mixtures of pure butane with air are described by the airline. As shown in Figure 1.2 the airline crosses the explosive region. The intersections of these are called the explosive limits. For butane the lower explosive limit (LEL) is at 1.4 vol.% butane, while the upper explosive limit (UEL) is at 9.4 vol%. [31]

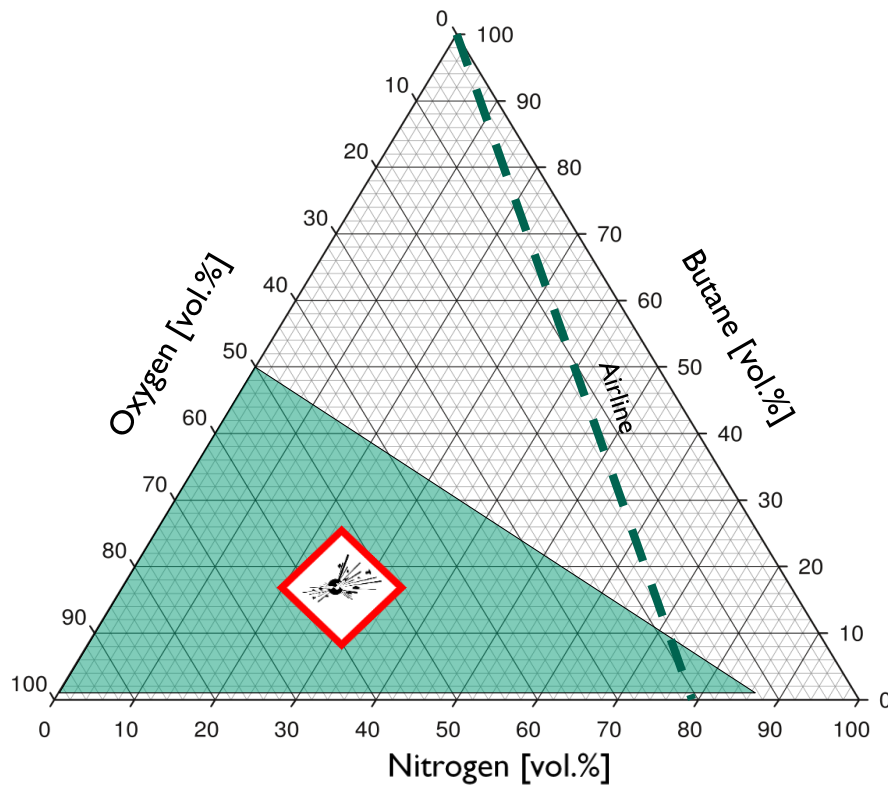


Figure 1.2: Ternary plot of butane, nitrogen, and oxygen. Explosive mixtures indicated by green area. Mixtures between air and pure butane are indicated by the airline (—).

While it is possible to perform experiments with explosive mixtures, special requirements are to be met, see ATEX directives (ATmosphères EXplosives) [32, 33]. Generally, when performing experiments with butane, the formation of explosive mixtures should be prevented. To assure a safe working environment, different layers of protection are installed. In the following the distinct layers of protection used in the experimental setup of this work are presented. The setup itself was installed during the work of Sluyter [34, 35] and is described in detail in chapter 3.2.

First: no explosive mixtures are used as feed gas in the experiments and a safety distance to the UEL is maintained. For this thesis the lowest applied butane content is 14 vol.%. The performed reaction converts butane and oxygen in a stoichiometric amount. Additional oxygen is consumed by the maintenance metabolism of the bacteria. The applied gas mixture is therefore getting richer in nitrogen, leading away from the explosive region.

Second: a gas-tight reactor is used. As a bubble column reactor is used, no bearings for the drive shaft needs to be sealed. Furthermore, the absence of moving parts

prevents the creation of sparks. Before and during an experiment the tightness of the reactor is checked by the operator.

Third: in the case of an undetected leakage, the reactor is placed in a fume hood at a ventilation of $650 \text{ m}^3 \text{ h}^{-1}$ ($> 10500 \text{ L min}^{-1}$). A stream of pure butane at $\sim 150 \text{ L min}^{-1}$ would be needed to reach the LEL at this dilution. The usually applied gas feed rates are between 0.75 and 2.5 L min^{-1} and 14 to 40 vol.\% .

Fourth: a gas sensor, ExSens(-I)/ExTox/Germany, is installed in the fume hood. This sensor measures the butane content inside the fume hood. At a value of 20% of the LEL (0.28 vol.\% Butane) a visual warning starts. At 40% of the LEL (0.56 vol.\% butane) an acoustical signal starts, and the butane feed gas is stopped by closing a magnetic valve. As a normally closed magnetic valve is applied, the valve closes in the case of a power shortage.

These independent layers of protection allow for a safe execution of experiments.

2 Aim and Objective

The aim of this study is the independent investigation of three biocatalytic approaches for the oxyfunctionalisation of butane in bubble column reactors. Subsequently, these systems are to be compared and their potential for industrial applications are to be discussed, see chapter 8. For the independent investigation this work is divided into the following topics:

“Construction of a Gas Mixing Station”

Previous works at the Institute of Technical Biocatalysis [34, 35] on the oxyfunctionalisation of butane were performed using premixed gas bottles. These butane air mixtures limit the range of possible reaction conditions. To perform experiments at conditions not reachable so far, the construction of a gas mixing station (GMS) is described in chapter 4.

“Whole Cell Catalysed Oxidation of Butane to Butyric Acid”

Using the newly constructed GMS the aforementioned previous works on the whole cell catalysed butane oxidation is continued. The optimised usage of the biocatalysts and the multivariable investigation of the system to define a process window are described in chapter 5.

“Utilisation of Butane as Energy- and Carbon-Source”

The whole cell catalysed oxidation of butane to butyric acids requires glucose for the cell’s maintenance and cofactor recycling. An enhanced strain, which can metabolise the oxidation products of butane, butanol and butyric acid, is investigated in respect to its growth rate on butane and its derivatives. The feasibility of this glucose free butane oxidation is examined in Chapter 6.

“Butane Hydroxylation by Unspecific Peroxygenase”

The unspecific peroxygenases (UPO) are a recently emerging family of enzymes. They are capable of the oxyfunctionalisation of various organic compounds, requiring only hydrogen peroxide as co-substrate. The first application of the UPO for the hydroxylation of butane outside of analytical scale, kinetic measurements and a scale up to preparative scale are described in chapter 7.

3 Materials, Reactors and Methods

3.1 Materials

If not otherwise stated, all used chemicals had a purity greater than 99%. Salts mixtures and stock solutions were prepared in advance according to the recipes given in the Appendix 11.1.

3.1.1 Biocatalysts

In this work three different biocatalysts were used: Two whole cell systems, expressed in *Escherichia coli*, and one free enzyme.

Whole Cell Systems

The Evonik Creavis GmbH supplied the strains for the whole cell systems. Both strains are deviates of *E. coli* W3110:

E. coli W3110 pBT10

This strain contains the pBT10 plasmid, which holds the genetic information for the alkBGT-operon. Dicyclopentyl ketone (DCPK) in a concentration of 0.025% (v/v) is used for induction. Additionally, the plasmid provides an antibiotic resistance against 50 mg/mL Kanamycin.

E. coli W3110 pBT10 pJ294

This strain contains the pBT10 (described above) and pJ294-plasmid. On pJ294 the genetic information for the ato-operon is encoded, which is induced by isopropyl β -d-1-thiogalactopyranoside (IPTG) in a concentration of 1 mM. Additionally, the plasmid provides an antibiotic resistance against 100 mg/mL Ampicillin.

Free Enzyme

The enzyme, unspecific peroxygenase, was kindly supplied by Prof. F. Hollman, TU Delft/The Netherlands. The concentration and purification were performed by S. Bormann, DECHEMA-Forschungsinstitut/Frankfurt am Main/Germany. The

methods have been published in Perz et al. [36] and are reproduced below, according to the Wiley-VCH Article Sharing Policy [37].

Enzyme production

For the fermentative production of the recombinant evolved unspecific peroxygenase mutant from *Agrocybe aegerita* (*rAaeUPO*) recombinant expression in *Pichia pastoris* was used, following a previously reported protocol.[38, 39] In short: 800 mL of a pre-culture of recombinant *P. pastoris* (overnight cultivation in BMGY medium containing Zeocin (25 µg mL⁻¹) at 140 rpm and 30 °C) were used to inoculate 6 L fermentation medium (basal salts medium, pH 5 with PTM1 trace salts (4.35 mL L⁻¹) and antifoam C 0.2 mL L⁻¹). The fermentation was run at 30 °C and 600 rpm. During the first 48 h, glycerol was fed to the cultivation broth at rates to maintain the dissolved oxygen around 30-40 % saturation. After 48 h, glycerol feed was stopped and 0.5 % (v/v) of methanol were fed to the fermentation to induce the overexpression of *rAaeUPO*. Again, great care was taken to adjust the methanol feed rate such that the dissolved oxygen remained at approx. 30 % saturation. The feed rates were adjusted to until a rapid increase of the dissolved oxygen concentration was observed. Using this procedure, the cell density reached 165 g L⁻¹ after 160 h and the fermentation was stopped. At this point, the volumetric peroxidase activity (determined using the ABTS assay, Chapter 3.4.3) [38, 39] was 170 U mL⁻¹.

The culture broth containing *P. pastoris* cells and *rAaeUPO* was clarified by centrifugation (8000 rpm, 2 h and 4 °C). The *rAaeUPO*-containing supernatant was stored at -80 °C for further use.

Enzyme purification

For the experiments reported in this work, about 700 mL of crude *rAaeUPO* (approx. 90 µM) were concentrated twice by crossflow ultrafiltration (10 kDa cut off, PES, Vivaflow 200, Sartorius) and diluted with 300 mL 100 mM potassium phosphate buffer pH 7. The washed, crude enzyme was then concentrated to a final volume of 450 ml. The concentration of the enzyme preparation, as determined from three independent dilution series using the ABTS assay, was 127 ± 3 µM (3566 ± 88 U mL⁻¹). The enzyme solution was stored in falcons at 4 °C or, for longer storage at -80 °C.

3.2 Experimental Setup

In the following the experimental setups used in this work are described. This includes the gas mixing station and the used reactors: A stirred tank reactor/fermenter for the cultivation of the bacteria and two independent bubble column reactors (0.2 and 2 L). Additionally, special configurations of the bubble column reactors are described.

3.2.1 Gas Mixing Station

The design and construction of the GMS will be described in more detail in chapter 4. In the following the final design is described:

The piping and instrumentation diagram (P&ID) and a picture of the gas mixing station are shown in Figure 3.1 a) and b), respectively.

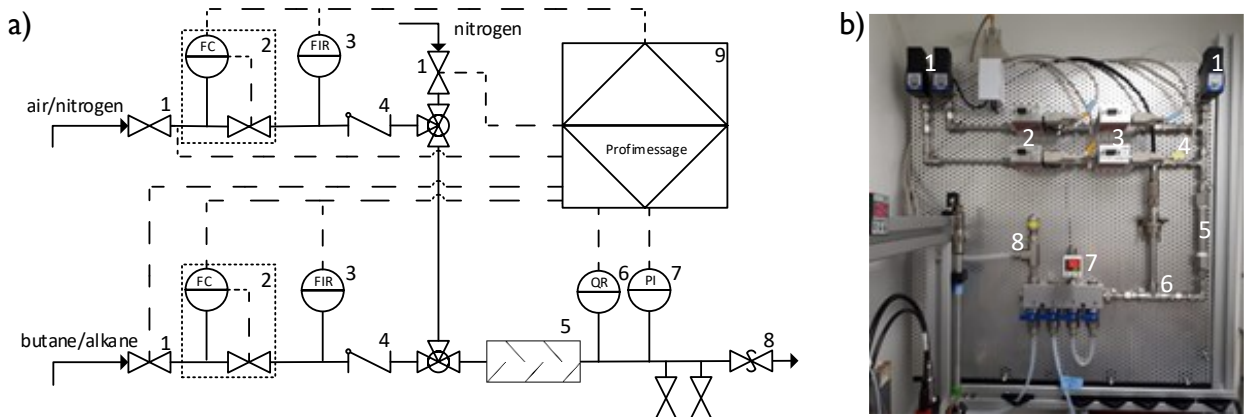


Figure 3.1: a) P&ID and b) picture of the gas mixing station. Used components: 1 magnetic valve, 2 MFC, 3 MFM, 4 check valve, 5 mixing chamber, 6 oxygen sensor, 7 pressure indicator, 8 relief valve, 9 PLC.

The GMS has two inputs for the gases to be mixed and a separate input for an inert or purge gas, nitrogen by default. These inputs are barred by “normally closed” magnetic valves. The feed lines for the gases to be mixed have the same structure: a mass flow controller (MFC), EL-FLOW® Select with valve/Bronkhorst®/The Netherlands, followed by a mass flow meter (MFM), EL-FLOW® Select/Bronkhorst®/The Netherlands, and in the end a check valve, SS-4C-1/3/Swagelok®/USA , to prevent back mixing. The maximum flow rate for air or nitrogen is $24.9 \text{ L}_N \text{ min}^{-1}$. The maximum flow rate for butane depends on the setting of the mass flow meter/controller, either 1.7 or $5.7 \text{ L}_N \text{ min}^{-1}$. The gases pass a self-build mixing chamber, made of a double nipple (DN 10, 10 cm length LN 38100-ES /Riegler Druckluft und Pneumatik/

Germany) and a stationary flow breaker. Before ending in a distribution station the mixed gas passes a sensor for oxygen partial pressure, OXYPro® Wide-Range/PreSens®/Germany,. Here the total over pressure is measured, dual display digital pressure sensor (DP-102A-E-P)/ Panasonic Corporation/Japan, and the mixed gas can be taken off, the outlets are sealed via ball valves, 377.01-ES/Riegler Druckluft und Pneumatik/Germany. The outlet pressure is regulated by a relief valve, SS-RL3S4/Swagelok/USA. All tubing inside the GMS is from stainless steel, 1/4 in. outer diameter. All inlets and outlets of the GMS can be connected via quick connector, 6 mm outer diameter. All connectors and fittings inside the GMS, except for the quick connectors, are from Swagelok/USA. The GMS is controlled by a programmable logic computer (PLC), ProfiMessage and the program ProfiSignal (Version 4.2.0.45) from Delphin Technology AG/Germany.

3.2.2 Reactors

In this work mainly three different reactors were used. As these reactors, one stirred tank reactor (STR) as well as a small and big bubble column reactor (BC), are placed in the same fume hood (see Figure 3.2), they share the available utilities that will be described further below. The main features of the three reactors are summarized in Table 3.1.



Figure 3.2: Experimental setup with the STR/Fermenter (left), the 2 L (middle) and 0.2 L (right) bubble column reactor inside the fume hood.

All reactors are additionally equipped with ports for an oxygen sensor with integrated temperature measurement, Mettler Toledo InPro 6800, and pH-sensors, Mettler Toledo

405-DPAS-SC-K8S, a sampling port and different septa for, possible sterile, addition of liquids. All connections of the STR are on the top side. The big BC has additional septa on the bottom side. The small bubble column has an additional port, for 6 mm tubes, at the bottom as well as septa at the side, at the height of the gassing adapter and symmetrically at the upper end of the column. The engineering drawing of the top and bottom plates of the 2 L bubble column reactor can be found in G. Slyters dissertation [35], the drawing for the plates of the 0.2 L reactor are shown in the appendix (Figure A.6).

Table 3.1: Main features of the three applied reactors.

Reactor	STR	Big BC	Small BC
Working volume	Up to 2.5 L	~ 2 L	0.2 – 0.3 L
Height (working volume)	~20 cm	~ 40 cm	~ 20 cm
Inner diameter	12 cm	8 cm	4 cm
H/D ratio	1.6	5	5
Gassing adapter: height h, diameter d	2 µm sinterstone h = 4 cm; d= 2.2 cm	2 µm sinterstone h = 4 cm; d= 2.2 cm	2 µm sinterstone h = 4 cm; d= 2.2 cm
Stirrer	2x Rushton turbine and 1x pitched blade	-	-
Max. overpressure producer	-	500 mbar [35]	500 mbar self-constructed

All reactors are controlled via ProfiMessage/Delphin Technology AG/Germany. The PLC to control these reactors are described in detail in the thesis of G. Sluyter [35]. The temperature and the pressure have to be adjusted manually.

Figure 3.3 shows the universal valid P&ID for the three reactor systems and their utilities exemplified for a bubble column reactor setup. For the addition of liquids a number of pumps are available. For the titration of base or acid in each reactor a separated peristaltic pump, Watson Marlow SCI Q 400/Watson-Marlow Fluid Technology Group/Great Britain, is used. The pumps are controlled through a digital signal by the PLC and the flow rate can be adjusted manually. An additional peristaltic pump, meredos SP-GLV/Meredos GmbH/Germany, is used for feed solutions, mainly for glucose feed during fermentation. The pump is controlled by an analogue signal and the flow rate is regulated by the PLC, a timed feed rate as well as different feed strategies can be implemented. Smaller amounts of liquids, e.g. antifoam, can be fed by syringe pumps, Aladdin Single Syringe Pump/World Precision Instruments/USA.

For all liquids silicone hoses are used for tubing and Luer-Lock fittings are used as connectors.

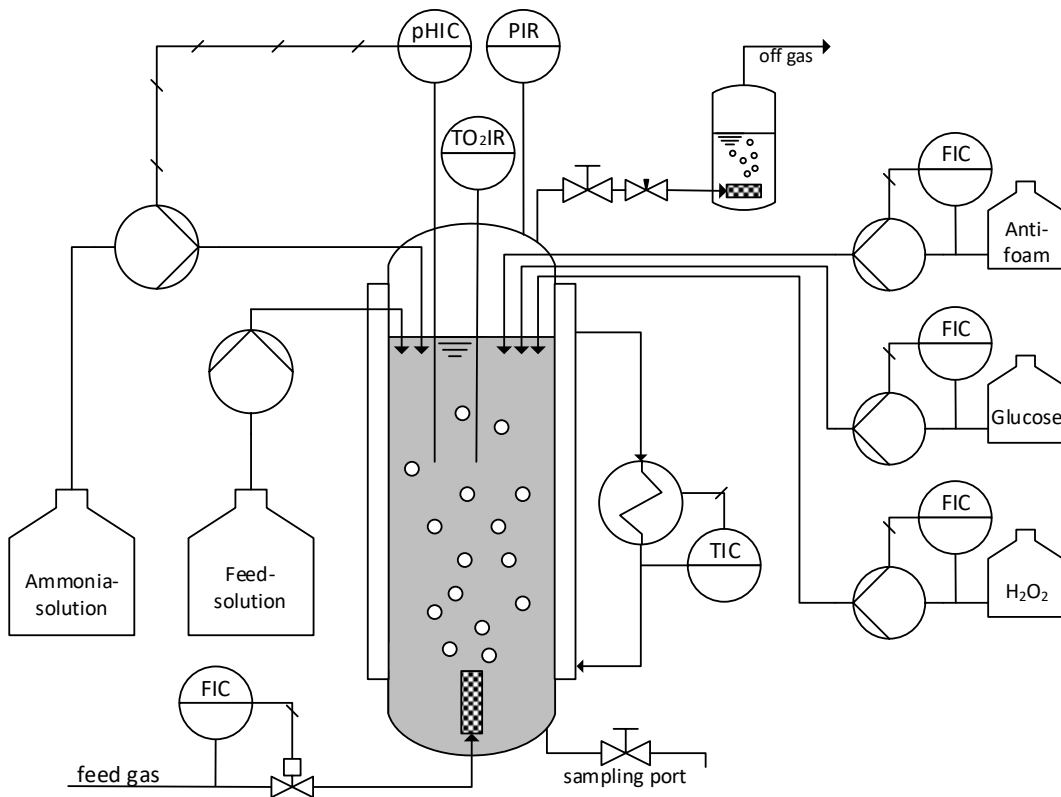


Figure 3.3: General P&ID for the three reactor systems with all available utilities, here shown for a bubble column setup.

Air and nitrogen, for the calibration of the oxygen sensors, are provided for all reactors via manually adjustable flowmeters, Honsberg Instruments GmbH/Germany. During experiments gassing is controlled for each reactor individually by a MFC, EL-FLOW® Select with valve/Bronkhorst®/The Netherlands, which are connected with the PLC. The MFC of the STR is usually connected to the in-house compressed air line. The MFCs of the BCs can be connected to the GMS or directly to the supply line of the gas cylinder cabinet. Additionally, all MFCs can be bypassed and the GMS can be directly connected to one or more reactors.

For temperature control a cooling circulator, Thermo Haake Phoenix II P2-C35P/Thermo Haake/Germany, is used. The reactors can be connected separately to its supply pipe. For this the BCs are equipped with a double jacket and the STR with an

internal rod. The temperature is manually set for the receiver tank or an external temperature probe (only STR) is used.

The off-gases can be washed in washing bottles, which are also used for pressure generation in the head spaces of the BCs. For an increased pressure generation, the gas enters the wash bottle through a sinterstone (2 or 10 µm pore size). Additionally, the pressure is adjusted via a ball and or needle valve. With a combination of these the pressure can be adjusted between 0 and 500 mbar(g) independent of the applied gassing rate.

For safety measurements the fume hood, containing the experimental setup, and the gas cylinder cabinet are equipped with a butane sensor each, ExSens (-I)/Extox/Germany. When a sensor measures 0.28 vol.% butane in the atmosphere, corresponding to 20% of the lower explosive limit, a flashing light is triggered. At 40% of the or the lower explosive limit (0.56 vol.%) the gas supply is stopped by a magnetic valve. A normally closed magnetic valve is installed, during a power shortage the valve would closed automatically.

Additional information can be found in the dissertation of G. Sluyter [35].

Special Reactor Configurations

For the two bubble column reactors additional configurations were used in specific studies. In the following the changes to the above-described system are explained.

Bubble column with external liquid loop

During the cultivation of *E. coli* in the 0.2 L bubble column reactor formation of singular big foam bubbles was observed. Bursting of these foam bubbles lead to an accumulation of biomass on the reactor walls. As the anti-foam agent had no effect on these bubbles a sprinkling with its own liquid was applied. [40] For this a liquid pump cycle was installed. A steady amount of medium was withdrawn from the bottom of the BC. Pumped, at 0.15 L min^{-1} , by a peristaltic pump, Watson-Marlow 323/Watson-Marlow Fluid Technology Group/USA, with a silicone tubing (inner diameter 5 mm) and entered the BC at the upper side port. This prevented foam formation and washed biomass from the reactor wall.

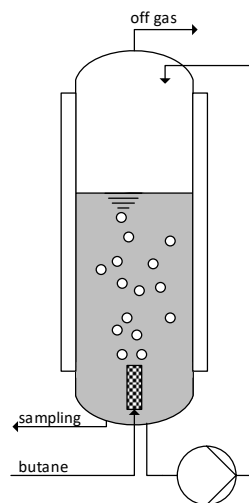


Figure 3.4: P&ID for the 0.2 L bubble column reactor with external pumping loop.

Bubble column reactor with external extraction column

In the scale up experiment of the rAaeUPO system (chapter 7.5.2) an additional liquid-liquid extraction was applied. For this the two bubble column reactors were connected as shown in Figure 3.5. Aqueous reaction media was withdrawn at the bottom of the 2 L bubble column reactor. Pumped by a peristaltic pump, to the top of the 0.2 L column which was used as an extraction column. After passing the organic phase, n-decanol, the aqueous media was pumped backed into the 2 L bubble column reactor. To ensure a constant volume flow in and out of the extraction column a dual channel peristaltic pump, REGLO/Ismatec®/ Germany, is used.

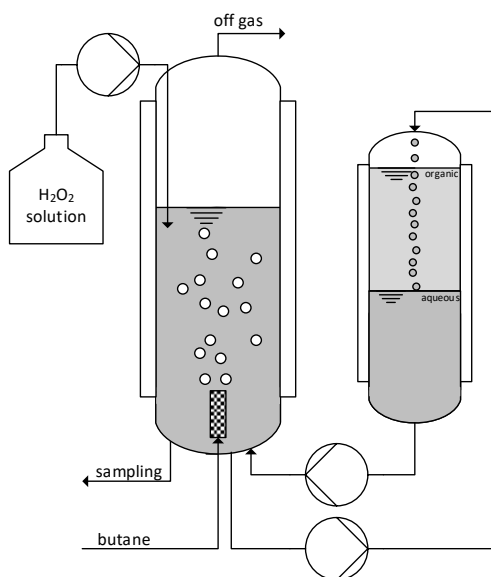


Figure 3.5: 2 L bubble column reactor setup with external extraction column (0.2 L)

3.3 Experimental Procedure

In this chapter the experimental procedures, which were used in this work, are described.

3.3.1 Bacteria Cultivation

In the following the general workflow for bacteria cultivations in shaking flask and stirred tank reactor are described.

Shaking Flasks

Cultivations in shaking flask were performed as a pre-culture for the high cell density (HCD) fermentation (see next subchapter) and the cultivation on butane derivatives (see chapter 6.2). The protocols and standard operation procedure (SOP) are attached in Appendix 11.4.1 and Appendix 11.4.3. The general procedure for both experiments is the same and is therefore described in a general manner. System specific information are listed in Table 3.2. A list of contents and the procedure for the preparation of all stock solutions is attached in Appendix 11.1.

All work is performed in a clean bench. The autoclaved stock solution is measured and transferred to a sterile flask. Either directly into a shaking flask with baffles or, when several shaking flasks are to be prepared, in an appropriate sized reagent bottle. Further compounds are directly pipetted into the flask, according to the concentration depicted in Table 3.2.

Table 3.2: System specific information for the bacteria cultivation in shaking flasks.

	HCD	Butane derivatives
Volume of shaking flask	1 L	0.3 L
Filling volume	0.1 L	0.05 L
Salt stock-solution	HCD	M9
HCD-Feed	30 mL L ⁻¹	-
NH ₄ Fe-Citrate-Stock	17 mL L ⁻¹	-
MgSO ₄ -Stock	-	2.45 mL L ⁻¹
NH ₄ Cl-Stock	-	9.09 mL L ⁻¹
US3 Trace Element-Stock	3 mL L ⁻¹	15 mL L ⁻¹
Kanamycin	50 µg mL ⁻¹	50 mg L ⁻¹
Ampicillin	-	100 mg L ⁻¹
DCPK	-	250 µL L ⁻¹
IPTG	-	1 mmol L ⁻¹

If a reagent bottle was used, the cultivation media is distributed to the shaking flasks. For the cultivations on butane derivatives the desired amount of butanol or butyric acid is then added to the shaking flask according to planned experiments.

The *E. coli* W3110 pBT10 strain, containing only the alkBGT system, is inoculated with two beads from long term cryo-conservation. The shaking flask is placed in a shaking incubator at 37°C and 180 rpm. After 9 h of cultivation the culture is used for the inoculation of the STR Fermenter, see next section: high cell density fermentation.

The *E. coli* W3110 pBT10 pJ294 strain, containing the alkBGT and ato system, is inoculated with 1 to 5 mL of active culture (see chapter 6.2), depending on the OD of the active culture and desired starting OD of the new culture. When an active culture with low OD had to be used the *E. coli* were centrifuged (10 min at 5000 rpm, UNIVERSAL 320R/Hettich/Germany) and resuspended in a smaller volume puffer. The shaking flasks were then placed in a shaking incubator at 30°C and 180 rpm.

High Cell Density Fermentation

The high cell density (HCD) fermentation was only used for the *E. coli* W3110 pBT10 strain to generate cell mass for further bubble column experiments. The protocols for laboratory usage are attached in Appendix 11.4.1. A list of contents and the procedure for the preparation of all stock solutions is attached in Appendix 11.1.

The HCD fermentation is performed over the course of three days. On the first day the fermenter is prepared. On the second day the preculture is started, the preparation of the fermenter finalized, and the main culture started. Harvest and cleaning are performed on the third day. In the following the procedure is described in detail.

First day

On the first day the in advanced prepared HCD salt stock (see appendix, Table A.1) is dissolved in 2 L Millipore water. 1.88 L of this salt solution are transferred to the fermenter and the residual in a reagent bottle. The pH probe is calibrated using calibration solutions with pH values of 4 and 7. After calibration the pH probe as well as the dissolved oxygen probe are placed into the corresponding ports at the top of the STR and screwed tightly. The connectors for the cables of the probes are covered. Afterwards the filling level of the culture medium is marked. The fermenter, the

reagent bottle with media, a reagent bottle with deionized water (>200 mL) and necessary tubing are autoclaved overnight.

Second day

On the second day the reactor is taken from the autoclave, placed in the fume hood, and the power supply for the dissolved oxygen sensor is connected for polarisation. Afterwards the HCD medium, which was autoclaved in a reagent bottle, is used to start the preculture (see above).

To compensate evaporated water during autoclaving of the reactor, autoclaved water is added sterile to the fermenter, using the a peristaltic pump and sterile tubing. After the previously marked filling level is reached the reagent bottle is exchanged with a reagent bottle containing further nutrients (see Table 3.3). Preparation of this nutrients, in a sterile reagent bottle, and exchanges of the tubing is performed under a clean bench.

Table 3.3: Nutrients for the HCD fermentation. Added after autoclaving.

Compound	Final concentration in reactor
HCD-Feed	30 mL L ⁻¹
NH ₄ Fe-Citrate-Stock (10 g L ⁻¹)	17 mL L ⁻¹
US3 Trace Element-Stock	15 mL L ⁻¹
Kanamycin	50 µg mL ⁻¹

While the nutrients solution is added to the reactor, all utilities are connected. This includes: the engine for the stirrer, the connection to the cooling circulator, the external temperature sensor of the circulator, the feed for ammonia solution, the cable to the pH-sensor, the cooling water for the exhaust gas cooler, the antifoam feed and the air inlet. After the complete nutrients solution is added to the reactor, the tubing is steriley switched to a bottle containing the HCD-feed (see appendix, Table A. 3). The pH-value is adjusted to pH 6.8 and this value is set into the PLC.

Approximately 7 hours after the preculture was put in the incubator, the reactor temperature is set to 37°C and a low stirring rate is applied. When the reactor reaches 37°C, the DO-sensor is calibrated.

After 9 hours of preculture ~ 50 mL of preculture are steriley transferred to a syringe and added to the reactor in steps. After each addition the OD₆₀₀ is measured. Addition of preculture is stopped when an OD of 0.1 is reached. The fermentation is started by

setting the starting time for the glucose feed, 8 hours after induction at a dilution rate of 0.004 h^{-1} and an increase in dilution rate by 0.001 h^{-1} every 1.25 hours. The cooling circulator is set to cool the reactor after 7 hours to 30°C , at a cooling speed of 7°C h^{-1} and the antifoam (Delamex 180, Bussetti & Co GesmbH/Austria) feed is started at $50 \mu\text{L h}^{-1}$.

Third day

During the fermentation the OD_{600} and glucose concentration are measured regularly. At a DO level of ~ 40 , or 3 hours before the DO level is expected to reach 10-20 %, the induction is started by the addition of $250 \mu\text{L L}^{-1}$ DCPK. Three hours later the fermentation is stopped, and the cells are harvested. For this all utilities are disconnected, with the second last being the engine for the stirrer and the last the air supply. The culture medium is transferred to centrifugation bottles, which are balanced and put into the centrifuge, Avanti J-25 with J-10 rotor/Beckman Coulter/USA, at 5000 rpm for 15 minutes and 4°C . After centrifugation, the supernatant is discarded and the cell pellets aliquoted into 50 mL falcons. The falcons are weighted, labelled, and stored at -80°C . To be able to distinguish between different fermentations and be able to compare bacterial activity between these, each fermentation was labelled with a running number (HCD#). It is assumed that the maximum activity for each cell aliquot of the same fermentation is constant.

Lastly, the reactor is filled with water and autoclaved. Subsequent to autoclaving, the reactor is cleaned and assembled for the next use.

3.3.2 Bubble Column Experiments

The general procedure for all bubble column experiments is the same and is therefore described in a general manner. The system specific information are listed in Table 3.4. Additionally, the method for the addition of the biocatalyst to the bubble column is described separately. The protocols for laboratory usage are attached in Appendix 11.4. A list of contents and the procedure for the preparation of all stock solutions is attached in Appendix 11.1.

Table 3.4: Overview over the applied conditions for the different reaction systems.

Biological System	alkBGT	alkBGT/ato	rAaeUPO
Medium	M9	M9+	potassium phosphate 0.1 M pH 7
O ₂ -Sensor	Yes	Yes	Yes
pH-Sensor	Yes	Yes	No
Titration with	25 % ammonia solution	-	-
Gassing	butane-air	butane-air	butane-nitrogen
Feed of	glucose	-	H ₂ O ₂
Antibiotic	Kanamycin	Kanamycin and Ampicillin	-

The day before the experiment, the DO-sensor is mounted in the reactor and attached to power supply for polarisation. On the day of the experiment the bubble column is filled with the corresponding medium and the antibiotic is added, if necessary (see Table 3.4). The temperature is set and a low air gassing is applied for mixing. The pH-sensor is calibrated (pH 4 and 7) and mounted in the reactor. Then the utilities are connected as needed: glucose feed, anti-foam feed, base feed and/or H₂O₂ feed. A drop of antifoam is added in the 0.2 L bubble column reactor or 3 drops in the 2 L bubble column.

When the temperature reached the set point, the DO-sensor is calibrated. For this pure nitrogen and air at an absolute pressure of 1 atm is used. After the calibration the bubble column is checked for air-tightness.

The addition of the biocatalyst is depending on the reaction system and is therefore explained separately:

AlkBGT-System

A falcon with *E. coli* biomass is taken from -80°C storage and placed in a container with warm water. When the biomass at the wall is visibly liquefied, the falcon is taken out and the content is shaken and squeezed into a syringe. For a 50 mL falcon a 50 mL syringe is used. Using the sampling port, the biomass is resuspended in the bubble column. The OD is measured until consecutively measurements are constant, difference less than 0.5 OD. The glucose feed rate ($\dot{F}_{Glucose}$ [mL h⁻¹]) is calculated using eq. 13 and the feed rate set.

$$\dot{F}_{Glucose} = f_{Glucose} \cdot V_R \cdot OD \cdot \frac{500 \text{ g}_{\text{glucose}} \cdot \text{kg}^{-1}}{w_{\text{applied}}} \quad 13$$

$f_{Glucose}$ [mL_{Glucose-solution} h⁻¹ L⁻¹ OD⁻¹] is the glucose factor (see 5.2.3), V_R [L] the reactor volume, and w_{applied} [g kg⁻¹] the glucose concentration in the stock solution. Normally in the 0.2 L bubble column reactor 50 g_{glucose} kg and in the 2 L bubble column reactor 250 g_{glucose} kg solutions were used. At very high ODs (> OD 20) 500 g_{glucose} kg could be used in the 2 L bubble column reactor.

The experiment starts with the supply of butane.

AlkBGT/Ato-System

The OD of the preculture is measured and the required volume to reach the desired starting OD is calculated. This volume of starting culture is then transferred to a 50 mL falcon, centrifuged (5000 rpm, 10 minutes, 4°C). The supernatant is discarded and the cells are resuspended with medium from the bubble column. Using a syringe the cells are transferred via the sampling port into the bubble column. When the reactor with external loop is used (see chapter 3.2.2), the pump is started right after addition of the bacteria.

If needed, liquid substrate (butyric acid and or 1-butanol) is added to the bubble column via the sampling port. After ~30 seconds a to sample is taken. For dual substrate cultivations (chapter 6.3) 50 mL of the medium, including cells and liquid substrate, are withdrawn and transferred to a 300 mL shaking flask. This flask is placed in a shaking incubator at 120 rpm and the same temperature as the bubble column.

The experiment starts with the supply of butane.

UPO-System

Using the APTS assay the UPO concentration of the stock solution (see chapter 3.1.1) is measured in triplicates. From this result the required volume of the stock solution is calculated. The corresponding amount is transferred into a syringe and added to the bubble column via the sampling port. A to sample is taken and the UPO concentration is directly measured.

The butane feed is started, as described in the following subchapter for all bubble column experiments in a general matter. After the pressure is adjusted to the desired value the experiment starts with the feed of hydrogen peroxide.

Start of the Experiments

Except for the experiments with the UPO system, the experiments start with the gassing of butane, pure or in mixtures. To prevent explosive mixtures in the bubble column reactor, the system is flushed with pure nitrogen until the DO-value decreases significantly. The nitrogen flow is then stopped and the gas supply pipe is connected to the outlet of the mass flow controller or directly to the mixing station. The gas flow is set to the desired value and the back pressure is manually adjusted. The adjustment of the pressure is performed in steps to give the mass flow controller time to adapt to the pressure changes. When the pressure reaches the desired value the t_0 sample is taken. Samples are withdrawn regularly and directly measured. Depending on the experiment the OD₆₀₀ or active enzyme concentration is determined. The substrate/product concentrations are determined via GC, after extraction (see chapter 3.4.1). Over the course of the experiments pressure and temperature are regularly manually adjusted.

At the end of the experiment the butane flow and all additional feeds (anti-foam, H₂O₂, glucose) are stopped. After flushing the system with nitrogen, a low gassing with air is applied to prevent clogging of the sinter stone. The reaction media is withdrawn, if necessary autoclaved and discarded. The gassing with air is stopped. The pH- and DO-sensors are cleaned with 70 vol.% ethanol solution and stored for later use. Lastly the bubble column is filled with a 2 vol.% Korsolex (Korsolex®basic/PAUL HARTMANN AG/Germany) solution. On the next day the Korsolex solution is transferred back into a storage container and the bubble column is flushed with water while being gassed with air until no foam formation visible.

3.3.3 Thermovessel Experiments: UPO Process Curve Analysis

Subsequent reactions of the UPO were investigated with process curve analysis (see chapter 7.3.2). For this thermovessels with a working volume of 50 mL (100 mM KP_i pH 7) were placed on a magnetic stirrer. The vessel was connected to the refrigerated circulator and the temperature set to 25 °C. Using the APTS assay the UPO concentration of the stock solution (see chapter 3.1.1) is measured in triplicates. From this result the required volume of the stock solution is calculated. The corresponding amount is transferred to the vessel and the substrate, 2-butanol, is added. For H₂O₂ feed (100 mM) a syringe pump is used. After starting the pump a t_0 sample is taken and directly analysed, active enzyme concentration and extraction for GC. The experiment

is continued, while regularly sampled, until no more enzyme activity is measured or 1.5 times the amount of H₂O₂ was added (mol/mol).

3.4 Analytics

3.4.1 GC Analytics

Aqueous product and substrate concentrations were determined via gas chromatography. For the analysis 500 µL of aqueous sample are mixed with 500 µL of organic solvent. Depending on the reaction system the extraction mixture was acidified with 50 µL of 3 M HCl-solution. For solvent selection refer to Table 3.5.

Table 3.5: Overview of the extraction system depending on the reaction system and products and/or substrates.

Reaction System	alkBGT	alkBGT+ato	rAaeUPO
Organic solvent	ethyl acetate	MTBE	MTBE
Measured compounds	1-butanol & butyric acid	1-butanol, butyric acid, acetic acid	2-butanol & butanone
Acidulation	yes	yes	no

All samples were vortexed for 2 min and centrifuged for 3 min at 13000 rpm for phase separation. The upper organic phase was transferred into GC-vials with inlets and analysed in a gas chromatography set-up (HP 6890 GC, Agilent). The inlet temperature was 250 °C and a split of 50:1 (1-butanol and butyric acid) or 30:1 (2-butanol, butanone) was applied. A hydrogen flow rate of 1.5 mL min⁻¹ was used as the carrier gas and a FFAPplus column (Macherey-Nagel, 30 m x 250 µm x 25 µm) was installed. A FID detector operating at 250°C analysed the samples. The initial oven temperature was set to 45°C and was held for 4 min. Afterwards, the oven temperature increases at 20 °C min⁻¹ to 200 °C.

Changes to the above-described procedure were performed for some experiments. In the beginning of the UPO experiments ethyl acetate (for 2-butanol) and heptane (for butanone) was used as organic solvent. The solvent was changed to MTBE to measure both concentrations in parallel. In the scale-up of the UPO decanol (chapter 7.5.2) was used as extractant. For direct measurement the same methods was used but with a temperature ramp up to 220°C.

The retention times are 1.3, 2.0, 3.8 and 8.6 min for butanone, 2-butanol, 1-butanol and butyric acid, respectively. Exemplary chromatograms are given in appendix 11.5.

3.4.2 Glucose

The glucose concentration during fermentation of the *E. coli* was determined by a blood sugar analyser „ACCU-CHEK“, F. Hoffmann-La Roche AG/Switzerland. The system employs single use measuring strips, which are dipped into the sample. High cell concentrations can interfere with the measurement leading to measurement failure. In these cases, the measurement is repeated with a centrifuged sample. A measuring result of “LOW” corresponds to a glucose concentration below 10 mg L⁻¹ (0.6 mmol L⁻¹).

3.4.3 ABTS Assay

The amount of active UPO inside the reaction media can be determined via the 2,2'-azino-bis(3-ethylbenzthiazoline-6-sulfonic acid) (ABTS) assay. For this an initial reaction rate measurement with a defined reaction system is performed. In a 1 mL poly(methyl methacrylate) (PMMA) cuvette ($d=1\text{ cm}$) the reactants are mixed. Final concentration of 0.3 mM ABTS (c_{ABTS}), 2 mM H₂O₂ in a 100 mM Na₂HPO₄/citrate buffer (pH 4.4) are applied, see Table 3.6. The reaction starts by the addition of 100 µL sample. The sample is diluted beforehand to achieve an adsorption increase (dA) between 0.1 and 1 cm⁻¹ min⁻¹ at 420 nm. The extinction coefficient for ABTS ($\varepsilon_{ABTS,420\text{nm}}$) is 36 mM⁻¹ cm⁻¹.

Table 3.6: Pipetting scheme for the ABTS assay. Reactants are prepared in buffer.

Liquid	Volume [µL]
Na ₂ HPO ₄ /citrate buffer	750
H ₂ O ₂ (40 mM)	50
ABTS (3 mM)	100
Sample	100

Using eq. 14 and the kinetic parameters ($K_{M,ABTS} = 0.300\text{ mM}$, $k_{cat,ABTS} = 546\text{ s}^{-1}$) determined for rAaeUPO-PaDa-I expressed in *Pichia pastoris* by Molina-Espeja [39] the concentration of active enzyme (c_E [mM]) is calculated.

$$c_E = \frac{dA}{\varepsilon_{ABTS,420\text{nm}} \cdot d} \cdot \frac{(K_{M,ABTS} + c_{ABTS})}{k_{cat,ABTS} \cdot c_{ABTS}} \quad 14$$

An active enzyme concentration of 1 mM corresponds to volumetric activity of $3.3 \cdot 10^7$ U L⁻¹ regarding ABTS as substrate.

4 Gas Mixing Station

In this chapter the design and construction of the gas mixing station (GMS), which was used in all further experiments, is described.

4.1 Introduction

Generally, two possibilities exist to supply a bioreactor with a mixture of the gaseous substrates, butane and oxygen (or air): The use of pre-mixed gas bottles or the on-site mixing of the gases. The first method is normally quite easy and convenient. Only a low number of connections and instruments are needed, which makes the setup safe while being cheap. Usually, 50 L gas cylinders are used, which can be pressurised up to 200 bar(g). At an assumed gassing rate of 2 L min^{-1} , this would result in a theoretical experimental runtime of around 80 h. Unfortunately, butane has a vapour pressure of $\sim 2 \text{ bar}$ at 20°C [31]. This leads to the condensation of butane when its partial pressure exceeds these 2 bars. E.g. at 20 vol.% butane the possible maximum filling pressure is 10 bar. Additionally, a safety distance is applied. Furthermore 1 bar of the gas mixture remains in the gas bottle. Overall, usable 8 bar can be assumed, which leads to an experimental runtime (using 2 L min^{-1}) of approximate 4 h. This runtime would further decrease if higher butane contents, gassing rates, or pressures would be applied. To overcome this limitation and to be able of supplying a freely selectable gas composition a GMS was constructed.

4.2 Design

Design Boundaries

For the design of the GMS the current as well as possible future setups were considered. So far one 2 L bubble column reactor was used at a time, but an identical bubble column was available, which could be used in parallel at sufficient gas supply. Additionally, a possible scale up of the reactor was discussed, therefore, this should be taken into consideration for the design of the GMS.

One aspect, which should be kept constant at a scale up, is the height to diameter ratio (H/D). For the 2 L bubble column the H/D is approximately 6. In respect to the space in the fume hood a scale up to a ~14 L bubble column reactor with an inner diameter of 15 cm is possible. Depending on the used scale up criteria, different gassing rates could be used. Using the superficial gas velocity as criteria, a gassing rate of 2 L min^{-1} translates into a gassing rate of 7 L min^{-1} . When using a constant gas volume flow per reactor volume (VVM), which is a VVM of 1 in a 2 L reactor and a gassing rate of 2 Ln min^{-1} , a gassing rate of 14 L min^{-1} needs to be applied.

As described in chapter 1.3 the lowest applied butane content is 14 vol.%. The upper limit must be determined experimentally, but it was aimed at a butane content of 40 to 50 vol.% at every possible gassing rate.

Lastly, the outlet pressure of the GMS has to be discussed. The applied bubble column reactors are made of glass with a maximum allowed over pressure of 500 mbar, see chapter 3.2.2. Additionally, the pressure drop of the gassing adapter and potentially of an additional mass flow controller (MFC) needs to be overcome. At the same time the inlet pressure of the butane stream is approximately that of the vapour pressure of butane, 1 bar(g). Therefore, the outlet pressure therefore needs to be adjusted in-between these two values.

Final Design

The main features of the GMS are two MFC, one for butane and air respectively, a mixing chamber, distribution chamber, a pressure indicator and a relief valve. In Figure 4.1 a simplified P&ID of these components is shown. All components are specified, model/brand and Company, in the materials and methods (chapter 3.2.1).

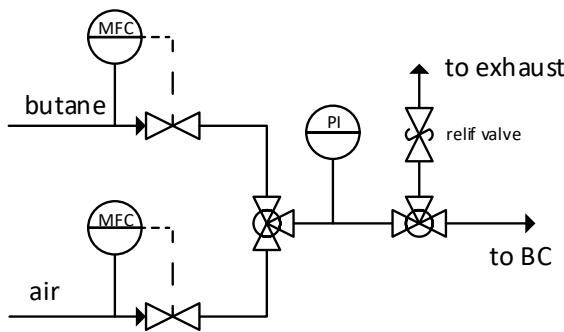


Figure 4.1: Simplified P&ID of the GMS for an arbitrary mixing of butane and air.

The volume flow of butane and air is controlled by a thermal mass flow meter, an EL-Flow Select by Bronkhorst. To account for a higher flow rate in a possible scale up the butane MFC is equipped with two different settings, see Table 4.1. Even in a scale up to a 14 L scale at 1 VVM, a butane content of up to 40 vol.% can be supplied. The two gas streams are mixed in mixing chamber. Using a relief valve, the pressure, measured by a pressure indicator, can be manually adjusted at the distribution chamber. In the absence of a consumer the gas stream is lead to the exhaust via this valve. The valve is also used to compensate small differences between the MFC of the GMS and the other MFCs used in the setup, see chapter 3.2. By adjusting the GMS to a slightly higher flow rate than the consumer, the desired pressure is kept constant. The surplus gas is led to the exhaust via the relief valve. This is specifically needed when two reactors are supplied in parallel.

Table 4.1: Maximum possible flow rate of the MFC installed in the GMS.

MFC	Air	Butane	
		Setting 1	Setting 2
Max flow [$\text{L}_\text{N} \text{ min}^{-1}$]	24.9	1.7	5.7

In addition, the GMS is equipped with several safety instalments. The main safety concern is the creation of explosive mixtures. The GMS is operated via the control program (ProfiSignal, see digital appendix) of the PLC (ProfiMessage). Using ProfiSignal the total volume flow and butane content are set. While the total volume flow can be freely chosen, only a pre-defined set of butane content are available, the lowest being 14 vol.%. Besides this programming that does not allow to actively mix explosive mixtures, two additional layers of protection are used. Firstly, both single gas streams are measured by thermal mass flow meters (MFM). Secondly the compositions of the final mixture is determined by an oxygen sensor. As air is mixed with butane, the mixed gas composition is on the airline and therefore describable by the sole measurement of oxygen, butane or nitrogen. If one of the three measurements (MFC, MFM or sensor), independently from the others, determines a butane content below 12 vol.%, the gas supply is stopped. For this “normally closed”-magnetic valves are used. Like the other magnetic valves, these valves close also in the case of a power shortage. To prevent a back mixing of gases, check valves are utilised behind the

MFMs. Additionally, the piping and mixing chamber behind these check valves can be flushed with nitrogen allowing for a safer start up and shut down procedure.

Validation

Before the use of the GMS, the produced mixed gas was validated by comparing it with a premixed gas bottle (butane content of 20 ± 1 vol.%) provided by Linde, Linde plc/Dublin/Irland, using a μ -GC (measurements performed by the Institute of Chemical Reaction Engineering (TUHH), Hamburg, Germany). The mixed gas of the GMS was inside the error margin ($\pm 1\%$) of the pre-mixed gas bottle.

5 Whole Cell Catalysed Oxidation of Butane to Butyric Acid

In this chapter the oxidation of butane to butyric acid using the alkBGT system in a whole cell (*E. coli*) concept is described. Previous results on this topic were published by Sluyter et al. [34]

5.1 Introduction and Fundamentals

The ability of microorganisms to utilise, or grow on, alkanes was already reviewed in the 1940s [41, 42]. Starting from the initial fundamental research, the recent years have shown industrial interest in the oxyfunctionalisation of alkanes and fatty acids. A special interest persists in the terminal hydroxylation since it is the generally more unfavoured reaction, as described in chapter 1.1. In this regard the cooperation partner, the Evonik Industries AG, holds several patents for the utilisation of the so called alkBGT enzyme system, which can catalyse these reactions [43–47].

Starting with an ACIB (Austrian Centre of Industrial Biotechnology) funded project in 2015 (ACIB Project 21.091), the hydroxylation of short chain alkanes was investigated at the Institute of Technical Biocatalysis (ITB). Here the alkBGT system was utilised heterologously expressed in *E. coli*. The focus at the ITB was the investigation of the upstream process development in a bubble column reactor setup. For this, a model system, in which butane is oxidised to butyric acid, was established and systematically examined. In the experiments a mass transfer limitation was observed. This led to the primary investigation of process parameters like gassing rate, overpressure in the bubble column, butane content in the feed gas and the reaction temperature. The main performance indicators were the \dot{Q}_P , in here the volumetric formation rate of butyric acid, and the yield, the percentage of butane that is converted to butyric acid.

With the previously described GMS, investigations of until then inaccessible process conditions were made possible and will be one focus of this chapter. Before the experimental results are described and discussed, the following subchapters will give

a brief introduction into whole cell biocatalysis, the alkBGT enzyme system and the optimisation method Design of Experiments.

In this chapter, unless otherwise stated, the volumetric productivity \dot{Q}_P [mol L⁻¹ h⁻¹] is defined as the formation rate of butyric acid and the yield Y [%] is defined as the percentage of butane that is converted to butyric acid.

5.1.1 Whole Cell Biocatalysis

In biocatalysis the general question arises if the applied enzyme is to be used as an enzyme (*in vitro*) or inside host cells (*in vivo*). The latter is also called whole cell biocatalysis. Both ways of applications offer advantages and disadvantages. Free enzymes often reach higher reaction rates as no transport through a cell wall is needed. Additionally, the microorganisms themselves demand certain additives, e.g. salts and a carbon source (often glucose), to survive. These would not be needed if the enzyme is applied in its free form. Additionally, to the target enzyme, the microorganism also brings further enzymes into the reaction media. Depending on the substrate, these additional enzymes could perform unwanted by-products.

On the other hand, the microorganism provides the target enzymes with several benefits. The most important ones are the protection from outside influences (the reaction conditions) and the regeneration of cofactors. Depending on the enzymes these cofactors are e.g. NAD(P)H or ATP. While in a reaction with a free enzyme these must be provided, the microorganism provides them while performing its maintenance metabolism. Some enzymes are quite complex structures, assembled by different subunits and/or bound to the cell membrane. In these cases, as with the alkBGT system, application without the cells protection is complicated and therefore unfavourable for an industrial process.

5.1.2 AlkBGT System

In 1963 the isolation of an *Pseudomonas* (later classified as *Pseudomonas putida* GPo1) capable to grow on hexane as sole carbon source was reported by Baptist et al. [48]. A cell free extract of the strain was able to catalyse the hydroxylation of octane to octanol. Three years later Peterson et al. [49] first reported on the structure of an alkane (Alk) utilising system. It was found that the system consists of three enzymes forming the AlkBGT system. Further genetic investigations decoded the whole pathway for the metabolism of alkanes, resulting in the AlkBGT(HJKL) system. After the first

oxyfunctionalisation by AlkBGT, the alcohol dehydrogenase (AlkJ) and aldehyde dehydrogenase (AlkH) oxidise the alcohol to the corresponding acid. The acyl-CoA synthetase (AlkK) finally activates the carbon acid to an acyl CoA, which can then be metabolised via β -oxidation. [50] Lastly, the alkL is a transport enzyme which guides longer chain substrates through the cell wall.

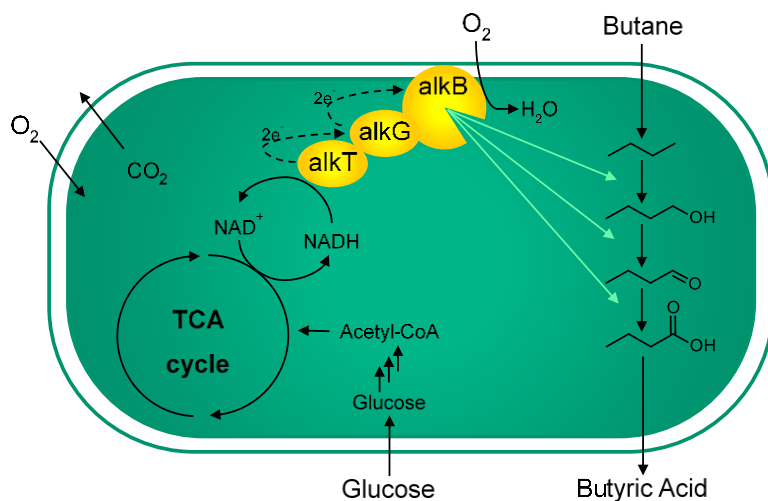


Figure 5.1: Schematic view of the alkBGT system expressed in *E. coli*. Additionally, cofactor regeneration via glucose supported maintenance metabolism is indicated.

In this chapter a heterologous expression of the AlkBGT enzymes in *E. coli* is utilised. Therefore, only these 3 enzymes are described in detail. The AlkB enzyme is an integral cytoplasmic membrane protein and non-heme di-iron (Fe^{2+}) mono-oxygenase.[51] The AlkG is a rubredoxin and the AlkT a rubredoxin reductase, both are cytoplasmic proteins. [51] For the overall system *in vivo* in *Pseudomonas van Beilen* [52] reports on a molar ratio of 50:10:1 (AlkB: AlkG: AlkT). In the system, AlkT performs the oxidation of NADH to NAD^+ and delivers the electrons to AlkG. Which passes the electrons to AlkB, at which the hydroxylation of the alkane takes place [52], see also Figure 5.1. Besides the initial hydroxylation, the AlkBGT system also performs the subsequent oxidations, effectively over oxidising the substrate. Therefore, the final product of this system is not butanol but butyric acid. Further (bio-)catalytic steps could be performed to generate higher value products from this.[53]

In this chapter the oxidation of butane to butyric acid is used as a model system to investigate the general utilisation of gaseous alkanes. In this regard butyric acid as the product is more favourable than butanol, as the latter is known to damage *E. coli* in higher concentration. [54] In contrast, the pH change, caused by the butyric acid, can be compensated by titration.

5.1.3 Design of Experiment

As described earlier, the whole cell catalysed oxidation of butane is normally performed under mass transport limited conditions. In recent years advances on the mathematical description of hydrodynamics and mass transport phenomena inside of bubble column reactors (BC) were achieved [55, 56]. But still huge efforts must be made to describe processes in BCs mechanistically. This is especially true for systems like the one applied in this work, as the cells can be considered a third phase. A model would need to incorporate the three phases as well as changing hydrodynamic aspects by the changing process parameters. For this work this effort is not worthwhile, as the investigations focus on a rather early stage of process development. In contrast a black box model can be easily implemented and provide all the information needed at this development state. A (statistical) Design of Experiments (DoE) offers an efficient way to set up these models. [57] Instead of varying “one factor at time” (OFAT), DoE tools offer a systematic method to plan and analyse experiments. Which leads to a reduced number of experiments and the possibility to describe interaction between the investigated parameters which are neglected in a classical OFAT experiments.

In the response surface methodology (RSM) a functional relationship between the input factors (herein process variables) and the response of interest (e.g. \dot{Q}_P or yield) is made. As the actual relationship is unknown it is approximated by a low degree polynomial model. Using this approximation, the response for a given setting of factors can be predicted. These predictions can be used to determine the optimal setting of factors for a chosen response. Effectively, making a process optimisation regarding the chosen response or combination of responses possible.

Linear, or first-degree, models are often used to screen for significant input factors but are insufficient when more complex phenomena are to be described. In this case second, or higher, order designs are used. For most industrial applications a second order design is sufficient. [57] As previous works already determined important factors, this work will directly work with a higher order design. The most frequently used designs for this are the 3^k factorial, central composite and Box-Behnken designs. [58] In a 3^k factorial design for each factor (k) three levels are defined, a low a medium and a high level (-1, 0, +1). Then every possible combination of the different factors with the different levels is examined, resulting in 3^k number of experiments. The resulting design space is illustrated in Figure 5.2 a for a three factor design.

The Box-Behnken design is similar to the 3^k factorial design. But the amount of performed experiments is reduced and only the “edges” of the design space are sampled, see Figure 5.2 b. This leads to regions of poor predictability, especially in the corner regions, but allows to skip extreme combinations of factors.

The central composite design (CCD) consists of a 2^k (two levels for each factor) design, which can be used in a first order model, e.g. for screening. To analyse the curvature of the response inside the design space the design is extended by a centre and several “star points”, see Figure 5.2 c. Accordingly, for each factor 5 different levels are included in the design.

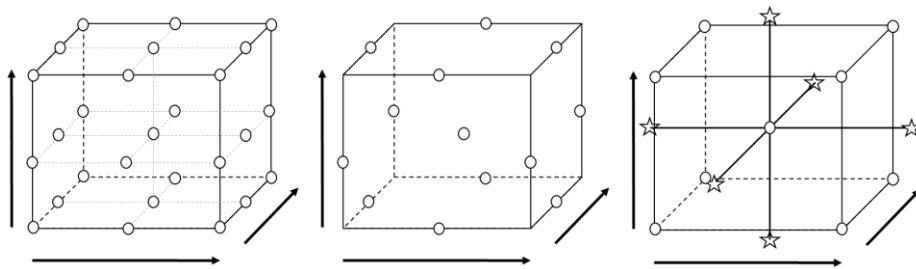


Figure 5.2: Graphical illustration for different three factor design. a) 3^k factorial, b) Box-Behnken, c) central composite design. Arrows indicate different factors.

Depending on the limitations of the design space, different versions of the CCD exist. If no limitations exist, e.g. experiments at all desired system pressures can be made, a circumscribed central composite design (CCC) should be performed. Here the corner points of the design represent the limits of the design space, the area of interest, and the star points are outside the design space, as shown in Figure 5.2 c. This design will yield the highest predictability for the area of interest.

If the experimental setup is limited, e.g. experiments with the maximum feasible pressure are to be included into the design, the design has to be changed. In an inscribed central composite design (CCI) the design is scaled down. The high and low levels are chosen in way that the experiments for the star points are performed at the minimum/maximum possible value for the corresponding factor. This reduces the area of validity of the final design but keeps the precision of a CCC. The alternative is the face centred central composite design (CCF). Here the star points are placed on the same level as the corner points. With this the whole design space can be described but some precision, especially for purely quadratic models is lost. [57]

5.2 Activity test

In the aforementioned studies empiric values for the activity of the whole cell biocatalyst and the necessary glucose supply were used. To quantify these parameters an activity test was established. From the previous experiments [34, 35] it was known, that the system is easily mass transport limited. In fact, it was made sure that the estimated maximum bacterial activity was higher than the expected mass transport of the butane. The goal for the activity test was to reduce the cell concentration, expressed in OD [-]. Below a critical value (OD_{crit}) the system is depending on the amount of cells and therefore being biologically limited. To reduce experimental labour, the experiments were conducted in the 0.2 L bubble column reactor (Chapter 3.2.2). While the OD was varied between the different experiments, all other parameters were kept constant (reactor volume 250 mL, temperature 30 °C, butane content 27 vol.%, overpressure 100 mbar, gassing rate 0.25 L min⁻¹ and a specific glucose feed rate of 4.17 mL OD⁻¹ h⁻¹ with a feed solution containing 50 g kg⁻¹ glucose). To exclude variations caused by different fermentations, cells from one high cell density fermentations (HCD#47) were used in all experiments. Figure 5.3 shows the measured \dot{Q}_P at the different applied ODs. Additionally, the activity (A [mmol L⁻¹ h⁻¹ OD⁻¹]) was calculated as the quotient of the \dot{Q}_P and the average OD, see eq. 15.

$$A = \frac{\dot{Q}_P}{OD_{600,avg}} \quad 15$$

In the beginning the \dot{Q}_P is proportional increasing with the OD. Starting from an OD of approx. 6 a plateau is reached, indicating the transition to mass transfer limitation. Accordingly, the activity is constant (0.35 mM h⁻¹ OD⁻¹) up to an OD of 6. At higher ODs the butane, which is transferred into the liquid phase, is shared between the cells, resulting in a lower activity. Based on this results it was concluded that the activity of a batch of fermented cells can be determined in an experiment with the aforementioned conditions and an OD of lower than 6. To be able to detect higher activity's an OD of 4 or below was usually applied in further activity tests.

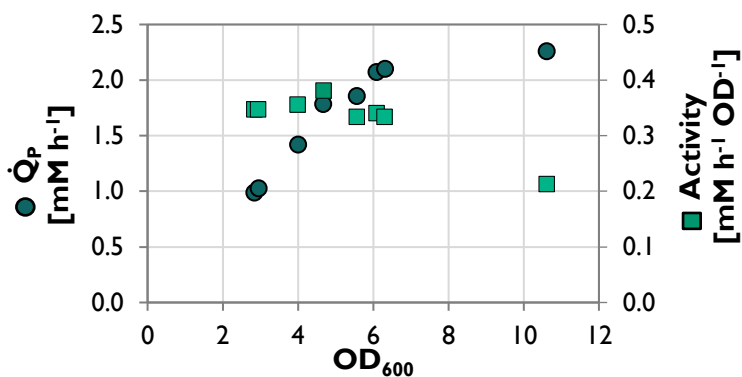


Figure 5.3: \dot{Q}_p for the formation of butyric acid (●) and associated activity (■) at varying ODs. Constant reaction conditions: 250 mL M9 medium, 30°C, gassing of 0.25 L min⁻¹ with 27 vol.% butane, overpressure of 100 mbar, specific glucose feed rate 4.17 mL h⁻¹ OD⁻¹ (glucose concentration 50 g kg⁻¹).

In the following this activity test was utilised to evaluate the used bacteria. The induction time during the fermentation, the effect of the freezing between bacteria fermentation and utilisation in the bubble column, and the specific glucose demand of the cells were investigated.

5.2.1 Induction Period

To determine the impact of different induction length on the bacterial activity, a high cell density fermentation was performed, and cells were harvested in intervals. After normal processing, centrifugation and freezing of the cell pellet at -80°C, activity tests were performed. The resulting activities in respect to the induction length are depicted in Figure 5.4. It is shown that the activity generally increases with increasing induction duration. The highest activity was measured for an induction period of 3 h, longer periods yielded no benefit. It must be noted that in the activity test with cells induced for 0.25 h, a lag phase was observed. Butyric acid was only measured after 1-1.5 hours and a constant \dot{Q}_p was reached another 0.5 hours later. This activation during the experiment can be explained by auto induction of the alkBGT operon by alkanes.[59] While the activity test is performed in minimal media, the frozen cell pellet still contains residual nutrients from the fermentation allowing *E. coli* to express enzymes at the beginning of the experiment. When all nutrients are consumed, all energy is put into the butane oxidation, resulting in the final constant \dot{Q}_p .

For all further experiments an induction time of 3 hours was used.

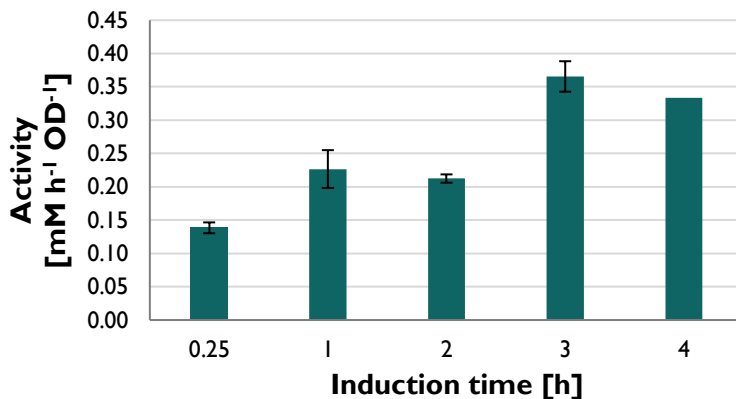


Figure 5.4: Influence of the induction time on the activity of alkBGT. Experiments with 0.25, 1 and 2 h were performed in duplicates, 3 h in triplicates and 4 h once. Constant reaction conditions: 250 mL M9 medium, 30°C, gassing of 0.25 L min⁻¹ with 27 vol.% butane, overpressure of 100 mbar, specific glucose feed rate 4.17 mL h⁻¹ OD⁻¹ (glucose concentration 50 g kg⁻¹).

5.2.2 Freezing of Cells

To determine, if the fermented cells lose activity during freezing and storage at -80 °C, activity tests with different treated cells were performed, see Figure 5.5. To determine the reference, the cells were harvested and instead of freezing the cell pellet, they were resuspended in minimal media and an activity test was performed directly.

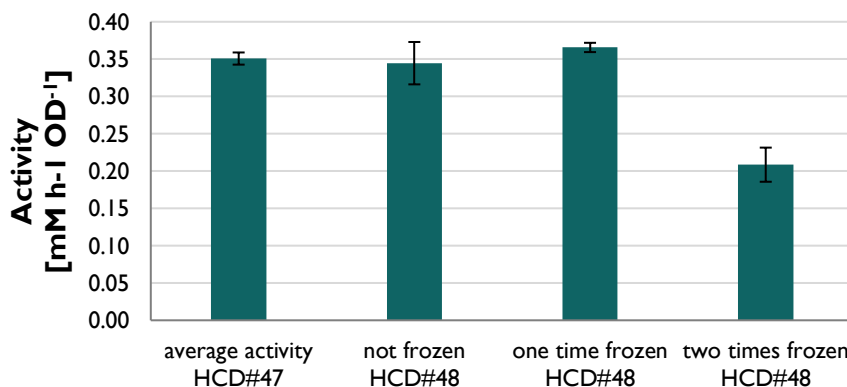


Figure 5.5: Impact of cell freezing on the alkBGT activity. HCD#47 represent the average activity during the implementation of the activity test. Constant reaction conditions: 250 mL M9 medium, 30°C, gassing of 0.25 L min⁻¹ with 27 vol.% butane, overpressure of 100 mbar, specific glucose feed rate 4.17 mL h⁻¹ OD⁻¹ (glucose concentration 50 g kg⁻¹).

Afterwards, activity tests with cells, which were frozen at -80°C, were performed. Additionally, these cells were harvested after the activity test, again frozen at -80°C and a second activity test was performed. For comparison the average activity from the development of the activity test is shown (HCD#47).

The results show that a singular freezing of the cells does not impact the activity of the cells negatively. However, it is not possible to reuse the cell after an experiment, as the activity after one time usage and a second freezing is reduced by ~40 %.

5.2.3 Glucose Demand

Like the OD_{crit} , it was suspected that a critical value for the specific glucose feed rate exists. Only when the cells metabolism provides enough NADH can the alkBGT system perform the biotransformation at maximum capacity. To determine the required glucose supply, activity test with varying specific glucose feed rates were performed. As described in chapter 3.3.2 the applied glucose feed ($\dot{F}_{Glucose}$) is calculated using eq. 13 and a glucose factor ($f_{Glucose}$). Figure 5.6 shows the results of the activity tests regarding the applied specific glucose feed rate as well as the glucose factor. With increasing glucose feed the activity increases until reaching a plateau at around $45 \text{ mg}_{\text{Glucose}} \text{ L}^{-1} \text{ h}^{-1} \text{ OD}^{-1}$, a glucose factor of $0.09 \text{ mL L}^{-1} \text{ h}^{-1} \text{ OD}^{-1}$. The highest activity achieved was $0.45 \text{ mM h}^{-1} \text{ OD}^{-1}$. The scattering of the data points can be explained by the use of three different batches of cells and the experimental variance. For further experiments it is assumed, that with a glucose factor of $0.1 \text{ mL L}^{-1} \text{ h}^{-1} \text{ OD}^{-1}$ maximum activity is achieved.

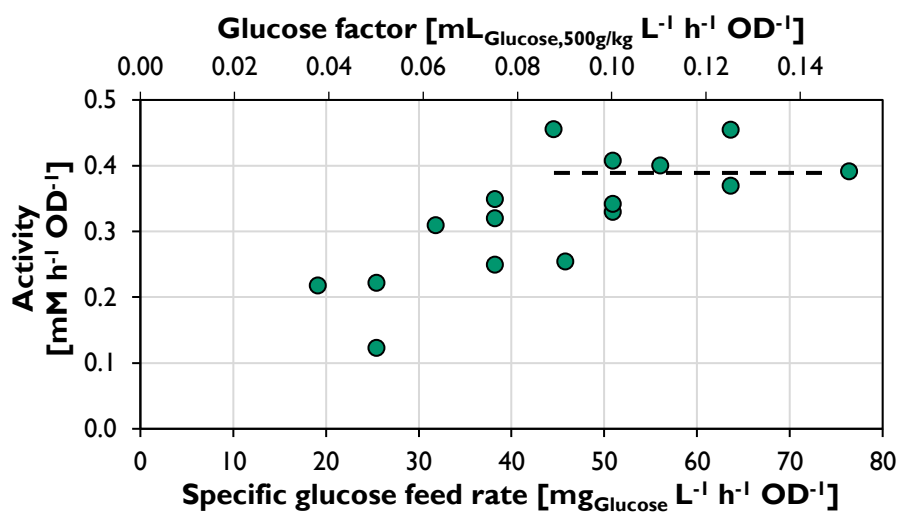


Figure 5.6: alkBGT activity (●) in dependency of the specific glucose feed rate and glucose factor. Reaction conditions: 250 mL M9 medium, 30°C, gassing of 0.25 L min⁻¹ with 27 vol.% butane, overpressure of 100 mbar, glucose concentration in feed 50 g kg⁻¹.

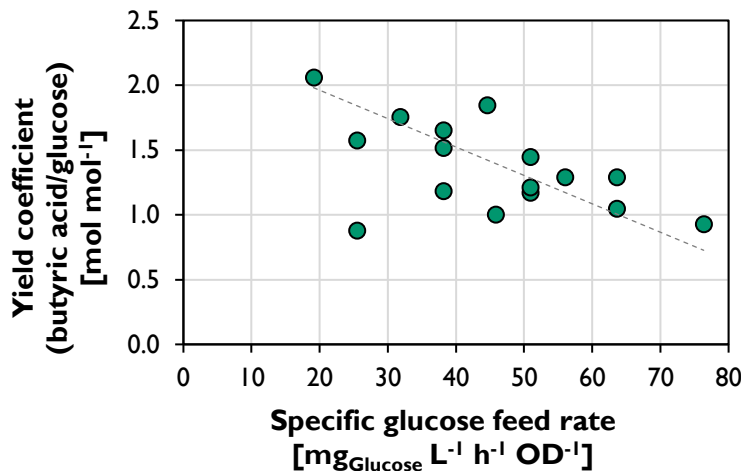


Figure 5.7: Product-substrate ration for butyric acid and glucose (●) during the investigation of the glucose demand. Reaction conditions: 250 mL M9 medium, 30°C, gassing of 0.25 L min⁻¹ with 27 vol.% butane, overpressure of 100 mbar, glucose concentration in feed 50 g kg⁻¹.

By forming the quotient from activity and applied molar specific glucose feed, the yield coefficient for the butyric acid in relation to glucose ($Y_{B-Ac/G}$ [mol mol⁻¹]) is calculated, see eq. 15. The yield coefficients for the glucose demand experiments are shown in Figure 5.7.

$$Y_{B-Ac/G} = \frac{A [mM h^{-1} OD^{-1}]}{\dot{F}_{Glucose,spec.} [mM h^{-1} OD^{-1}]} \quad 16$$

With increasing specific glucose feed the yield coefficient is decreasing, indicating that the bacteria become less efficient with increasing glucose supply. Based on the applied cellular pathways each oxidation of butane to butyric acid consumes 3 NADH, see chapter 5.1.2. While one molecule of glucose yields 8 NADH, which are 2 during glycolysis and in total 6 in the tricarboxylic acid cycle (TCA).[20] Neglecting the maintenance metabolism the theoretical maximum yield coefficient is therefore 2.67 mol mol⁻¹. It becomes clear that this value is not achieved during the experiments. When a glucose feed is chosen to reach maximum alkBGT activity the yield coefficient is reduced to 1-1.5 mol mol⁻¹. As a surplus of biomass is normally used the glucose yield decreases further. While this finding does not directly impact the further experiments, it would be important for an economic analysis.

5.3 Single Parameter Studies

One aim of this work was to perform a multivariable investigation of the alkBGT system (see chapter 2), for this the design space had to be determined. The basis for this was given by the works of Sluyter et al. [34, 35], were the parameters: gassing rate, pressure, butane content and temperature were investigated separately. As described in chapter 4, the GMS enables experiments to be carried out at higher butane contents. To determine the design space of the later performed DoE, the impact of butane on the \dot{Q}_P was reviewed. Additionally, because of a clogged sparger, the influence of the gassing had to be re-examined as well.

5.3.1 Butane

The aforementioned works [34, 35] have shown a unexpected impact of increasing butane content in the feed gas. With all other parameters kept constant and an increasing butane content, the \dot{Q}_P reached a maximum and then decreased significantly (■ in Figure 5.8-a). The butane partial pressure increases with rising butane content, which should lead to higher butane transfer. Since a butane limitation is assumed, higher \dot{Q}_P would be expected. Based on the dissolved oxygen measurements (■ in Figure 5.8-b) an oxygen limitation was suspected. Anti-foam agents are known to reduce k_{La} -values [23, 24, 60], therefore the dosage was generally optimised. Before optimisation 5-10 droplets of anti-foam at the beginning of the experiment and a constant feed $25 \mu\text{l h}^{-1}$ were used. The improved dosage, as described in chapter 3.3.2, consisted of 3 droplets at the beginning and single droplet addition when foaming was imminent (● in Figure 5.8).

It can be seen, that with the adjusted anti-foam dosage the \dot{Q}_P first increased with increasing butane content. At around 30 vol. % a plateau was reached, as further increase in butane content yielded no additional \dot{Q}_P . Only a pronounced decrease in dissolved oxygen was observed.

To verify that the increased \dot{Q}_P is not an effect caused by the use of the GMS, an experiment using a gas bottle (28.4 vol. % butane) was performed (▲ in Figure 5.8). Since this experiment is in good agreement with the other experiments, an effect caused by the GMS was dismissed.

Due to the plateau for \dot{Q}_P and the decreasing dissolved oxygen concentration no higher butane contents were examined.

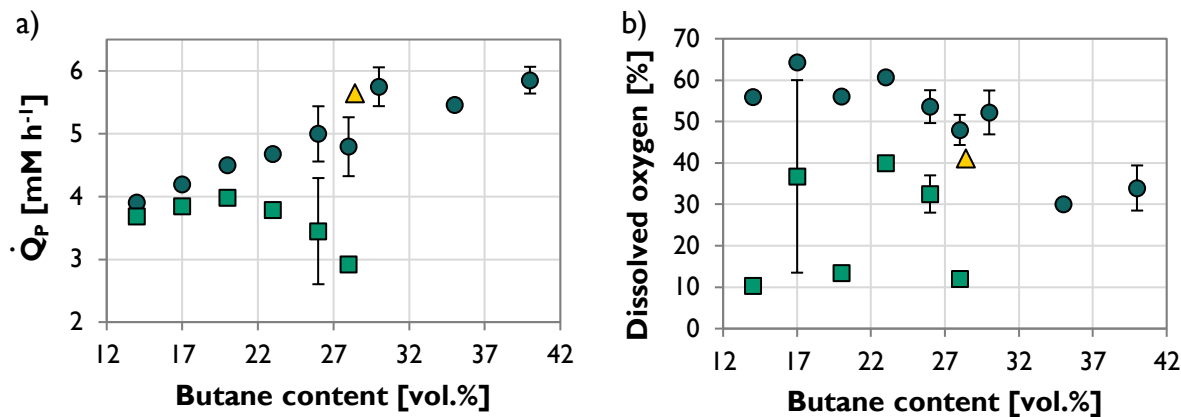


Figure 5.8: \dot{Q}_P (a)) and dissolved oxygen concentration (b)) for varying butane content in the feed gas. Improved anti foam supply and use of GMS (●) or premixed gas bottle (▲) and previous results from [35] using premixed gas bottles and old anti foam dosage(■). Constant reaction conditions: 2 L M9 medium, 30°C, gassing of 0.7 Ln min⁻¹, overpressure of 100 mbar, specific glucose feed rate 0.1 mg L⁻¹ h⁻¹ OD⁻¹(glucose concentration 500 g kg⁻¹).

5.3.2 Gassing Rate

As described in chapter 3.2.2 a sintered cylinder, with an average pore size of 2 µm, was used as a sparger inside the bubble column. To avoid clogging the sparger was regularly cleaned after each experiment. For this the sparger was flushed with corsolex-solution and rinsed with water. Still a clogging occurred hence the sparger had to be cleaned intensively. To check for changes of the spargers performance, experiments with this cleaned sparger (● in Figure 5.9) were compared with the previous results presented in [35] (▲ in Figure 5.9). Instead of an increasing \dot{Q}_P , no impact of the gassing rate on \dot{Q}_P was measured. Thus, a permanent change of the sparger was suspected, and a new sparger examined (■ in Figure 5.9). Again, no impact of the gassing rate on the \dot{Q}_P was measured. To verify that the differences are not caused by a change in the pre-pressure in front of the sparger, an experiment using a premixed gas bottle was performed (◆ in Figure 5.9). For gas bottle experiments the pre-pressure in front of the MFC is adjusted to 1 bar(g). While the pressure at the outlet of the GMS is ~0.75 bar(g), as described in chapter 4. This difference might change the bubble size distribution inside the bubble column [61, 62]. However, no significant difference between the experiments was visible.

Finally, the former experiments were reviewed with the knowledge gained through the activity test (chapter 5.2). It became clear that the activity for the experiment at 0.25 L min^{-1} was at $0.32 \text{ mM OD}^{-1} \text{ h}^{-1}$, which is the approximated maximum activity at the applied glucose factor of $0.075 \text{ mL}_{\text{Glucose},500\text{g/kg}} \text{ L}^{-1} \text{ h}^{-1} \text{ OD}^{-1}$ (see Figure 5.6). If this data point is excluded, the differences in the conclusion between the experiments is significantly reduced. Small differences are to be expected through the change of sinter stone and different dosage of anti-foam agent.

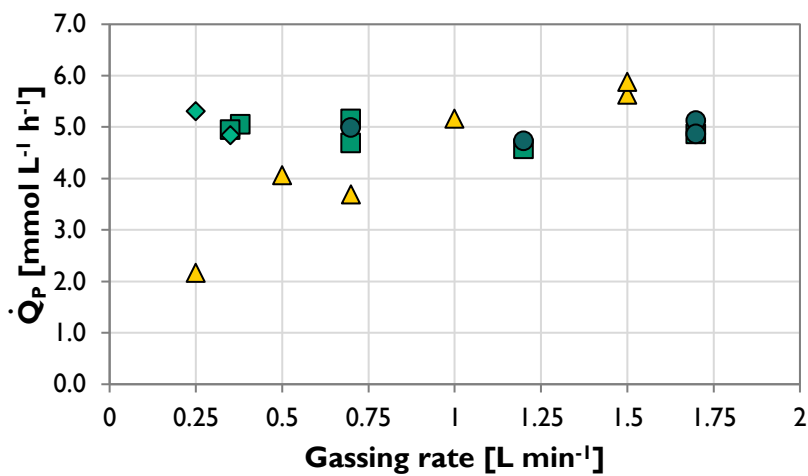


Figure 5.9: Comparison of the \dot{Q}_p for different spargers and feed gas supply. Old sparger and GMS (\bullet), new sparger and GMS (\blacksquare), new sparger and premixed gas bottles (\blacklozenge) and previous results from [35] with premixed gas bottles(\blacktriangle). Constant reaction conditions: 2 L M9 medium, 30°C , butane content in feed gas 14 vol.%, overpressure of 100 mbar.

5.4 Multivariable Process Analysis by DoE

Using the newly established GMS, the operation window for the 2 L bubble column reactor was expanded towards conditions which could not be reached so far. These were higher butane contents, gassing rates, pressures and especially combinations of these. To reduce the number of performed experiments “Design of Experiment” was used.

5.4.1 Design Space

To investigate the operation window of the bubble column setup a response surface methodology (RSM) using a central composite design (CCD) was chosen. It was expected that the highest \dot{Q}_P is achieved at the highest pressure. Therefore, the maximum pressure possible, 0.5 bar(g) predetermined by the reactor material, was to be included in the design space. Because of this limitation a “face centred” type (CCF) was chosen. In a CCF all experiments are performed within the design space, which can reduce precision compared to other CCD but retains the coverage of the area of interest.[57] The aforementioned parameters: gassing rate, butane content and pressures, were chosen as factors. Their lower and upper limited and the corresponding reasons are explained in the following.

Pressure

As mentioned before, the maximum pressure of 0.5 bar(g) was selected due to safety considerations. The lowest pressure, 0.1 bar(g), was chosen for comparability to the previously performed experiments using pre-mixed gas bottles.

Gassing Rate

Based on the previous results, the gassing rate was varied between 0.7 and 1.5 L min⁻¹. At higher gassing rates the pressure drop over the gassing adapter increased drastically which would require higher pressures at the outlet of the GMS. The pressure at the outlet of the GMS was always lower than the butane vapour pressure of 1 bar(g), see chapter 4. Additionally, a pronounced foam formation was observed at higher gassing rates. To keep similar hydrodynamic properties, a correction for the applied pressure was performed. According to eq. 17 the norm volume flow (\dot{V}_n) was calculated, which must be applied to reach the desired volume flow (\dot{V}) inside the reactor at a given pressure (p).

$$\dot{V}_n = \frac{\dot{V}}{p}$$

Butane Content

The design space for the butane content was chosen based on the single parameter investigation in chapter 5.3.1. The butane content in the feed gas was varied between 14 and 40 vol. %. Lower butane contents were avoided because of safety considerations, see chapter 1.3.

Constant Parameters

When possible, parameters were kept constant, e.g. the temperature was kept at 30 °C to prevent biological interferences and allow comparisons of the achieved activity with the introduced activity test. The applied biomass or OD was chosen based on the expectation for the single experiment to be not limiting. If limiting conditions were detected a repetition with higher OD was performed. The glucose factor was fixed to 0.2 mL L⁻¹ h⁻¹ OD⁻¹ (250 g kg⁻¹ glucose solution), according to chapter 5.2.3.

Final Design

Using the software Design-Expert® 12, Stat-Ease, CCF design with 19 experiments, including five centre points, was generated. For each factor three levels, see Table 5.1, were applied.

Table 5.1: Summary of factors and corresponding values

Parameter	Low value	Middle value	High value
Pressure [mbar(g)]	100	300	500
Gassing rate [L min ⁻¹]	0.7	1.1	1.5
Butane content [%]	14	27	40

All performed experiments, with the applied combination of factors and results for the different responses are summarized in Table A.6. The analysis for the individual responses, namely the \dot{Q}_P and yield, is performed in the following chapters.

5.4.2 DoE Response: Volumetric Productivity

The most important response is the \dot{Q}_P , as it describes the rate at which the butane is converted to the product. Based on the experimental results a reduced quadratic model was created in Design-Expert to calculate the \dot{Q}_P in dependency of the input factors. A summary of the ANOVA, fit statistics, and the model parameter are given in Appendix Table A. 7. It has to be noted, that the activities reached during the single experiments (see Table A.6) were in all cases below the activities of the applied cells, determined by the activity test (chapter 5.2). A selection of the predicted surface plots is shown in Figure 5.10.

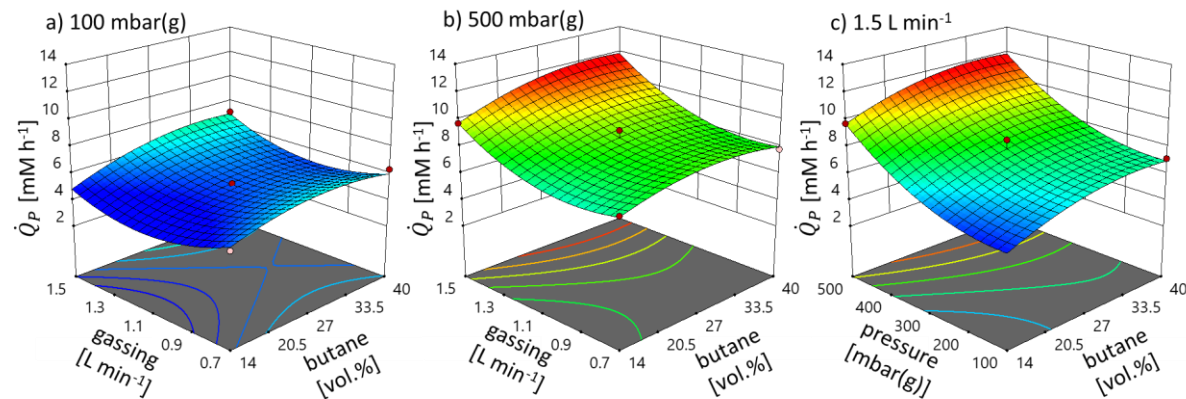


Figure 5.10: Response surface plots for the \dot{Q}_P depending on gassing rate and butane content at a) 100 mbar(g) and b) 500 mbar(g), as well as \dot{Q}_P depending on pressure and butane content at 1.5 L min^{-1} . Circles represent actual experimental data points. Constant reaction conditions: 2 L M9 medium, 30°C , glucose feed $0.2 \text{ mL L}^{-1} \text{ h}^{-1} \text{ OD}^{-1}$ (250 g kg^{-1} glucose solution).

The conditions shown in Figure 5.10 a in part match the conditions applied during the single parameter studies: Starting from a gassing rate of 0.7 L min^{-1} , with 14 vol.% butane and 100 mbar(g), and increasing either gassing rate or butane content. Comparable to the single parameter study, the \dot{Q}_P increases with increasing butane content, from a value around 4 mM h^{-1} , reaching a plateau of 6 mM h^{-1} .

However, for increasing gassing rates the \dot{Q}_P passes through a minimum until reaching the initial value. This opposes the findings of the single parameter study for the gassing rate. In which no influence of the gassing rate on the \dot{Q}_P under these conditions was measured, see chapter 5.3.2. This local minimum can be explained through the model design. This becomes clear when analysing the plot with the same conditions but at

500 mbar(g), see Figure 5.10 b. Here the increased gassing rate takes effect on the \dot{Q}_P , i.e. an increase in \dot{Q}_P . The interaction between gassing rate and pressure is additionally depicted in Figure 5.11 for a butane content of 14 vol%. For the model to incorporate this effect, a higher polynomial term is needed. In the face centred design the highest term allowed is a quadratic function, which leads to the anomaly of a local \dot{Q}_P minimum at low pressure and middle gassing rate.

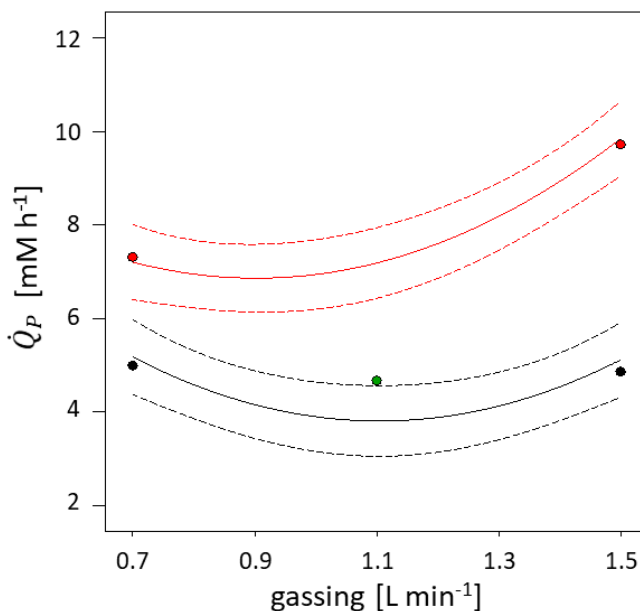


Figure 5.11: Parameter interaction for gassing rate with pressure, 100 mbar(g) (black lines and circles) and 500 mbar(g) (red lines and circles), at 14 vol% butane. Including a star point (green, 300 mbar(g)). Dotted lines represent 95% confidence interval. Constant reaction conditions: 2 L M9 medium, 30°C, glucose feed 0.2 mL L⁻¹ h⁻¹ OD⁻¹ (250 g kg⁻¹ glucose solution).

From Figure 5.10 b and c it can be concluded that the optima for gassing rate and pressure are outside of the design space. The optimum regarding the butane content was calculated to 35.5 vol%. Again, a plateau is predicted, similar to the one already found during the single parameter study. The highest measured \dot{Q}_P , which was achieved at the highest combination of the three factors, i.e. at a gassing rate of 1.5 L min⁻¹, 40 vol% butane, 500 mbar(g), is within the 95 % confidence interval of the calculated maximum \dot{Q}_P , 11.47 and 11.62 ± 0.76 mM h⁻¹, respectively. A distinct maximum could be located outside of the design space.

As described in the creation of the design space (chapter 5.4.1), the highest feasible conditions were already applied. For higher pressures and gassing rates the reactor setup has to be modified, including the installation of a pressure resistant reactor.

Thus, no optimal parameters for the overall process but an operation window for the used setup could be determined.

Two experiments were carried out to verify the predictions of the model, for which a point prediction was performed beforehand. The previous described single parameter studies offer already data points for comparison of the lower \dot{Q}_P regions. However, only qualitative comparison is appropriate as another gassing adapter was used. Hence, for the validation, conditions with higher expected \dot{Q}_P were chosen. The applied conditions, the prediction with 95 % confidence interval and the experimental results are given in Table 5.2. The deviation between predicted and experimentally measured \dot{Q}_P is with 0 and 2 % very low.

Table 5.2: Point prediction for \dot{Q}_P with applied conditions , prediction including with 95 % confidence and experimental result. Constant reaction conditions: 2 L M9 medium, 30°C, glucose feed 0.2 mL L⁻¹ h⁻¹ OD⁻¹ (250 g kg⁻¹ glucose solution).

Pressure [mbar(g)]	Butane content [%]	Gassing rate [L min ⁻¹]	\dot{Q}_P prediction [mM h ⁻¹]	Experiment [mM h ⁻¹]	Deviation
300	30	1.5	8.08 ± 0.72	8.24	2 %
400	30	1.4	8.71 ± 0.51	8.71	0 %

These results imply that the model is overall more accurate than the 95 % confidence intervals indicate. This would be a false conclusion, as the impact of the gassing rate at lower pressure (Figure 5.11) shows. Nevertheless, the model can predict the \dot{Q}_P for a complex system with different influencing factors, which would be very challenging with a mechanistic model. As the later has to include equations for mass transport phenomena for different substances, difficult to measure parameters, e.g. varying k_{LA} values for butane, or the changing hydrodynamics of a non-ideal three phase system - just to name a few.

5.4.3 DoE Response: Yield of Butyric Acid on Butane

As the total amount of butane fed into the reactor is differing between the experiments, the highest \dot{Q}_P does not necessarily correspond to the highest conversion of butane. Unfortunately, the amount of butane in the off-gas could not be measured and therefore no conversion calculated. Thus, a yield on butane, the percentage of the fed butane that was converted to butyric acid, is calculated. For this the molar butane flow

into the reactor is divided by the \dot{Q}_P of butyric acid. As only traces of butanol and no butyraldehyde was detected the conversion of butane can be approximated with the calculated yield on butane.

Based on the experimental results (Table A.6) and a logarithmic (log10) transformation a reduced quadratic model was created in Design-Expert to calculate the yield in dependency of the input factors. A summary of the ANOVA, the fit statistics and the model parameter are given in Appendix Table A. 8. A selection of the predicted surface plots is shown in Figure 5.12.

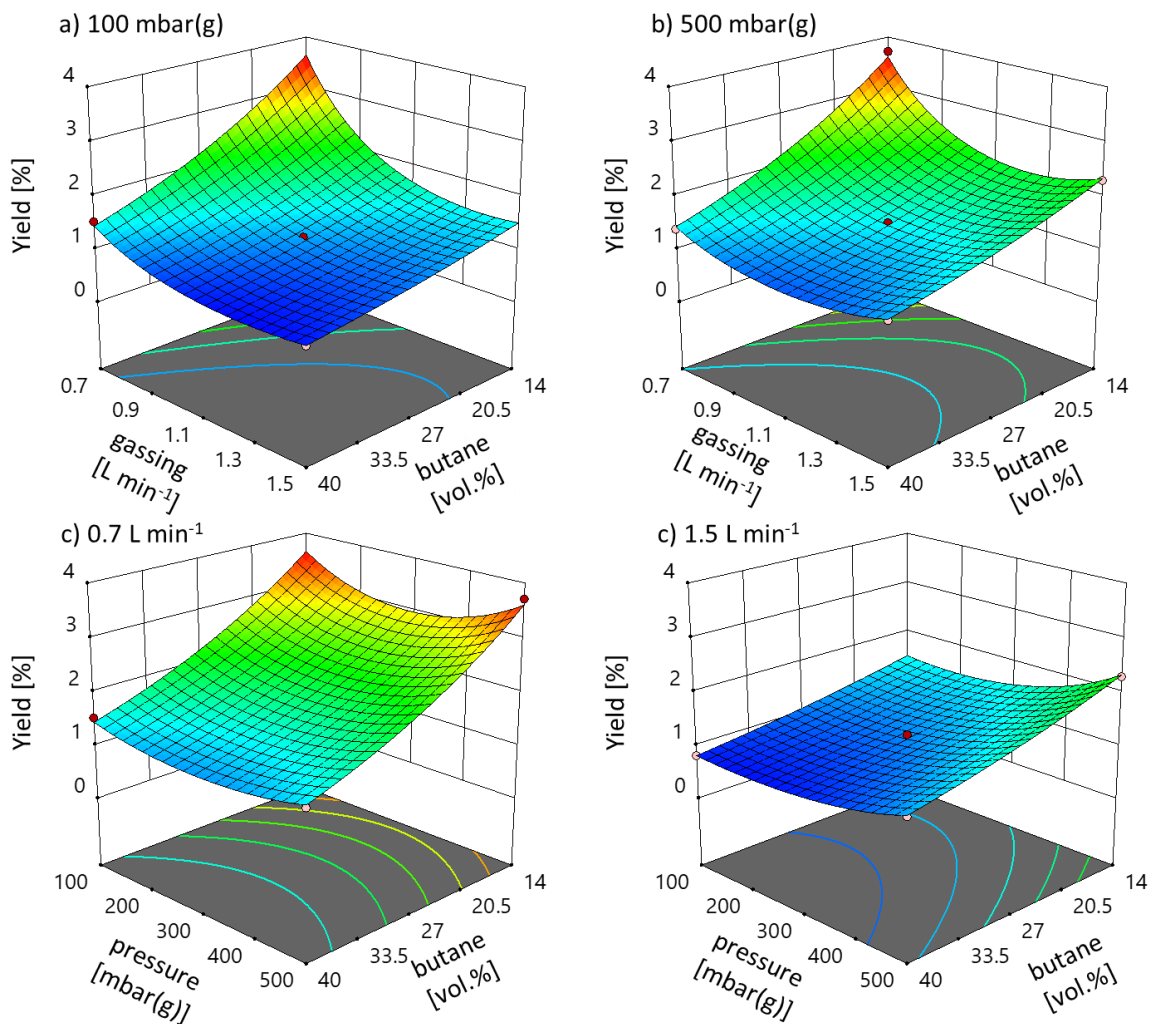


Figure 5.12: Response surface plots for the yield depending on gassing rate and butane content at a) 100 mbar(g) and b) 500 mbar(g) and response surface plots for the yield depending on pressure and butane content at c) 0.7 L min⁻¹ and d) 1.5 L min⁻¹. Circles represent actual experimental data points. Constant reaction conditions: 2 L M9 medium, 30°C, glucose feed 0.2 mL L⁻¹ h⁻¹ OD⁻¹ (250 g kg⁻¹ glucose solution).

It is shown, that at low pressures (Figure 5.12 a) only the combination of low gassing rates and low butane contents creates a significant increase in yield. At higher pressure (Figure 5.12 b) the yield increases over the whole design space with decreasing butane content. The highest yield is, again, reached at low gassing rates and butane content. The pressure only influences the yield in combination with another factor, here the gassing rate, see Figure 5.12 c and d. While at low gassing rates (Figure 5.12 c) the pressure does not affect the yield, an increase is visible for higher gassing rates (Figure 5.12 d). This is similar to the observations for the gassing rate regarding the \dot{Q}_P and also the cause for the parabolic form in Figure 5.12 c, which is again an result of a quadratic term.

Overall, the yield is nearly the reverse to the \dot{Q}_P , which is expected due to the theory. Lower gassing rates result in longer residence times, i.e. longer contact time, and thus a higher yield. Because the gassing rates are corrected for increasing pressures, the total (molar) amount of butane fed to the system increases with pressure. This counterbalances the higher mass transport resulting from the higher butane partial pressure.

5.4.4 Combined DoE Response: Process Window

The previously shown results of the DoE for the \dot{Q}_P and yield are combined in one graph to outline the process window, see Figure 5.13. For this, all possible combinations of the three parameters: gassing rate, butane content and overpressure, were used to calculate the \dot{Q}_P and the yield. For each process parameter 20 evenly distributed increments were used. For reference the results for “all low” (0.7 L min^{-1} , 100 mbar 14 vol.%) and “all high” (1.5 L min^{-1} , 500 mbar 40 vol.%) process conditions are marked in yellow. It should be noted, that for each parameter combination one dot is displayed. Areas where single dots cannot be differentiated indicate that several parameter combination result in this point of operation. While clearly distinct dots indicate areas for which only a certain parameter combination is possible. For these points a higher uncertainty is to be expected.

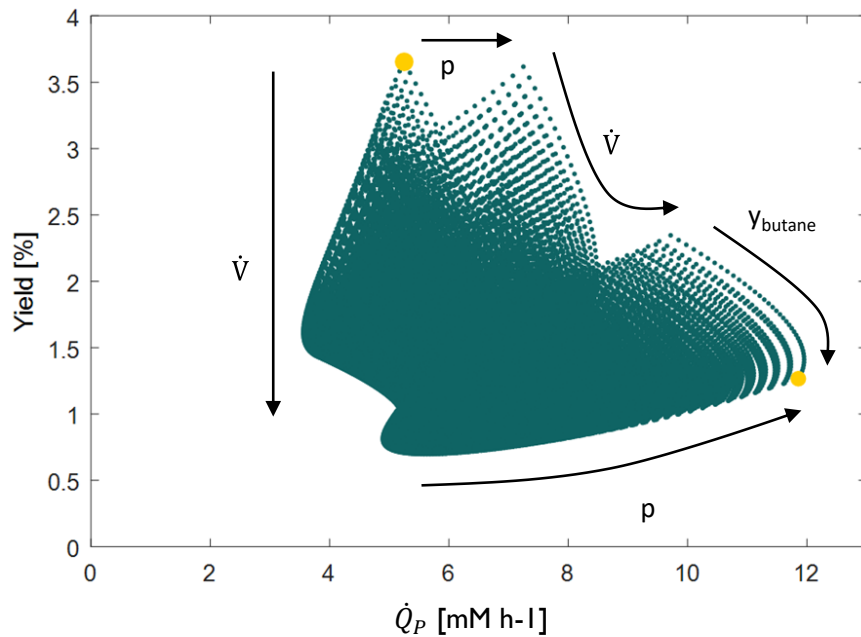


Figure 5.13: Process windows for the oxidation of butane by the alkBGT system heterologously expressed in *E. coli*. Data points for \dot{Q}_P and yield based on the predictions of the design of experiment. Any possible combination of the three parameters: gassing rate \dot{V} ($0.7\text{-}1.5 \text{ L min}^{-1}$), butane content y_{butane} (14–40 vol.%) and overpressure p (100–500 mbar) divided in 20 increments respectively is shown. Corner points of DoE for the “all low” and “all high” parameter combination ●, arrows indicate increasing parameter values.

As a combination of the separate DoE results is shown, the same characteristics are visible. For example, the decrease in \dot{Q}_P with increasing gassing rate at low pressure (left side of the diagram), is based on the usage of only quadratic terms. As discussed before, at these conditions, with only the gassing rate being changed, \dot{Q}_P should be constant. Similarly, the yield is decreasing with increasing pressure (at the upper part of the diagram), which is again caused by a quadratic term, see Figure 5.12 c). It is to be expected that yield does not decrease at constant conditions and increasing pressures. Overall, the following conclusions can be made:

- An increasing pressure has generally a positive effect on \dot{Q}_P and in combination with other parameters also on the yield.
- An increase in gassing rate decreases the yield and increases the \dot{Q}_P at higher pressures.
- Higher butane contents lower the yield but increase \dot{Q}_P .

Altogether these results are in line with the theoretical expectations.

5.5 Mass Transport Vectors

In Chapter 1.2 the three main influencing factors for mass transport were described: reactor type and configuration, operating conditions, and additives. The reactor type was, for the scope of this work, fixed, see safety considerations chapter 1.3. The operating conditions were, inside the limitations given by the reactor setup, exploited to their full potential by the DoE. Hence, the addition of mass transport vectors was investigated to further improve the mass transport and thereby the \dot{Q}_P .

Based on a literature study by A. Nahir [63] a selection of different vectors, a salt (magnesium sulfate), an organic liquid (dodecane) and a solid vector (Desmopan® DP9730A particles 4x2x2 mm), were examined in the 2 L bubble column setup. The increase in \dot{Q}_P compared to a control experiment is shown in Figure 5.14.

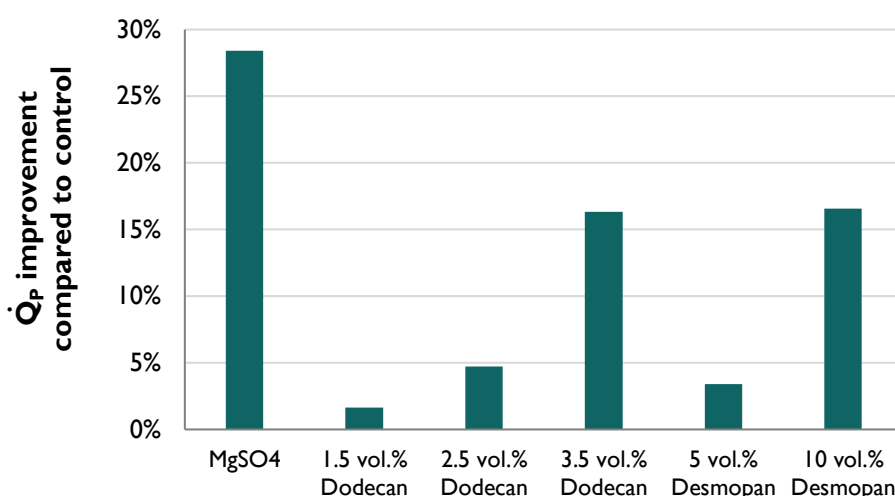


Figure 5.14: Increase in \dot{Q}_P for different mass transfer vectors, compared to a control without vectors. Butane was supplied by premixed gas bottles. Reaction conditions: 2 L M9 medium, 30°C, butane content in feed gas 20 vol.%, overpressure of 100 mbar, gassing rate 0.7 L min⁻¹. Desmopan: 10 vol.% correspond to 130 g particles.

It should be noted that for these experiments premixed gas bottles were used which were limited in the runtime. Additionally, for each vector only one experiment was conducted and the concentrations were stepwise increased, to screen for suitable vectors.

While the MgSO₄ addition yields with 28% the highest increases in \dot{Q}_P the data is unreliable. During the experiment strong precipitation was observed. It is assumed that magnesium hydroxide, which has low solubility in water (8.75 mg L⁻¹ at 20°C [64]), is formed. The measured cell activity for this experiment was 0.55 mM OD⁻¹ h⁻¹, which is also unreasonably high. The cause for this result was likely an interference of the precipitate during the extraction of sample preparation. Because of the precipitation, no further experiments were performed with MgSO₄.

Dodecan and Desmopan yielded higher \dot{Q}_P with increasing amounts applied, both up to a 15 % increase. For the former a maximum at 2.5 vol.% was estimated based on recent literature data [65]. As this study applied a STR setup and pure water, differences were expected. The calculated activity was at the upper limit for both experiments at the respective highest concentration, indicating a biological limitation. Nevertheless, a \dot{Q}_P increase of 15% is a significant increase that was deemed worthy for application.

The above-described experiments were performed at comparable low \dot{Q}_P of 5 to 6 mM h⁻¹. This was done to reduce the necessary biomass in each experiment, allowing to perform all experiments with the bacteria from one single fermentation. Thereby the effect of different cells was minimised. To validate the effects at higher \dot{Q}_P the two vectors dodecane and Desmopan were added in their highest concentration/amount in the point validation experiments described in chapter 5.4.2. The addition was performed after 4 h of experiment. The difference in \dot{Q}_P before and after addition of the vector is shown in Figure 5.15.

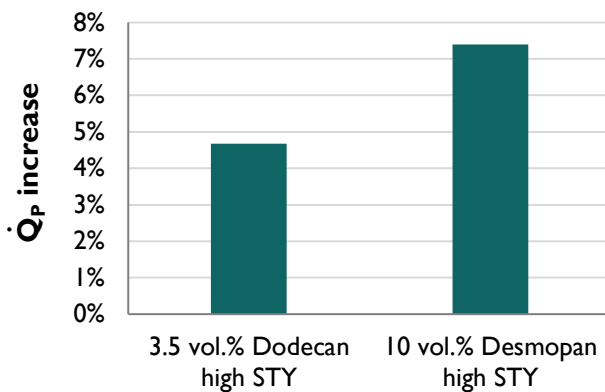


Figure 5.15: \dot{Q}_p increase conditions a) 300 mbar and 1.5 L min^{-1} , b) 400 mbar and 1.4 L min^{-1} . Constant reaction conditions: 2 L M9 medium, 30°C , butane content in feed gas 30 vol.%, overpressure of 100 mbar, gassing rate 1.4 and 1.5 L min^{-1} . Desmopan:10 vol.% correspond to 130 g particles.

Compared to the previous experiments, the increase in \dot{Q}_p is significantly lower. First it has to be noted, that these experiments were not biologically limited. The cause for the lower improvement is unclear. A possible explanation are interactions between the applied process conditions and the amount of used vector. From literature [65–67] it is known that liquid vectors show a maximum for the increase in mass transfer. This maximum is specific for each system. The previously mentioned publication of Sinha et al. [65] found a maximum for a 1 L STR at 2.5 vol.% dodecane in pure a water. An older publication by Rols et al. [66] estimated maxima at around 14 and 23 vol.% dodecane in a 12 L STR with an ongoing fermentation of *A. aerogenes* and different dispersion methods. Both publications refer to the bubble size distribution and coalescence behaviour of the respective systems when explaining the experimental results. For the Desmopan experiment an accumulation of Desmopan particles at the bottom of the bubble column was observed. This reduced most likely the impact on the mass transport. An optimisation of the applied amount of vector is necessary for both vectors.

Since a more detailed and systematic investigation of these and different mass transfer vectors was outside of the scope of this work, further systematic investigations are recommended for the future, see chapter 8.1.

5.6 Interim Summary

- The oxidation of butane to butyric acid by a modified *E. coli* strain, containing the alkBGT system, was investigated in two bubble column reactor setups.
- An activity test for the used bacteria was established in a 0.2 L bubble column reactor and subsequently applied to further biological investigations.
The maximum achievable activity was $\sim 0.45 \text{ mM}_{\text{butyric acid}} \text{ h}^{-1} \text{ OD}^{-1}$. A glucose feed rate of $45\text{-}50 \text{ mg}_{\text{glucose}} \text{ L}^{-1} \text{ h}^{-1} \text{ OD}^{-1}$ is needed to achieve these activities.
- The process window of a 2 L bubble column reactor was determined by using Design of Experiments. The investigated parameters were gassing rate, butane content and overpressure. The highest \dot{Q}_P was measured with 11.47 mM h^{-1} .
The optimum is expected to be outside of the design space. But as the applied conditions were already maxed out, due to reactor limitations, the optimum could not be determined.
- Further potentials to increase the \dot{Q}_P are shown with the application of mass transfer vectors.

6 Utilisation of Butane as Energy- and Carbon-Source

In this chapter the utilisation of butane by a modified *E. coli*, containing the previously described AlkBGT system and the so called Ato system, is described. Preliminary work for this chapter was performed during the master thesis of Philipp Garbers [68].

6.1 Introduction and Fundamentals

While oxyfunctionalisation of butane, as it is described in the previous chapter, offers an alternative to burning butane, it suffers under the drawback of the glucose demand. Like the “Food or Fuel” debate [69] it can be argued that the production of butane derivatives using glucose contradicts the second UN goal for sustainable development. A more sustainable approach would be a glucose independent process, which uses butane as its single carbon source. In this regard Gehring et al. [53] demonstrated the synthesis of rhamnolipids in *Pseudomonas putida* using butane as (single) energy and carbon source.

In this chapter the previously utilised *alkBGT* system, from *P. putida* expressed in *E. coli*, is combined with the *ato*-system, see next subchapter, to investigate the feasibility of *E. coli* cultivation on butane and its derivatives.

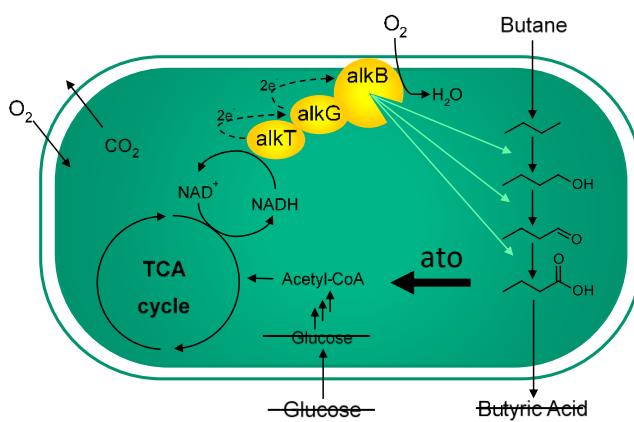


Figure 6.1: Schematic view of the changes, compared to chapter 5, to the applied *E. coli*.

6.1.1 Ato-Enzyme System

Many bacteria can utilise medium and long chain fatty acids via β -oxidation. The corresponding enzymes are encoded on the *fad* regulon.[70] In a first ATP consuming reaction step an acyl-CoA synthetase (Fadd) binds a CoA to the fatty acid, generating an Acyl-CoA. From here the β -oxidation cycle starts with an oxidation by FadF. In this reaction a double bond between the second (C_α) and third carbon (C_β) atom is inserted, while reducing an FAD^+ to $FADH$ in the process. Subsequently this bond is hydrated by FadC and a hydroxyl group is formed at the C_β . Further oxidation of the hydroxyl group by FadB leads to a keto group, while yielding one NADH. Lastly FadA, a thiolase, releases an acetyl-CoA while at the same time attaching a CoA to the residue. This reforms the acyl-CoA but with a residue shortened by two carbons. Further cycles lead to the complete degradation of the fatty acid.

Normally this system is used for medium and long chain fatty acids. Using the ato system also butyric acid, as a short chain fatty acid, can be utilised, see Figure 6.2. Instead of the ATP consuming Fadd, the AtoA, a CoA-transferease, transfers a CoA from an acetyl-CoA to a butyric acid. The formed acyl-CoA then enters the β -oxidation and is in the end cleaved to two acetyl-CoA, either by the FadA or by AtoB, another thiolase. While one acetyl-CoA is needed for the initial transferase yielding an acetate, the other acetyl-CoA enters the TCA cycle. Here it can be used for generating energy or in the anabolism and therefore growth of the bacteria.

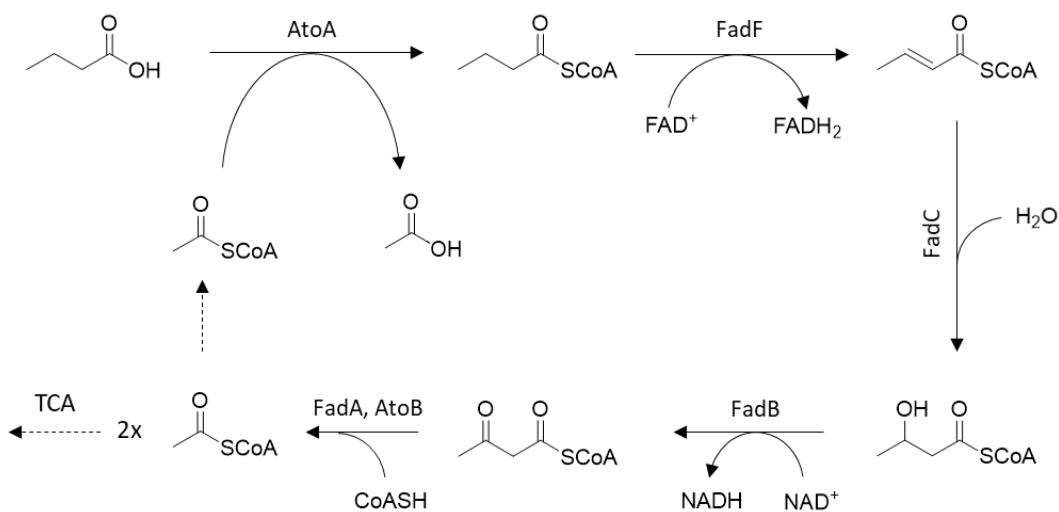


Figure 6.2: Overview of the *ato* and *fad* system for the conversion of butyric acid to acetyl-CoA. Adapted from Pauli and Overath [71].

6.1.2 Bacterial Cell Growth

The macroscopically growth of a bacteria culture can be divided into four main phases, with transition stages in between, see Figure 6.3. After the inoculation of a reaction/growth media with bacteria a lag (I) phase might occur. In this phase the cells adjust to the new environment before they start to grow. When the growth is not limited the cells will proceed to double continuously, resulting in the exponential (II) phase. At the time, when an essential nutrient is depleted and no feeding of the substance is applied, the growth transitions to the stationary phase (III). The accumulation of inhibiting compounds can also lead to the third phase. Whichever the case, the growth and death of the bacteria balance each other out, resulting in a constant amount of living bacteria. At some point the stationary phase transitions into the death (IV) phase, here the dying of the bacteria exceeds the growth.

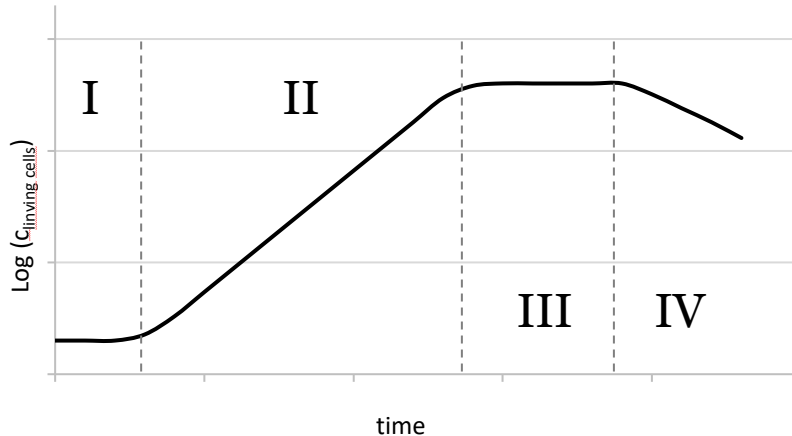


Figure 6.3: Phases of bacterial growth. (I) Lag phase. (II) Exponential phase. (III) Stationary phase. (IV) Death phase.

Depending on the cells and surrounding conditions the phases can be longer or shorter. E.g the use of a new substrate leads generally to a longer lag phase as the bacteria must adjust their catabolism. If the carbon/energy source was the limiting factor the stationary phase can be very short.

For fermentation processes the mathematical description of the exponential growth phase is of great interest. In the following the mass balance for a fermentation inside a batch reactor will be described. Afterwards the changes which are needed to describe the special case of a bubble column reactor with a gaseous substrate are explained.

For the mass balance the general scheme (eq. 3) as introduced in chapter 1.2 is used. As in a batch reactor nothing is added or withdrawn the equation can be reduced as follows, eq. 18.

$$\frac{dc_i}{dt} = \dot{F}_{in} \cdot c_{in} - \dot{F}_{out} \cdot c_{out} \pm r \quad 18$$

To describe the cultivation two concentrations must be accounted for. The biomass concentration c_x (OD) and the substrate concentration c_s [mmol L⁻¹]. Herein, it is assumed that the exponential growth of the bacteria is only limited by this substrate. All other substrates are provided in excess. As the biomass increases and the substrate decreases no steady state conditions are applicable. Instead, ordinary differential equations (ODE) are used. The concentration of the cells or biomass is described by differential eq. 19.

$$\frac{dc_X}{dt} = \mu \cdot c_X \quad 19$$

Herein the biomass concentration is depending on the growth rate μ [h^{-1}] and the biomass concentration. A simple model to describe the growth rate depending on the limiting substrate is given by Monod [72], eq. 20. In this the maximum possible growth rate μ_{max} is reached when a huge surplus of the limiting concentration is present and no other factors are limiting the growth rate. The second parameter is the saturation constant K_s [mmol L^{-1}]. At a corresponding substrate concentration the half maximal growth rate is reached.

$$\mu = \mu_{max} \cdot \frac{c_S}{K_S + c_S} \quad 20$$

In the case of an inhibition of the growth by the used substrate Adrews [73] proposed eq. 21. In this a parameter that is expressing the inhibitory effect K_i [mmol L^{-1}] is introduced.

$$\mu = \mu_{max} \cdot \frac{c_S}{K_S + c_S + \frac{c_S^2}{K_i}} \quad 21$$

When the bacteria grow, they take up the substrate. This is described by the specific uptake rate q_S [$\text{mmol L}^{-1} \text{ OD}^{-1}$]. For simplicity it is assumed that all substrate that is taken up by the bacteria is used for growth. So, the substrate which is used for the maintenance metabolism of the cell is neglected. As the bacteria is not completely made of the one substrate and the anabolism takes energy as well a correlation between the formed biomass and used substrate is needed, see eq. 22.

$$\frac{dc_S}{dt} = q_S \cdot c_X = - \frac{\mu}{Y_{X/S}} \cdot c_X \quad 22$$

The biomass yield coefficient $Y_{X/S}$ [OD mM^{-1}] describes the formed biomass per utilised substrate and can be calculated as follows.

$$Y_{X/S} = \frac{dX}{dc_S} \approx \frac{c_{X,End} - c_{X,Start}}{c_{S,End} - c_{S,Start}} \quad 23$$

In a bubble column reactor where a gaseous feed of the substrate is applied, the initial mass balance must be changed, but only for the substrate ODE. The system boundaries

for the applied mass balance are placed around the liquid media. Therefore, the transfer rate (TR) of the gaseous substrate increases the substrate concentration, eq. 24. It is assumed that the volume increase by the steadily dissolving gas is neglectable.

$$\frac{dc_S}{dt} = q_S \cdot c_X + TR \quad 24$$

6.2 Cultivation on Butane Derivatives

To prove the functionality of the ato-system, first cultivations were performed in shaking flasks. Instead of butane the derivatives butanol and butyric acid were used as substrate. Growth on butyric acid indicates a working ato-system. While growth on butanol implies that the “overoxidation” through the alkBGT-system is occurring. Shaking flasks offer the possibility to parallelise the experiments, making investigations of growth rates easier. For the first proof of growth on butanol or butyric acid an overnight culture in LB-medium was transferred to an induction culture, M9+ medium with yeast extract. After 24 hours of induction the cells were washed and transferred to two cultures of M9 media without any additional carbons source except for butanol or butyric acid. The concentration profiles for these two cultures are shown in Figure 6.4. In both cultures the substrate concentration was decreasing but for the first three days no growth was detected. As the substrate was eventually depleted, the cultures were fed with butanol and butyric acid, marked by the dashed lines. After the third day growth was detected in both cultures.

To verify the growth on butanol and butyric acid the two cultures were pooled and used to inoculate four new cultures, with 20 and 50 mM of butanol or butyric acid, respectively. An increase in OD and decreasing substrate concentrations were directly measurable (data not shown).

To maintain an active cell culture a new culture was inoculated from an active culture every or every other week. Regular determination and feeding of butyric acid and butanol assured the supply of substrate. Additionally, parts of the previous culture were centrifuged, and the cell pellet stored at -80°C as a backup in case of contaminations or other interferences.

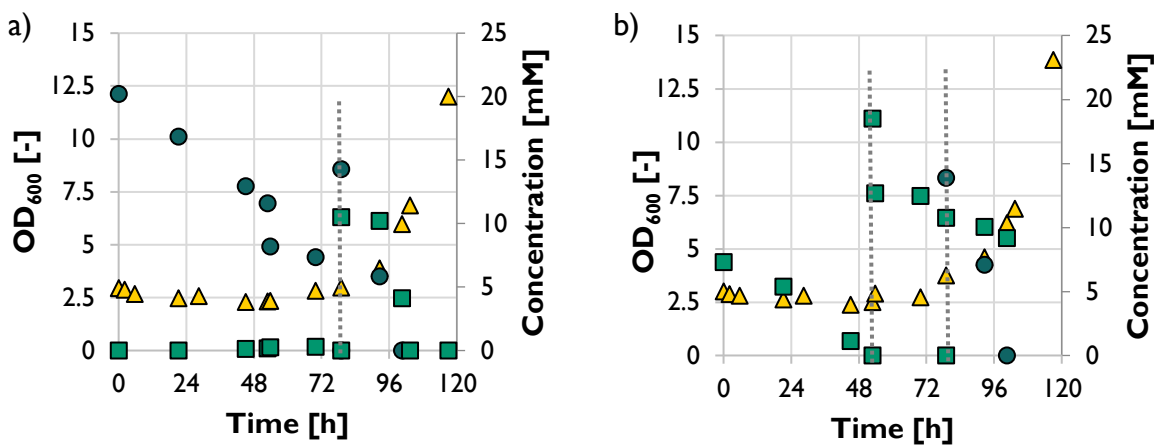


Figure 6.4: Concentration profiles during the initial activation of the cells with a) butanol and b) butyric acid as starting substrate: OD (Δ), butanol (\bullet) and butyric acid (\blacksquare). Reactions conditions: 300 mL shaking flask with 50 mL M9 minimal media, 120 rpm and 30°C. Addition of butanol and/or butyric acid indicated by dashed lines.

Growth Rates

Batch cultivations were performed in shaking flask to determine growth rates on butanol and butyric acid. Figure 6.5 shows the measured growth rates over the applied starting substrate concentrations at 30°C. For both substrates a substrate inhibition is detected. The maximum measured apparent growth rate is 0.13 h⁻¹ for both substrates.

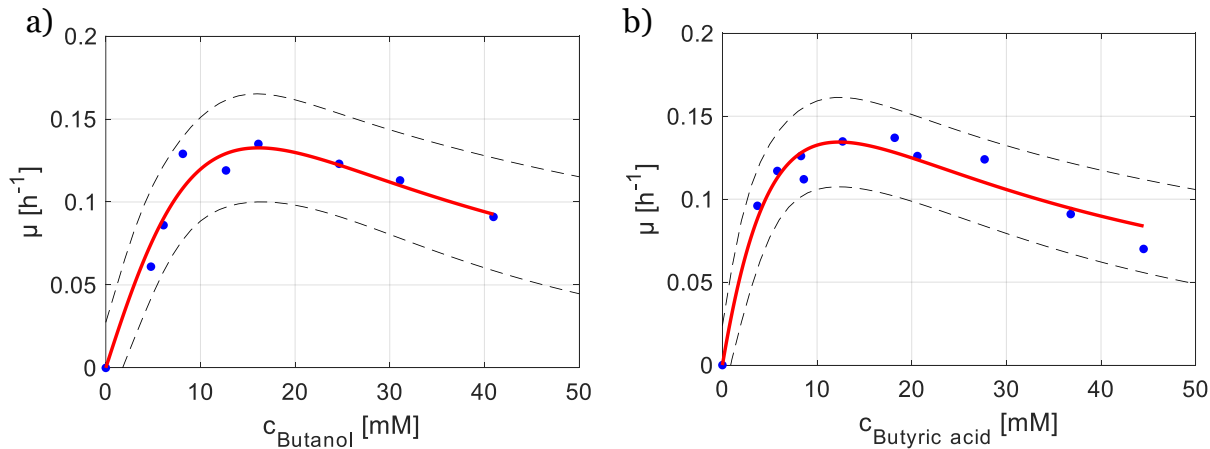


Figure 6.5: Measured growth rates (\bullet) depending on the initial substrate concentration for a) butanol and b) butyric acid. Fit (-) with 95% confidence interval (--) of substrate inhibited Monod kinetic. Reaction conditions: 300 mL shaking flask with 50 mL M9 media, 30°C and 120 rpm, starting substrate concentration as depicted and a starting OD of ~1.

The measured data were fitted using the Monod kinetic with substrate inhibition (eq. 21). The obtained kinetic parameters are listed in Table 6.1. Additionally, as the

kinetic parameter do not reflect the actual optimal growth parameters, the optimal substrate concentrations ($c_{s,\text{opt.}}$) and corresponding growth rate ($\mu_{\text{max,app}}$) are calculated. The high confidence intervals are caused by the substrate inhibition term of the kinetic and the natural occurring deviations of the experiment. Another factor is the measurement in batch mode. In a batch cultivation the substrate concentration decreases over time, leading in theory to heterogeneous growth rates over the course of the experiment. Further experiments, in a batch or continuous reactor, could improve the accuracy. As the focus of this work was the utilisation of butane, the growth kinetics were not pursued further.

Table 6.1: Fitted kinetic parameters, including 95% confidence interval, and apparent optimal conditions for the growth on butanol and butyric acid.

Parameter	Substrate	
	Butanol	Butyric acid
$\mu_{\text{max}} [\text{h}^{-1}]$	2.1 ± 36.8	0.37 ± 0.41
$K_S [\text{mM}]$	130 ± 2120	11 ± 18
$K_I [\text{mM}]$	2.2 ± 32	14 ± 22
$\mu_{\text{max,app}} [\text{h}^{-1}]$	0.13	0.13
$c_{s,\text{opt.}} [\text{mM}]$	~ 17	~ 12

6.3 Cultivation with Butane

To verify the growth on butane as single carbon and energy source, experiments in the 0.2 L bubble column reactor (chapter 3.2.2) were performed. Unexpectedly no growth could be detected in multiple experiments. As also some cultivations in shaking flask, with butanol or butyric acid as substrate, inexplicably did not grow, the applied cells were checked. For this, parallel experiments with butane, butyric acid and a combination of both were performed in three small stirred-tank reactors (50 mL STR, chapter 3.2.2). Additionally, the 0.2 L bubble column reactor was inoculated, and butane was applied as single substrate. Oxygen supply was ensured by gassing with air or, in the cases of butane as substrate, a butane-air mixture. The resulting OD measurements are shown in Figure 6.6.

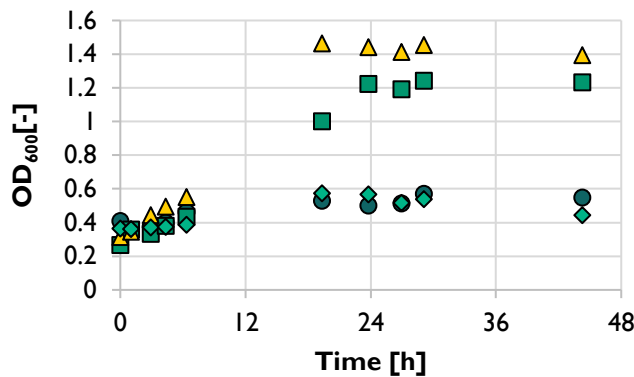


Figure 6.6: Parallel cultivation in 50 mL STR and different substrates: only butane (●), butyric acid (■), butane and butyric acid (▲). Cultivation in 0.2 L bubble column and only butane (◆).

It becomes visible that the cultures with butane as single substrate did not grow, while the two others, containing butyric acid, did grow. Indicating that the ato-system is functioning. Additionally, the final OD of the culture with butane and butyric acid as substrates was about 15 % higher than the OD of the culture with butyric acid as single substrate. This implies that the alkBGT system is working and converting butane to butyric acid if the cells have supply of another energy source.

Dual Substrate Cultivation

Based on these results a dual substrate cultivation approach was used in further investigations. For this, the cultivations were prepared in the bubble column reactor, including the addition of butanol or butyric acid. After inoculation 50 mL of culture medium were withdrawn and cultivated in a 300 mL shaking flask. This shaking flask was used as a reference without the gassing of a butane-air-mixture. The OD and substrate concentrations were regularly measured in the bubble column, gassed with a butane-air-mixture, and the shaking flask. The comparison of the separate results gives insights into the fixation of butane by the bacteria. It has to be noted, that at higher biomass concentrations stable foam bubbles were generated, which led to adhesion of the cell on the wall of the bubble column. To counteract this an external pump cycle was implemented (see Figure 3.4 in Chapter 3.2.2).

To verify that the difference in cultivation conditions did not influence the growth behaviour of the cells, two experiments in which the bubble column was only gassed with air were performed. The measured ODs for the shaking flask and bubble column are depicted in Figure 6.7. In both experiments no significant difference in growth rate or total cell concentration at the end of the experiment was detected. From these

experiments it can be concluded that the different reactors, bubble column or shaking flask, have no impact on the growth behaviour under the applied conditions.

For the actual dual substrate cultivations gassing with a 27 vol.% butane in air mixture at 300 mbar overpressure was applied. The resulting ODs as function of time are shown in Figure 6.8.

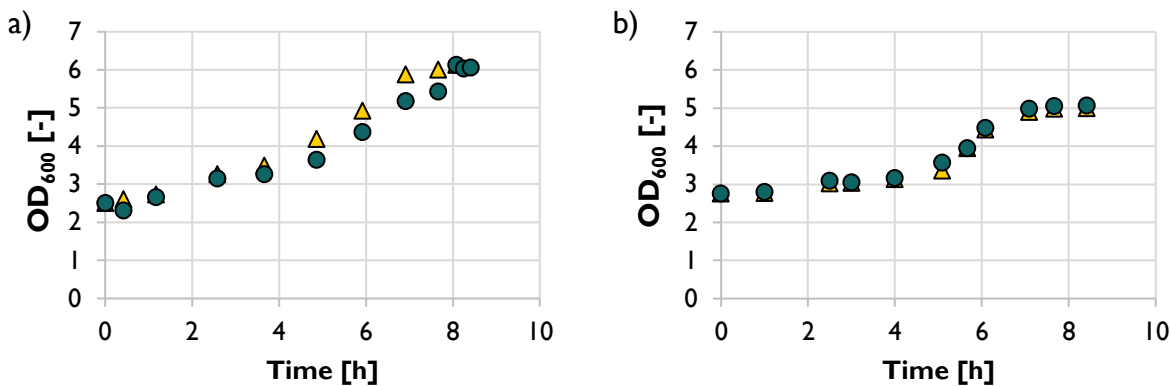


Figure 6.7: Control experiment for the dual substrate cultivation. OD in bubble column reactor (●) and shaking flask (▲) with butyric acid as single substrate. Reaction conditions: Temperature 30°C, Initial butyric acid dosage a) 20 mM b) 15 mM. Bubble column: 250 mL M9 medium, gassed with air at 0.2 L min⁻¹ and an over pressure of 300 mbar. Shaking flask: 50 mL M9 medium in 300 mL flask, shaken at 120 rpm.

The starting OD was chosen based on the previous observation that low initial ODs often showed a high lag phase, or no growth (data not shown) and the results gained from the activity test of the previous used *E. coli* strain (chapter 5.2). During the activity test, using the same conditions but a different medium, mass transfer limitation started to occur from an OD of 6 and higher. At higher ODs the liquid substrates, butanol or butyric acid, would quickly be consumed while not enough butane would reach the bacteria.

In all experiments the maximum OD was higher for the cultivations in the bubble column reactor. At the same time the growth rate stayed similar between the two applied reactors, except for the first experiment (Figure 6.8. a)), where a lag phase in the bubble column was observed. In all bubble column cultivations, no further growth after total depletion of the liquid substrates was measured. Which is in accordance with the initial statement, that no growth on butane as single carbon source could be detected. But as the maximum OD is higher in the bubble column reactor butane had

to be fixated. In this context this means, that butane is hydroxylated to butanol, further oxidized to butyric acid and then metabolised by the bacteria via the ato-system. Table 6.2 summarises the above-described experiments for the growth rates, the difference in maximum OD (OD_{max} , between bubble column and shaking flask) and the yield coefficient. For the latter, an apparent value (see eq. 23 in chapter 6.1.2) is used as the amount of butane which was fixated by the bacteria could not be measured directly. For the yield coefficient additionally the difference between the reactors is given as percentage. It has to be stressed that this difference is caused by the fixation of butane and not by biological differences between the cells in the different reactors.

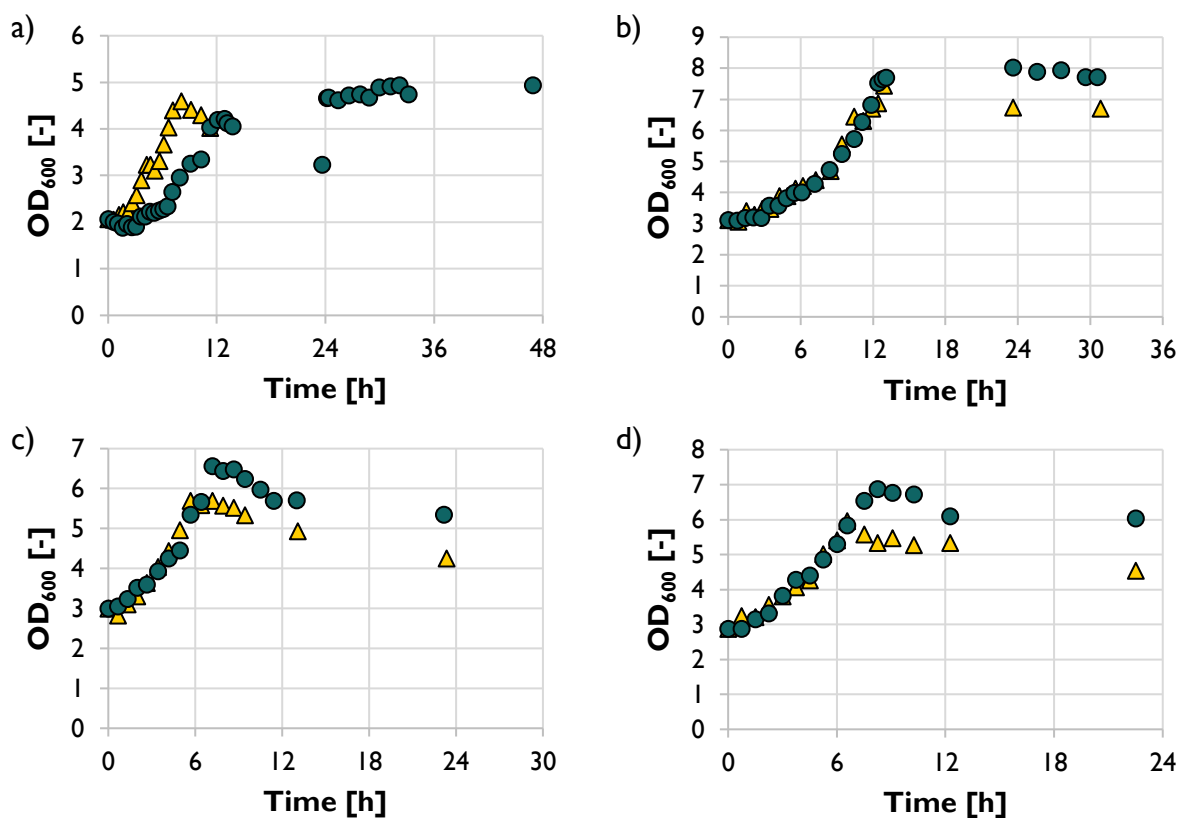


Figure 6.8: Cultivation in a bubble column (with butane, ●) and shaking flask (without butane, ▲). Constant reaction conditions: 30°C 200 mL, initial substrate dosage: a) 15 mM_{butyric acid} b) 15 mM_{butyric acid} + 10 mM_{butanol} c) 15 mM_{butyric acid} d) 10 mM_{butanol}. Bubble column: 250 mL M9 medium, gassed with a butane air mixture of 27 vol % at 0.2 L min⁻¹ and an over pressure of 300 mbar. Shaking flask (▲), 50 mL M9 medium in 300 mL flask, shaken at 120 rpm.

Table 6.2: Summary of the experimental data for the dual substrate cultivation.

Experiment (Figure 6.8)	μ [h ⁻¹]		Difference in OD _{max}	Y _{X/S, app.} [OD mM ⁻¹]		
	Shaking flask	Bubble column		Shaking flask	Bubble column	dif. [%]
I (a)	0.13	0.10	0.34	0.164	0.186	13.3
II (b)	0.10	0.09	0.58	0.168	0.190	13.4
III (c)	0.14	0.12	0.86	0.223	0.293	31.9
IV (d)	0.12	0.12	0.92	0.250	0.324	29.9

When the yield coefficient ($Y_{x/s,SF}$ [OD mM⁻¹]), that is calculated for the shaking flasks, is applied to the cultivations in the bubble column, the amount of fixated butane ($c_{butane,fixed}$ [mM]) can be estimated. For this, the difference in maximum OD between the bubble column ($OD_{max,BC}$ [-]) and shaking flask ($OD_{max,SF}$ [-]) is divided by the yield coefficient, see eq. 25.

$$c_{butane,fixed} = \frac{OD_{max,BC} - OD_{max,SF}}{Y_{x/s,SF}} \quad 25$$

The calculated fixated butane concentration, the average fixation rate, based on the time until maximum OD was reached, and a specific fixation rate, with the basis of the average OD, are summarised in Table 6.3. The fixation rate and specific fixation rate correspond to the \dot{Q}_P and activity used in the previous chapter, respectively. Additionally, the amount of fixed butane is related to the initial liquid substrate concentration. These values correspond to the increase in the yield coefficient from Table 6.3 and are shown for comprehensibility.

Table 6.3: Amount of fixated butane, the rate of fixation and the OD specific fixation rate for dual substrate cultivations.

Experiment (Figure 6.8)	c _{butane, fixed} [mM]	c _{butane, fixed} /c _{s,0} [%]	fixation rate [mM h ⁻¹]	spec. fixation rate [mM OD ⁻¹ h ⁻¹]
I (a)	2.1	13.3	0.06	0.02
II (b)	3.5	13.4	0.25	0.04
III (c)	3.9	31.9	0.45	0.09
IV (d)	3.7	29.9	0.51	0.11

Compared to the maximum activity of the alkBGT-system, which is around 0.45 mM OD⁻¹ h⁻¹ (see Chapter 5.2), the highest calculated specific fixation rate is significantly lower, 0.11 mM OD⁻¹ h⁻¹. As mentioned before, the average OD is used for

calculation. Even when the starting OD is used for calculation, the specific fixation rate is less than half of the observed maximum activity of the alkBGT system. Possible reasons are discussed collectively for the whole system in the next subchapter.

From the results shown in Table 6.2 and Table 6.3 differences between the first and last two experiments become visible. Especially the yield coefficient is important to note, as the later experiments exhibit significant higher values. For one when looking only at the results of the shaking flask experiments. But also, for the increased yield coefficient between shaking flask and bubble column. A possible reason for this is a difference in cell stock. The first two experiments were performed in December 2020 while the latter two in January 2021. As mentioned before, an active cell culture was maintained, as the initial activation of the bacteria is time consuming, see chapter 6.2. Consequently, for the time between the experiments, the bacteria were cultivated in shaking flasks and were frozen at -80°C during the Christmas break. A different conditioning of the cells is therefore likely. Furthermore, mutations during the repeated batch cultivations are possible. As the strain was provided by the Evonik Creavis sequencing and other DNA investigations were refrained.

6.3.1 Discussion of Cultivations with Butane

In this chapter the possible reasons for the lack of growth on butane as a sole substrate and possible future approaches are discussed.

A possibility which needs to be mentioned is the loss of the genetic information for the alkBGT system during the initial activation phase (chapter 6.2), e.g. by release of the corresponding plasmid. This can be excluded, as the *E. coli* repeatedly grew in fresh medium containing kanamycin as antibiotic, indicating the existence of the antibiotic resistance. Another indicator for the presence of the alkBGT system is the significant increased OD during the dual substrate cultivations, compared to the control. This proofs that some butane was fixated.

Additionally, the conditioning of the bacteria should be considered as a factor. As mentioned in the previous sub chapters, replicability was a challenge, e.g. only the results for the cultivations on butane derivatives at 30°C are shown as cultivation at 37°C showed inconsistencies. The growth rates differed by a factor of 10 (data not shown) between the cultivations and were not reproducible. To verify that during the bubble column experiment active cells were used the dual substrate cultivation was

applied. The bacteria were expected to grow on the liquid substrate and thereby show an active ato system. Afterwards a slower growth on butane as single substrate was anticipated. Nevertheless, as shown in Figure 6.8 this was not the case.

Another aspect of conditioning is the induction. As stated in the last chapter, the calculated activity of the alkBGT system during the dual substrate cultivation was significantly reduced compared to the maximum activity measured during the activity test (chapter 5.2). An insufficient induction could lead to a lower alkBGT activity and thus to a low rate of butane hydroxylation. The resulting supply of butyric acid could be too low to keep the maintenance metabolism or induce growth. But as the inductor, DCPK, was added in all cultivations (see chapter 3.3) and the alkBGT system is also induced by butane, no deficiency in the alkBGT system should exist. In further studies viability assays could be performed to determine if the bacteria in the bubble column reactor retain their viability longer when gassed with butane than with air. This would indicate an uptake of butane for maintenance. Alternatively, an (off-)gas analysis could be implemented. By measuring the butane in the feed and off gas, the butane uptake by the bacteria could be detected. As the calculated butane fixation rate (Table 6.3) is low during the cultivation, the measurement needs to be very sensitive to detect changes.

So far, the bacteria were seen as a black-box and discussion was focused on macroscopic effects, since this was the scope of this work. In the following the intracellular level is shortly addressed.

According to literature, see chapter 5.1.2, the alkBGT-system uses three NADH for the complete oxidation of one molecule butane to butyric acid. The ato-system converts one molecule of butyric acid net into one acetyl-CoA, one acetate and yielding an additional NADH, see chapter 6.1.1. In the TCA cycle one molecule of acetyl-CoA yields three NADH, one FADH and one ATP(GTP). Through the acetyl-CoA synthetase [74] the above-mentioned acetate can be converted to acetyl-CoA. This also enters the TCA, providing additional energy or a foundation for the anabolism. The metabolisation of acetate is proven by the lack of it's accumulation. In total seven NADH, three FADH and two ATP are provided, while only three NADH and two ATP are consumed. This surplus on energy should be enough to grow on butane as single substrate.

The examination of the intercellular NADH concentration, by internal flux analysis, could allow the investigation of this bias between theory and experimental results. Measurements over the course of a cultivation or during constant conditions, e.g. in a continuous bubble column experiment, can show the availability of NADH at different stages. During cultivation on butyric acid a higher NADH concentration is expected and parts of it would be used for the hydroxylation of butane. With depletion of butyric acid, with a higher apparent rate than the butane hydroxylation, the NADH concentration decreases. When this NADH is completely consumed for maintenance no further butane can be hydroxylated and the supply of butyric acid is stopped. By investigating the bacteria with only the alkBGT system, the NADH concentration during the different activities/glucose feed rates could be measured. A comparison of the NADH concentration could explain the lower activity for the alkBGT-ato bacteria.

6.4 Interim Summary

- The growth of a modified *E. coli* strain, containing the alkBGT and the ato-system, was investigated. As substrates butane, butanol, butyric acid and a combination of these were used.
- For the growth on butanol and butyric acid a maximum apparent growth rate of 0.13 h^{-1} and a substrate inhibition was found.
- For the use of butane as single carbon and energy source no growth was detected.
- In dual substrate cultivations, with butane and butyric acid or butanol, the activity of both systems (alkBGT and ato) could be shown.

7 Butane Hydroxylation by Unspecific Peroxygenase

In this chapter the hydroxylation of butane catalysed by an unspecific peroxygenase (*rAaeUPO*) is described. Parts of the results were already published by Perz et al. [36].

7.1 Introduction and Fundamentals

As described in chapter 5.1.1 the application of whole cell systems and free enzymes offer both advantages and disadvantages. In the regard of free enzymes the superfamily of cytochrome P450 monooxygenases is one of the most extensively studied enzymes for the oxyfunctionalisation of inactive C-H bonds. Despite their complex structure and need of NAD(P)H as cofactors, their capability for selective oxyfunctionalisation, especially in complex molecules, is of great interest. Screening and genetic engineering lead to the discovery of soluble, self-sufficient and/or single component enzymes, e.g P450 BM3. While the research mainly focused on fine chemicals and pharmaceuticals, where the product can cover the expenses, also P450 enzymes were discovered that perform the C-H activation for short chain alkanes. Nevertheless, the P450 catalysed hydroxylation of short chain alkanes did not exceed the analytical scale.

In recent years a new enzyme family, the unspecific peroxygenases (UPO), gained increased attention.[75] These enzymes can catalyse similar reactions as the P450 while only needing hydrogen peroxide (H_2O_2).[76] Compared to the expensive NAD(P)H, H_2O_2 can be easily and cheaply produced, also *in-situ* by electrochemistry from water and oxygen. For the oxyfunctionalisation of butane this has the additional benefit of needing no molecular oxygen in the feed gas, therefore pure butane can be applied. This improves the mass transport, which is the main challenge in the whole cell catalysed oxidation of butane to butyric acid (see chapter 5). Additionally, no butane air mixture needs to be prepared. This makes the preparation of the feed gas easier and in consequence safer.

Before the experimental results are described and discussed, the following subchapters will give a brief introduction into the UPO enzyme family and the fundamentals of enzyme kinetic.

In this chapter, unless otherwise stated, the volumetric productivity \dot{Q}_P [mol L⁻¹ h⁻¹] is defined as the formation rate of 2 butanol. The yield on H₂O₂ $Y_{H_2O_2}$ [%] is defined as the percentage of H₂O₂ that is converted to a measurable product (2-butanol and butanone). The active enzyme concentration c_E [mM] refers to the molar amount of enzyme as determined by the ABTS assay.

7.1.1 Unspecific Peroxygenase

As mentioned UPOs are, compared to the P450 monooxygenases which were discovered around 60 years ago [77], a recently emerging enzyme family. The first report of on a UPO was given by Ullrich et al. [78] in 2004. In this work a peroxidase (AaP) was isolated from *Agrocybe aegerita*, a bark mulch- and wood- colonizing basidiomycete. Because of its capability to utilise a variety of substrates it was later renamed to unspecific peroxidase. So far UPOs are exclusively found in fungi (excluding yeast).[76] Cultivation and especially downstream processing of *A. aegerita* is rather complicated. The main cause for this is the high protein content in the applied complex soy meal media. While different heterologous expression systems were found most suffered from low enzymes titres.[79] It took 10 years until Molina etc et al. [38] demonstrated in 2014 the heterologous expression of the so called AaeUPO-PaDa-I variant in *Saccharomyces cerevisiae*. This evolved mutant was also transferred in *Pichia pastoris*, an established expression host, which allowed protein titers of up to 200 mg L⁻¹. [39]

Besides its several applications [13, 80], the reaction mechanism of the UPO was investigated in recent years. [81] Figure 7.1 illustrates the catalytic cycle for the oxygenation as proposed by Wang et al.[82]. Additional the catalase reaction as well as the catalase malfunction pathway, as proposed by Karich et al. [83] are indicated. The active site of a UPO consists of a heme (Fe-protoporphyrin IX) with a cysteine-sulfur as the proximal ligand. A normal catalytic cycle starts with the activation of the resting state by H₂O₂, resulting in the formation of compound I. Depending on the substrate the activated enzyme can catalyses a oxygenation, as depicted, a oxidation or a halogenation. In the oxygenation a hydrogen atom of the organic substrate undergoes

a formal abstraction. In the process a substrate radical and the compound II are formed. By the so-called oxygen rebound the hydroxyl group is then transferred to the substrate resulting in the formation of the hydroxylated product. After this step the active centre returns to its resting state.

If instead of an organic substrate another H_2O_2 reaches the activated enzyme the catalase pathway is initialised. Again, compound II is formed but with a hydroperoxyl radical. Normally this results in the formation of molecular oxygen and water. But when a third H_2O_2 binds to the active centre, a hydroxyl radical is formed which results in the inactivation of the enzyme.

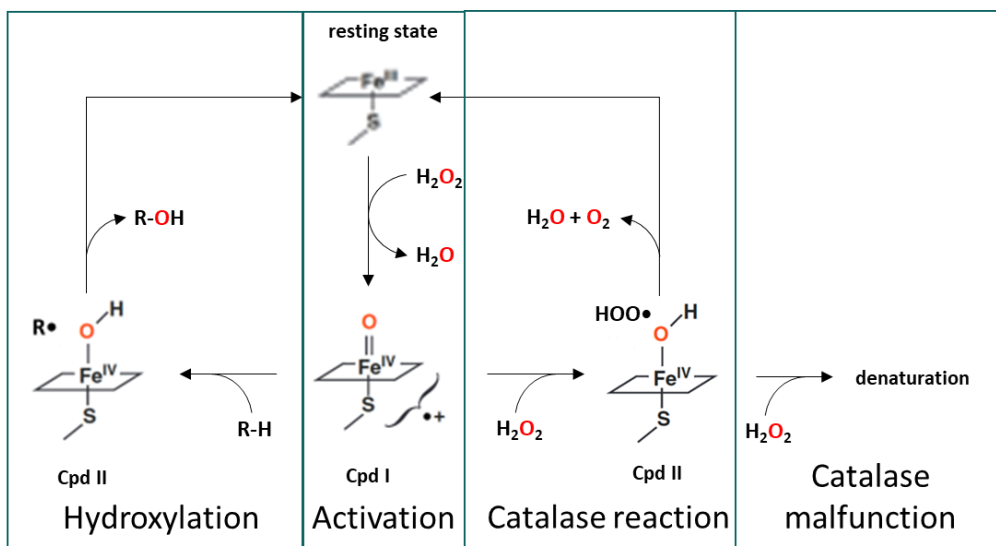


Figure 7.1: Simplified reaction mechanism of the UPO adapted from Hofrichter and Ullrich [81], including the catalase reaction and malfunction adapted from Karich et al. [83].

Use of UPO in this Work

Similarly, to the P450, investigation of the UPO focused on more complex hydrocarbons. Nevertheless, Peter et al. [84] demonstrated the conversion of short and medium chain alkanes (C3 to C8) by the UPO in analytical scale. While for higher alkanes, pentane and above, a mixture of 2- and 3-alcohols are formed, butane is hydroxylated to 2-butanol with a regioselectivity of 100% and an enantioselectivity of 30.8 ± 4.7 towards the (S) enantiomer.[84]

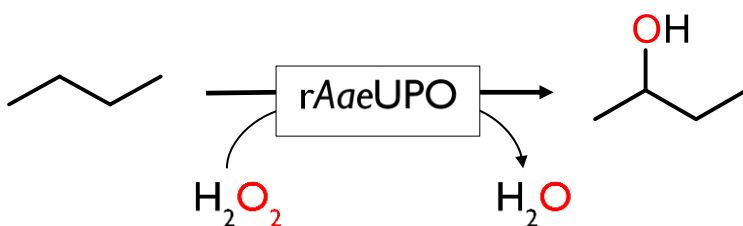


Figure 7.2: Reaction schema for the UPO catalyses hydroxylation of butane to 2-butanol using hydrogen peroxide as cosubstrate.

In this chapter the kinetics of this hydroxylation reaction are investigated as well as a transfer to the preparative scale conducted.

7.1.2 Enzyme Kinetic

The velocity of a chemical reaction is described by the reaction rate v [$\text{mmol L}^{-1} \text{s}^{-1}$]. For a simple, non-reversible, reaction where the substrate S is converted to the product P the reaction rate can be calculated by the change of concentration (dc_S or dc_P) over time dt (see eq. 26). In an ideal reaction, where the selectivity equals 1, the substrate decrease and product increase are inversely proportional which is described in the following equation.

$$v = -\frac{dc_S}{dt} = \frac{dc_P}{dt} \quad 26$$

In an enzymatic catalysed system, the enzyme E and substrate reversibly form an enzyme-substrate complex ES, which then can convert the substrate to the product (see eq. 27).



The time course for the individual concentrations is exemplified in Figure 7.3.a. After a brief initial phase, a pseudo steady-state (grey background) is reached for the enzyme-substrate complex and a constant reaction rate can be assumed: the initial reaction rate. As a rule of thumb, the constant reaction rate is assumed until a 10 % substrate conversion is reached. When the initial reaction rate is plotted over the starting substrate concentration, the enzyme kinetic becomes visible (see Figure 7.3.b). This kinetic can be described using the Michaelis-Menten-Equation (eq. 28) [85].

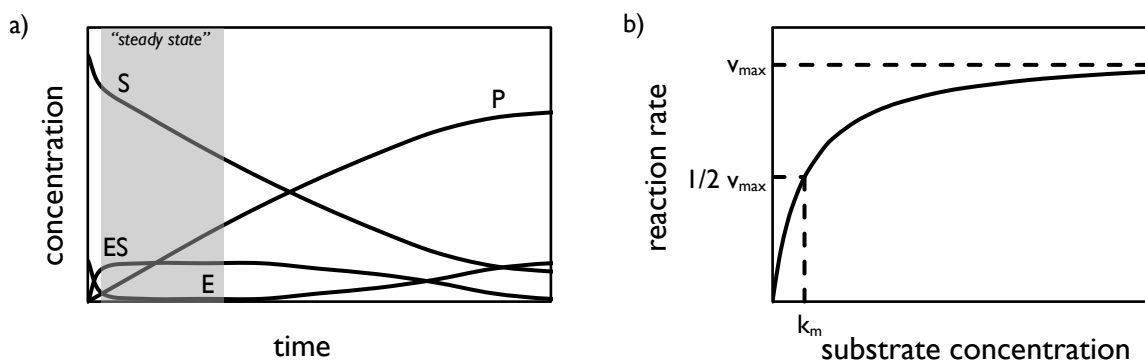


Figure 7.3: a) Schematic reaction progress of a simple enzymatic catalysed reaction. b) Visualisation of the dependency between reaction rate and substrate concentration for a simple Michaelis-Menten-Equation. E: enzyme, ES: enzyme-substrate complex, S: substrate, P: product.

$$v = v_{max} \cdot \frac{c_S}{c_S + K_M} \quad 28$$

The v_{max} [mmol L⁻¹ s⁻¹] represents the maximal possible reaction rate, which is achieved at high substrate concentrations. Under these conditions nearly all enzymes are saturated with substrate and the reaction rate is depending on the speed of conversion: The kinetic follows a zero-order reaction. The Michaelis constant K_M [mmol L⁻¹] indicates the substrate concentration at which the reaction rate is half v_{max} . For significant lower concentrations, a first order reaction can be assumed. A detailed derivation can be found in literature (e.g. Chmiel et al. [20]).

Depending on the concentration of active enzyme c_E [mmol L⁻¹] in an observed system, the value for v_{max} is changing. To enable comparisons an enzymes concentration independent variable, the catalytic constant k_{cat} [s⁻¹], is introduced. This constant describes the maximum number of reactions per time interval, which can be catalysed at the active site of an enzyme.

$$k_{cat} = \frac{v_{max}}{c_E} \quad 29$$

When eq. 29 is incorporated in eq. 28 a specific reaction rate, the turnover frequency TOF [s⁻¹], can be derived (eq. 30).

$$TOF = \frac{v}{c_E} = k_{cat} \cdot \frac{c_S}{c_S + K_M} \quad 30$$

Thereby the TOF describes the actual number of reactions that are catalysed by the enzyme under the applied conditions in a defined time.

The above-described equations are applied for simple one-substrate one-product reactions but can be extended for the use in a two-substrate reaction by multiplying with another substrate specific term (see eq. 31):

$$v = k_{cat} \cdot c_E \cdot \frac{c_{S,1}}{c_{S,1} + K_{M,1}} \cdot \frac{c_{S,2}}{c_{S,2} + K_{M,2}} \quad 31$$

7.2 Proof of Principle

The potential of the *AaeUPO* for the hydroxylation of butane in analytical scale was already demonstrated by Peter et al. [84], as mentioned before. Therefore, the transfer of this reaction to a preparative scale using a bubble column reactor was to be investigated in this work.

As the co-substrate, hydrogen peroxide, is known to inactivate the enzyme, especially at high concentrations[83], a feeding of H_2O_2 is advised. To estimate appropriate process conditions an experiment was performed, in which the H_2O_2 feed rate ($\dot{F}_{\text{H}_2\text{O}_2}$) was increased successively. In parallel the amount of active enzyme was measured regularly by an ABTS assay (see chapter 3.4.3), to follow enzyme deactivation. Figure 7.4 shows the resulting concentration profiles over the course of 4 hours, after which no more active enzyme could be measured. It is noteworthy, that the active enzyme concentration only started to decrease significantly at a H_2O_2 feed rate of 16 mM h^{-1} . For each individual H_2O_2 feed rate a constant \dot{Q}_P , the change in 2-butanol concentration over time, is measured.

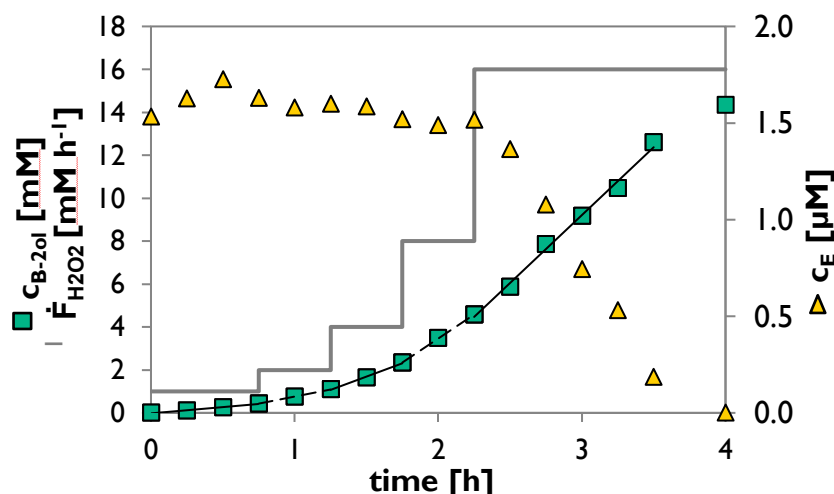


Figure 7.4: rAaeUPO catalysed butane oxidation with stepwise increase of hydrogen peroxide feed rate (—), ■ 2-butanol concentration and ▲ active enzyme concentration. Reaction conditions: Bubble column with 0.2 L KP_i-buffer (100 mM, pH 7), gassing of pure butane at 0.25 L min⁻¹, temperature 25 °C.

The impact of increasing H_2O_2 feed rates becomes visible when the \dot{Q}_P is plotted over the applied H_2O_2 feed rates (Figure 7.5.a). Except for the highest H_2O_2 feed rate, a linear increase in \dot{Q}_P with increasing H_2O_2 feed rates is observed. The highest H_2O_2 feed

rate yields a comparatively lower \dot{Q}_P . As at the same time the active enzyme concentration is decreasing, no sound conclusion to the cause can be made. Possible reasons are a limitation by the butane mass transport, the saturation of the UPO with H₂O₂ or overoxidation of the product. An indication for the overoxidation is the yield on H₂O₂ and TOF. The apparent yield on H₂O₂ ($Y_{H_2O_2,app}$, eq. 32) is the number of measured reactions divided by the amount of supplied H₂O₂. In this semi continuous system, this is the \dot{Q}_P divided by the H₂O₂ feed rate.

$$Y_{H_2O_2,app.} = \frac{\dot{Q}_P}{\dot{F}_{H_2O_2}} \cdot 100 \quad 32$$

The $Y_{H_2O_2,app.}$ for the different feed rates is shown in Figure 7.5.a. For the highest feed rate a decrease in yield of about 20% is measured, indicating parallel or subsequent reactions. Additionally, the TOF can be calculated and plotted over the enzyme specific H₂O₂ feed rate (eq. 33 and Figure 7.5.b).

$$\dot{F}_{H_2O_2,spez} = \frac{\dot{F}_{H_2O_2}}{c_E} \quad 33$$

For the lower feed rates, an average value was calculated (●). To account for the decrease in active enzyme concentration at the highest H₂O₂ feed rate a data pair of TOF and specific feed rate was calculated for each measuring point (◆). Even though the later points are not in line with the lower feed rates, a linear dependency of specific feed rate and TOF is visible, this shows that the enzyme is not saturated with H₂O₂.

Based on these results a differentiation for further investigations was made:
 Chapter 7.3 and 7.4 describe the kinetic characterisation and stability of the UPO, using low enzyme concentrations to prevent mass transport limitations. Whereas in chapter 7.5 higher UPO concentrations are applied to investigate the performance of the overall system.

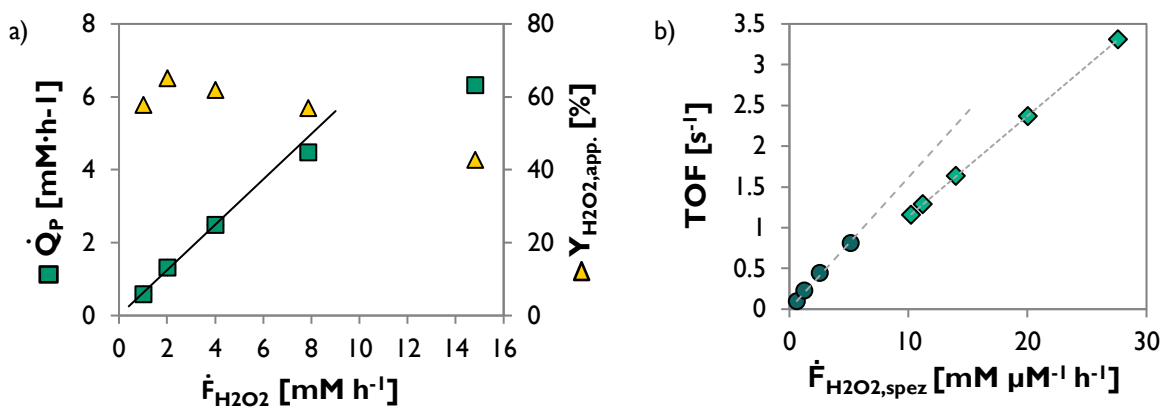


Figure 7.5: a) \dot{Q}_P (■) and H₂O₂-yield (▲) in dependency of the step wise increase in H₂O₂ feed rate, corrected for the volume change. b) TOF in dependency of the enzyme specific H₂O₂ feed rate. Data points at nearly constant active enzyme concentration and H₂O₂ feed rates below 8 mM h⁻¹ (●) and data points for decreasing active enzyme concentrations, a TOF calculated for every measurement point (◆).

7.3 Kinetic Characterisation of rAaeUPO

Kinetic characterisations can be performed in two ways: measuring the initial reaction rate or performing process curve analysis. In the former case, a constant reaction rate is assumed at the beginning of an experiment, while back reactions are neglected. To meet these conditions the conversion is generally kept below 5%. In the latter case the course of substrate and product concentrations is followed over a longer period, e.g. until steady state or depletion of catalyst. Afterwards the kinetic data can be derived by non-linear regression.

The hydroxylation of butane to 2-butanol is characterised using a modified initial rate measurement. To investigate the subsequent reaction, 2-butanol to butanone, process curve analysis was performed.

7.3.1 Kinetic for the Hydroxylation of Butane to 2-Butanol

As mentioned earlier, the maximal solubility of butane under standard conditions is low, around 1 mM [31]. At the same time, precise measurement of changes in this concentration range are quite challenging. To overcome this, the kinetic measurements were performed in the 0.2 L bubble column reactor (see chapter 3.2.2) at a constant gassing with butane. At a very low enzyme concentration, the reaction rate is only limited by the enzymes performance. The comparable high mass transfer results in a

constant butane concentration near maximal solubility. As the UPOs reaction mechanism (see chapter 7.1.1) does not allow back reactions the initial reaction rate stays constant until either significant amounts of enzyme are deactivated, or a subsequent reaction occurs (see Figure 7.6).

By changing the butane content in the feed gas, the partial pressure of butane can be influenced and thus, according to Henry's law (see chapter 1.2) the maximal solubility. Using the gas mixing station butane-nitrogen mixtures can be prepared and the investigated concentration range broadened. The maximum partial pressure to be applied is 1500 mbar, using pure butane and elevated pressure. Higher pressures are excluded because of safety considerations regarding the glass reactor.

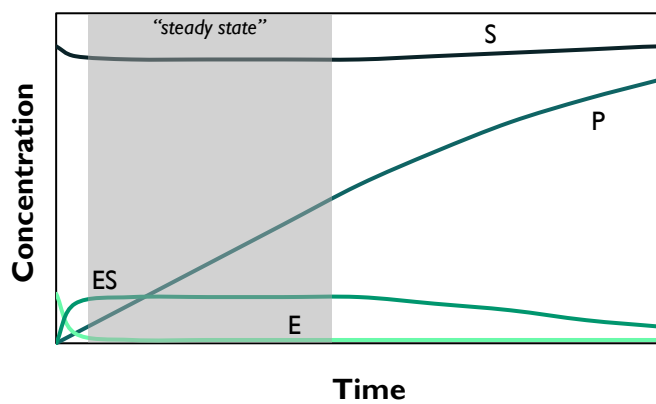


Figure 7.6: Visualisation of the concentrations profiles under constant supply of substrate and irreversible reaction. E: enzyme, ES: enzyme-substrate complex, S: substrate, P: product. Compare to Figure 7.3.

Providing a high H_2O_2 concentration at the start of the experiment would inactivate the enzyme. Changing H_2O_2 concentrations would also influence the reaction rate. In consequence H_2O_2 has to be fed to the reactor as well. Unfortunately, measurement of the H_2O_2 concentration was not possible. It is assumed that the feed and the simultaneously performed reaction will result in a steady state H_2O_2 concentration, simplified in eq. 34. This equation can be transformed, under the premise of a constant active enzyme concentration, into the dependency shown in eq. 35.

$$\frac{dc_{\text{H}_2\text{O}_2}}{dt} = \dot{F}_{\text{H}_2\text{O}_2,\text{in}} - v_i(c_{\text{H}_2\text{O}_2}) = 0 \quad 34$$

$$c_{H_2O_2} \sim \dot{F}_{H_2O_2,in}$$

35

To account for this changes eq. 31 (double substrate kinetic) has to be adjusted to describe the investigated reactions (see eq. 36):

$$v = k_{cat} \cdot c_E \cdot \frac{p_{butane}}{p_{butane} + K_{M, butane}} \cdot \frac{\dot{F}_{H_2O_2}}{\dot{F}_{H_2O_2} + K_{F, H_2O_2}} \quad 36$$

Here p_{butane} [mbar] describes the applied partial pressure of butane and $\dot{F}_{H_2O_2}$ [mmol L⁻¹ h⁻¹] the hydrogen peroxide feed rate. The constant K_{F, H_2O_2} [mmol L⁻¹ h⁻¹] can be defined similarly to a K_m value, as the H₂O₂ feed rate at which the reaction rate is half maximal.

Butane-dependent Kinetics

To investigate the butane kinetic independently from the hydrogen peroxide feed rate and to test the assumption of using the butane partial pressure instead of the concentration, a series of experiments with butane partial pressures from 60 to 1500 mbar and a constant, low H₂O₂ feed rate of 2.5 mM h⁻¹ were conducted. Over the course of one hour, a linear increase of the butanol concentration was measured for all experiments. At the same time the active enzyme concentration decreased in average to 86±7 %. For comparison, the TOF was calculated based on the starting amount of active enzyme.

Figure 7.7 (●) shows the TOF in respect to the applied partial pressures. As expected for a Michaelis-Menten kinetic the reaction rate is in the beginning proportionally increasing with butane partial pressure. Afterwards a saturation is reached. The obtained data were fitted (see red line - in Figure 7.7) using a single substrate equation and the script described in Appendix 11.3.1. The obtained kinetic parameters are listed in Table 7.1.

Table 7.1: Fitted kinetic parameters for the hydroxylation of butane by rAaeUPO at a constant hydrogen peroxide feed rate of 2.5 mM h⁻¹. Temperature 25°C, Medium of 100 mM KP_i at pH 7.

Parameter	Value	Unit	
k_{cat}	0.969 ± 0.065	s ⁻¹	± 6.7%
$K_{M, \text{butane}}$	80 ± 26	mbar	± 33%

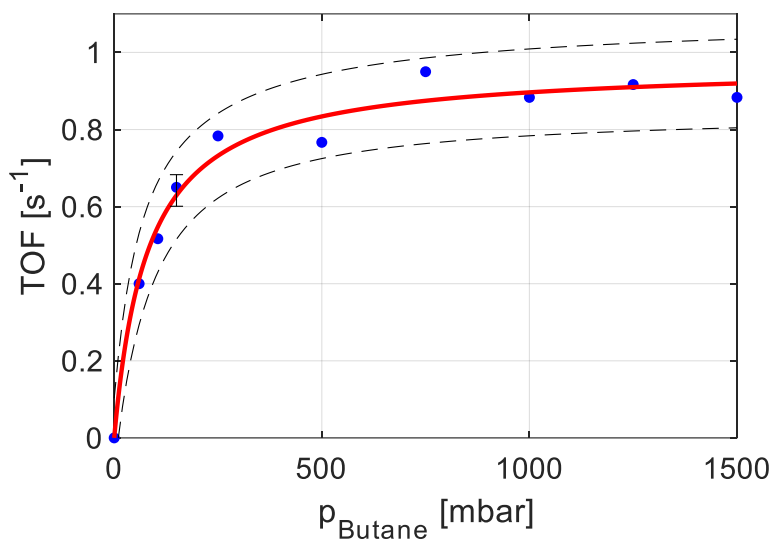


Figure 7.7: Measurement results (●) and Michaelis-Menten fit (-), including 95 % confidence interval (---), for the hydroxylation of butane by rAaeUPO. Reaction conditions: Bubble column with 0.2 L KP_i-buffer (100 mM, pH 7), gassing of butane nitrogen mixtures at 0.33 L min⁻¹ (0.5 Ln min⁻¹), total pressure 1500 mbar, temperature 25 °C, constant H₂O₂ feed rate of 2.5 mM h⁻¹, average starting enzyme concentration 0.582 ± 0.038 μM.

According to the Henry equation (eq. 2) a partial pressure of 80 mbar corresponds to a butane solubility of 0.088 mM. This low K_M value is beneficial for its application, as an increasing enzyme concentration will result in a lower dissolved butane concentration. The calculated k_{cat} (see Table 7.1) is low in comparison to the observed TOFs during the pre-study (up to 3 s⁻¹). This is a result of the use of a single substrate kinetic at low H₂O₂ feed rates. Therefore, the k_{cat} will be discussed within the double substrate kinetic later in this chapter.

To verify, that no transport limitation is measured at low butane partial pressures, the experiment at a butane partial pressure of 150 mbar was repeated with a reduced enzyme amount. Figure 7.8 compares the measured \dot{Q}_P , which is depending on the enzyme concentration, with the TOF, the concentration independent variable. While the \dot{Q}_P differs for the three experiments significantly, the TOF shows no significant differences. This confirms the assumption that mass transfer limitations can be neglected at the applied enzyme concentrations.

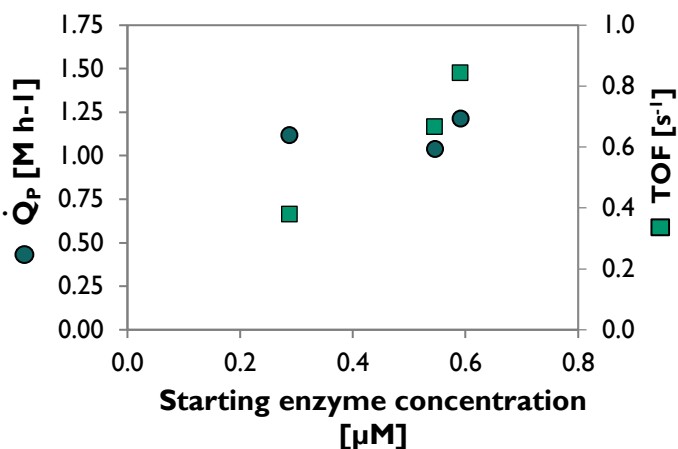


Figure 7.8: \dot{Q}_P (●) and corresponding TOF (■) at 150 mbar butane partial pressure and different enzyme concentrations. Reaction conditions: Bubble column with 0.2 L KP_i-buffer (100 mM, pH 7), gassing of 10 vol.% butane mixture with nitrogen at 0.33 L min⁻¹ (0.5 Ln min⁻¹), total pressure 1500 mbar, temperature 25 °C, constant H₂O₂ feed rate of 2.5 mM h⁻¹.

H₂O₂ Kinetics

Analogous to the butane single substrate kinetics, the impact of changing hydrogen peroxide feed rates was investigated. To realise this, the butane partial pressure was kept constant at 1500 mbar to avoid possible mass transfer limitations at high H₂O₂ feed rates. Based on the results in the pre-study (see chapter 7.2) the H₂O₂ feed rates from 1 to 20 mM h⁻¹ were investigated. For all applied feed rates a linear increase in Butanol concentration was observed, *i.e.* a constant \dot{Q}_P . At the highest H₂O₂ feed rates, 15 and 20 mM h⁻¹, a slight overoxidation of butanol to butanone was detected. The TOF was therefore calculated based on the total amount of hydroxylations detected, *i.e.* the change in 2-butanol and butanone concentration. For reference the starting enzyme concentration was used again. As depicted in Figure 7.9 a linear increase of the TOF with increasing H₂O₂ feed rates becomes visible. This indicates, that the H₂O₂ concentration inside the bubble column reactor stays on a low level, significantly lower than the K_M value and thus in the region of a first order kinetic. Due to the rapid enzyme deactivation no higher H₂O₂ feed rates were investigated.

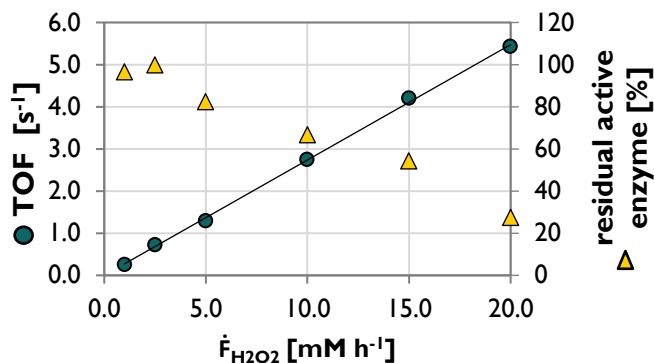


Figure 7.9: TOF (●) in dependency of the applied hydrogen peroxide feed rate and residual amount of active enzyme (▲) after 1 hour. TOF is calculated for linear region. Reaction conditions: Bubble column with 0.2 L KP_i-buffer (100 mM, pH 7), gassing of pure butane at 0.33 L min⁻¹ (0.5 Ln min⁻¹), total pressure 1500 mbar, temperature 25 °C, average starting enzyme concentration 0.603 ± 0.032 μM.

In contrast to the butane kinetic, the residual active enzyme concentration after 1 hour experimental time varies significantly. With increasing H₂O₂ feed rates the residual active enzyme concentration decreases almost linearly (Figure 7.9). It is important to note, that the \dot{Q}_P s were constant over the whole course of the experiments. This means, that the calculated TOFs does not change if only data up to a defined residual activity was used. For a detailed discussion about the stability of the enzyme, see chapter 7.4.

Double Substrate Kinetic

The previous shown data were combined with additional experiments, at varying butane partial pressure (150, 500, 750 and 1500 mbar) and increased H_2O_2 feed rate (15 mM h^{-1}), to calculate a double substrate kinetic. The TOFs in dependency of partial pressure and H_2O_2 feed rate for all experiments are shown in Figure 7.10 (●).

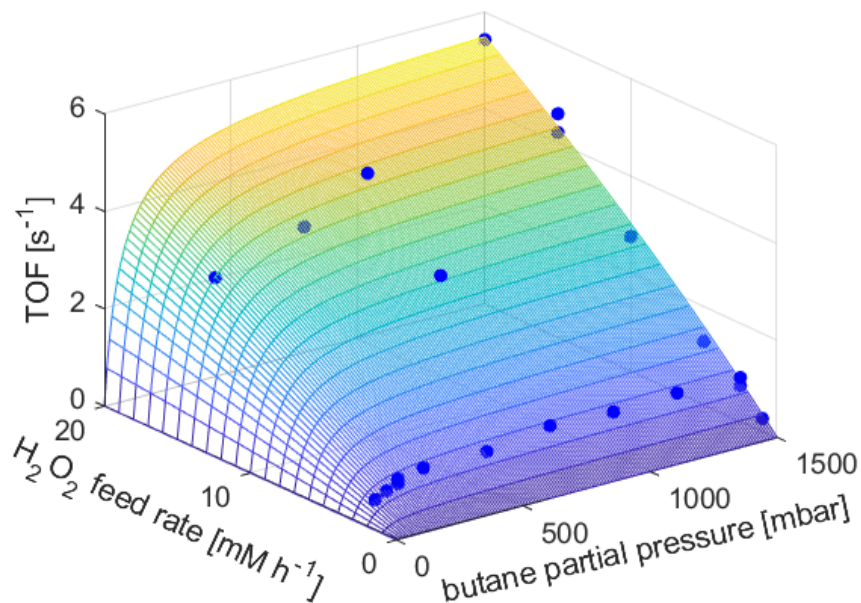


Figure 7.10: Experimental data (●) and fitted kinetic (surface) for the two substrate kinetic of the rAaeUPO catalysed hydroxylation of butane. Reaction conditions: Bubble column with 0.2 L KP_i-buffer (100 mM, pH 7), gassing of butane nitrogen mixtures at 0.33 L min^{-1} (0.5 Ln min^{-1}), total pressure 1500 mbar, temperature 25 °C, average starting enzyme concentration $0.590 \pm 0.033 \mu\text{M}$.

Again, slight overoxidation occurred at H_2O_2 feed rates above 10 mM h^{-1} (data not shown) and the amount of hydroxylation reactions, *i.e.* 2-butanol and butanone, were used to calculate the TOF. In all additional experiments, a linear increase in hydroxylations, *i.e.* \dot{Q}_P , was observed over the course of 1-hour experimental runtime. The only exception was the experiment at 150 mbar butane partial pressure and 15 mM h^{-1} . Here the \dot{Q}_P started to decrease after ~40 minutes due to enzyme deactivation. Hence, the \dot{Q}_P was determined only using the linear region, up to 40 minutes.

The experimental data were fitted using eq. 36 and the script described in Appendix 11.3.2. The result of the fitting is illustrated in Figure 7.10 (surface) and the determined kinetic parameter listed in Table 7.2. The RMSE was calculated to 0.17 s^{-1} .

The $K_{M, \text{butane}}$ is comparable to the previously estimated value and corresponds to a butane concentration of 0.072 mM. For the $K_{M, \text{H}_2\text{O}_2}$ a high variance ($\pm 87\%$) was calculated. This results from measuring in the first order kinetic region for hydrogen peroxide. In consequence, the k_{cat} value is estimated with a high error ($\pm 74\%$).

Table 7.2: Fitting results for the two-substrate kinetic of rAaeUPO catalysed hydroxylation of butane; with 95 % confidence interval as total values and percentage.

Parameter	Value	Unit	Variance
k_{cat} , butane	32 ± 24	s^{-1}	$\pm 74\%$
$K_{M, \text{butane}}$	65 ± 27	mbar	$\pm 42\%$
$K_{F, \text{H}_2\text{O}_2}$	92 ± 80	mM h^{-1}	$\pm 87\%$

From these results, it is obvious, that the hydrogen peroxide feed rate is the factor mainly regulating the reaction rate. It is important to note, that because of the changes to the applied Michaelis-Menten kinetic (use of partial pressure and H_2O_2 feed rate) these results reflect the UPOs performance only at the given experimental conditions. For the applied low enzyme concentration, a butane concentration around maximal solubility is assumed. At higher enzyme concentrations an equilibrium between mass transport, the butane transfer rate BTR, and reaction rate is reached, see Eq. 37 & 38.

$$\frac{dc_{\text{butane}}}{dt} = 0 = BTR - v \quad 37$$

$$k_{\text{cat}} \cdot c_E \cdot \frac{c_{\text{butane}}}{c_{\text{butane}} + K_{M, \text{butane}}} \cdot \frac{\dot{F}_{\text{H}_2\text{O}_2}}{\dot{F}_{\text{H}_2\text{O}_2} + K_{F, \text{H}_2\text{O}_2}} = k_L a \cdot (c_{\text{butane}}^* - c_{\text{butane}}) \quad 38$$

With an increased amount of enzyme, left side of eq. 38, the concentration gradient, right side of eq. 38, has to increase, resulting in a lower dissolved butane concentration. Hereby the TOF would decrease. In this respect, the low $k_{M, \text{butane}}$ will enable high TOFs when approaching mass transfer limited conditions. Likewise, a steady state concentration for hydrogen peroxide is assumed. Higher enzyme concentrations lead to lower hydrogen peroxide concentrations and thus lower TOF. To compensate the latter, an enzyme specific H_2O_2 feed rate can be used. For a precise determination of the kinetic parameter the measurement of the H_2O_2 concentration directly in the bubble column reactor would be needed. For a full enzymatic characterisation a higher H_2O_2 concentration, or feed rate, should be investigated as well. Here shorter

experiments with a higher number of samplings might enable measurements outside of the linear region. But as the full characterisation was not in the scope of this work and was therefore not pursued.

7.3.2 Kinetics for the Oxidation of 2-Butanol to Butanone

During the pre-study and the butane double substrate kinetic, overoxidation of the target product, 2-butanol, to butanone was suspected or observed, respectively. To quantify these, process curve analysis was performed. The advantage of process curve analysis is, that with a few experiments the kinetic can be estimated and at the same time subsequent reactions are revealed. The goal of this investigation was not a full enzyme characterisation with precise kinetic parameters but an estimation regarding the order of magnitude for the kinetics of the subsequent reaction.

For the analysis, the depletion of 2-butanol at two starting concentrations, 5 and 10 mM, and three different H_2O_2 feed rates, 2.5, 5 and 10 mM h^{-1} , was observed. Additionally, the active enzyme concentration as well as butanone concentration were measured. The results are shown in Figure 7.11 (single data points).

At the beginning of all experiments the 2-butanol concentration decreases linearly and butanone is formed. With decreasing 2-butanol concentration the reaction rate, 2-butanol to butanone, decreases. It becomes apparent, that the butanone reacts in a subsequent reaction, as the butanone concentration decreases again. Unfortunately, no additional peaks were detected in the GC measurements and the product of the butanone reaction could not be determined and quantified. It is noteworthy that active enzyme concentrations is decreasing linearly over the whole course of the experiment. When this enzyme deactivation rate $k_{\text{deact.}}$ is plotted against the H_2O_2 feed rate (see Figure 7.12) again a linear trend becomes visible, with increasing feed rates the deactivation rate increases. For calculation of a general deactivation rate the amount of data is deemed too low. In the following non-linear regression for determination of the kinetic data, the experimental determined deactivation rates were used. Additionally, specific H_2O_2 feed rates are calculated to account for the significant decrease in active enzyme concentration (see eq. 33).

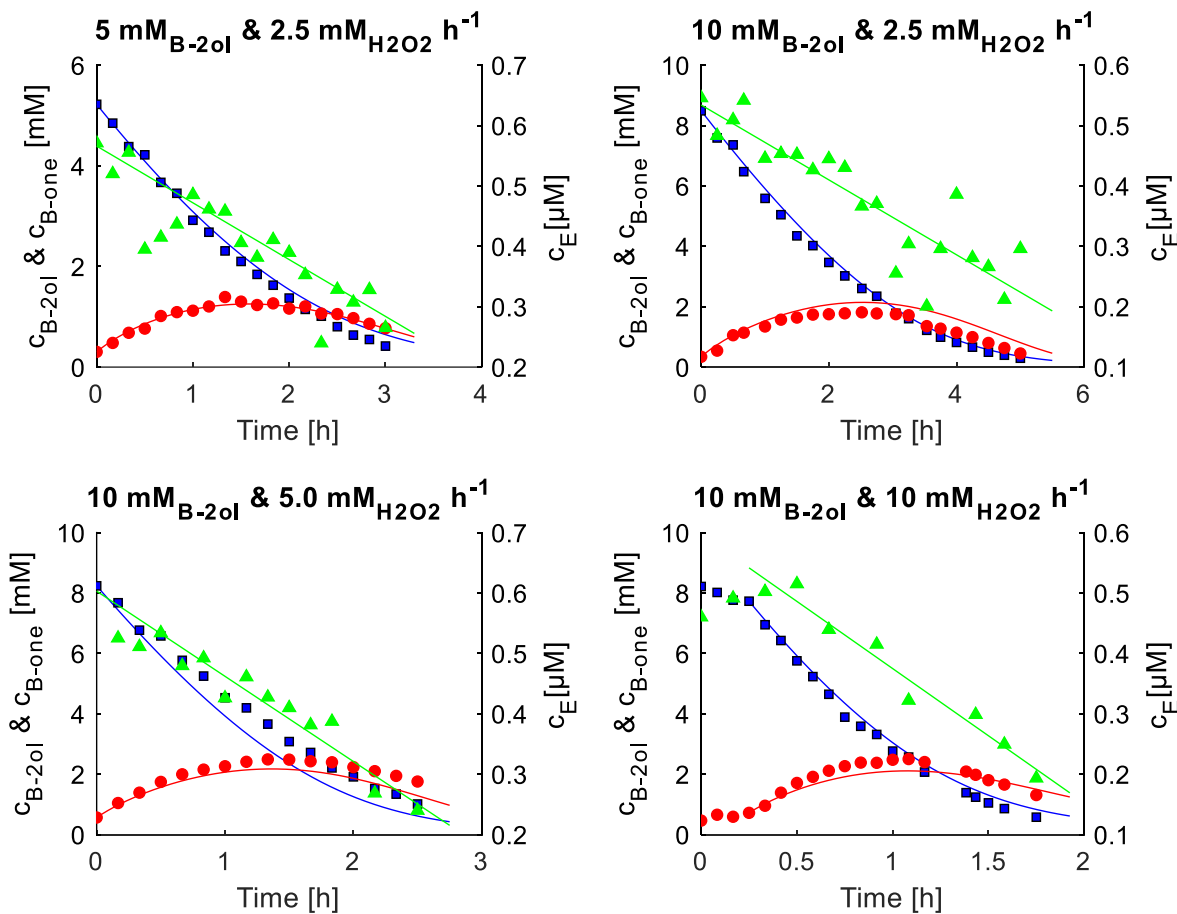


Figure 7.11: Measured (single data points) and simulated (lines) concentration for 2-butanol (blue), butanone (red) and active enzyme (green). Reaction conditions: Thermovessels with 0.05 L KP_i-buffer (100 mM, pH 7), temperature 25 °C, average starting enzyme concentration 0.540 ± 0.022 μM. Starting substrate concentration and applied H₂O₂ feed rates are depicted above the corresponding diagram. The start of the experiment with 10 mM and 10 mM h⁻¹ was delayed due to air bubbles in the feed tube.

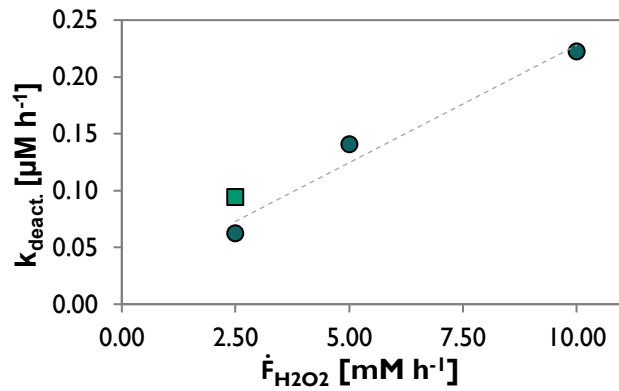


Figure 7.12: Enzyme deactivation rate during process curve analysis for 2-butanol starting concentrations of 5 (■) and 10 mM (●).

The kinetic parameters of the two observed reactions were estimated using the scripts given in Appendix 11.3.3. The kinetic expressions, double substrate Michaelis-Menten kinetics, for the oxidation of 2-butanol to butanone and the subsequent oxidation of butanone are given in eq. 39 and 40, respectively. Differential equations (dt [s] for 2-butanol [mM], butanone [mM] and the enzyme concentration [μM] are given in eq. 41-43. If needed, conversion of units was performed in the script. While the liquid organic substrates could be measured, again the H_2O_2 feed rate was used instead of the actual concentration.

$$v_{B-2ol} = k_{cat,B-2ol} \cdot c_E \cdot \frac{c_{B-2ol}}{c_{B-2ol} + K_{M,B-2ol}} \cdot \frac{\dot{F}_{H_2O_2,spez.}}{\dot{F}_{H_2O_2,spez.} + K_{F,H_2O_2,B-ol}} \quad 39$$

$$v_{B-one} = k_{cat,B-one} \cdot c_E \cdot \frac{c_{B-one}}{c_{B-one} + K_{M,B-one}} \cdot \frac{\dot{F}_{H_2O_2,spez.}}{\dot{F}_{H_2O_2,spez.} + K_{F,H_2O_2,B-one}} \quad 40$$

$$\frac{dc_{B-2ol}}{dt} = -v_{B-2ol} \quad 41$$

$$\frac{dc_{B-one}}{dt} = +v_{B-2ol} - v_{B-one} \quad 42$$

$$\frac{dc_E}{dt} = -k_{deact.} \quad 43$$

The six estimated kinetic parameters are summarised in Table 7.3, the errors are given as 95% confidence interval. The numerical solution of the differential equation systems is visualised in Figure 7.11 (lines).

Table 7.3: Results of the parameter fitting for the process curve analysis of the oxidation of 2-butanol to butanone and subsequent reactions. With 95 % confidence interval in absolute numbers and percentage.

Parameter	Value	Unit	Variance
$k_{cat, B-2ol}$	15.2 ± 2.9	s^{-1}	$\pm 19\%$
$K_M, B-2ol$	2.74 ± 0.79	mM	$\pm 29\%$
$K_F, H_2O_2, B-2ol$	33.9 ± 6.8	$\text{mM}_{H_2O_2} \mu\text{M}_{\text{enzyme}}^{-1} \text{h}^{-1}$	$\pm 20\%$
$k_{cat, B-one}$	7.9 ± 2.1	s^{-1}	$\pm 27\%$
$K_M, B-one$	1.07 ± 0.93	mM	$\pm 87\%$
$K_F, H_2O_2, B-one$	19.1 ± 5.9	$\text{mM}_{H_2O_2} \mu\text{M}_{\text{enzyme}}^{-1} \text{h}^{-1}$	$\pm 31\%$

Overall a good fitting with variances for most parameters below 30% was achieved. The applied 2-butanol concentration is up to a factor of 4 higher than the estimated $K_{M,B-2ol}$. This was beneficial for the fitting as the kinetic is calculated for a wide concentration range, *i.e.* high concentrations for the maximum reaction rate as well as the low concentration region with the transition to first order kinetic. In contrast the maximum reached butanone concentration is on the same level as the $K_{M,B-one}$, if the variance is included. This limited data result in the high variance of 87%.

Since the aim of this analysis was no in-depth reaction kinetic study of the liquid substrates, 2-butanol and butanone, but an estimation of the potential overoxidation of butane, no further studies were performed. The different kinetic measurements are compared and discussed in the next chapter.

7.3.3 Discussion of Kinetic Investigations

In the following two main aspects of the previously described results are to be discussed. For one the comparison of the estimated parameters and their impact on the hydroxylation of butane in a bubble column reactor. On the other hand, the assumptions made to calculate these parameters are discussed.

Comparison of the Kinetic Parameters

It is important to remember, that in the bubble column reactor butane is continuously gassed into the reaction media, thus a steady supply of butane is guaranteed. At the same time the reactions are limited by the supplied H_2O_2 . Hence, in a reactor with all organic substrates, *i.e.* butane, 2-butanol and butanone, present, the ratio of the different reaction rates depends on the individual kinetic parameters, K_m and k_{cat} , and the corresponding substrate concentration. For the comparison of the kinetic parameters the impact of H_2O_2 can be neglected. As described in chapter 7.1.1 the UPO is working in a ping pong mechanism. First H_2O_2 reacts with the active centre forming the “Compound I”. This activated enzyme catalyses in the following the oxidation of the organic substrate.

Table 7.4: Summary of determined kinetic parameter for the organic substrates

Species	$k_{cat,i} [s^{-1}]$	$K_M [\mu M]$
Butane	32 ± 24	0.072 ± 0.030
2-butanol	15.2 ± 2.9	2.74 ± 0.79
Butanone	7.9 ± 2.1	1.07 ± 0.93

Since the K_M values are low compared to the reached concentrations, a simplification is made. For all reactions the saturation with the organic substrate is assumed. Regarding the rate of overoxidation of 2-butanol, it is the worst case scenario. By this assumptions the kinetic equations are reduced to zero order and the selectivity can be derived as follows:

$$c_{B-2ol}(t, c_E) = (+k_{butane} - k_{B-2ol}) \cdot t \cdot c_E \quad 44$$

$$c_{B-one}(t, c_E) = (+k_{B-2ol} - k_{B-one}) \cdot t \cdot c_E \quad 45$$

$$c_{oxi.\ product.}(t, c_E) = +k_{B-one} \cdot t \cdot c_E \quad 46$$

$$k_i = k_{cat,i} \quad 47$$

$$S_i = \frac{c_i}{\sum_1^n c_j} = \frac{k_i}{\sum_1^n k_j} \quad 48$$

With the above made assumptions, which can be compared to a very long, not butane limited experiment, the selectivity for each species was calculated (see. Table 7.5). It becomes obvious that in such an experiment ~40 % of the 2-butanol are overoxidised. Usually, overoxidation would be reduced by optimising the experimental runtimes and thereby lowering final product concentrations. In the semi-continuous bubble column, an *in situ* product removal is advised. This would keep the 2-butanol concentration at a low level while fully utilising the enzyme.

Table 7.5: Selectivity for the rAaeUPO catalysed butane oxidation at infinite runtime and no mass transport limitation.

Species	Selectivity [%]
2-butanol	61.9
Butanone	18.3
Oxidised product	19.8

It has to be emphasised, that none mass transport limiting conditions are assumed. As already discussed (see. eq. 38), at higher enzyme concentrations the dissolved butane concentration can decrease and thereby the hydroxylation rate of butane. At the same time overoxidation rates stay the same resulting in a decreased 2-butanol selectivity.

Assumptions for Kinetic Investigation

Unfortunately, it is not meaningful to simulate the reaction sequence quantitatively. The reason for this are the assumptions that had to be made for the integration of the two substrates in the kinetic expression, as both concentrations could not be measured. For hydrogen peroxide a steady state concentration is assumed (see Eq. 34 in chapter 7.3.1). In this assumption only one reaction consuming H₂O₂ is included. While the effective H₂O₂ concentration might not change, when several parallel reactions occur, the reaction speed of the single reactions would differ. During the progress curve analysis this bias was accepted as the main focus of this work was the investigation of the butane hydroxylation and only an estimation was to be made for the overoxidation. For a thorough process optimisation the H₂O₂ concentration needs to be measured and the subsequent reactions characterised in detail. Besides the known reaction, also the unknown H₂O₂ consuming reactions need to be investigated. During the kinetic investigation of the butane hydroxylation the average H₂O₂ selectivity is calculated to be 60±11 %. While in some experiments slight overoxidation was observed, in the majority no 2-butanol or butanone was detected. It can be assumed that the UPO oxidises components present in the enzyme stock solution. Experiments with a purified enzyme could help to close the mass balance. Nonetheless, inline measurement of H₂O₂ is essential to generalise the kinetic.

While it should be possible to measure the H₂O₂ concentration with commercially available sensors, the measurement of the actual butane concentration remains a challenge. Because of the low concentrations applied, online process analytic technologies are challenged as well. Instead, Eq. 38 (page 90) can be utilised. For this the BTR needs to be calculated for a steady state by balancing the feed- and off-gas, e.g. measured by a micro-GC. In steady state the BTR is equal to the reaction rate and thereby it is possible to calculate the only missing variable, the dissolved butane concentration. Following this approach also the k_{la} value for the transfer of butane into the reaction media under the given process conditions can be calculated.

Regardless of these possible improvements, the established kinetic equation and parameters can be used for a non-mass transfer limited system.

7.4 Investigation of the Stability and TN of rAaeUPO

In comparison to the aforementioned TOF, the turnover number (TN [-]) describes the amount of catalytic cycles an enzyme can perform until its total denaturation, at given process conditions. The TN can be calculated by dividing the change in product or substrate concentration by the amount of enzyme, see eq. 49. To achieve a comparable TN it is important, that the enzyme is not limited by the amount of substrate or kinetic equilibria and the reactions are performed until all enzyme is denatured.

$$TN = \frac{c_{P,end} - c_{P,0}}{c_{E,0} - c_{e,end}} = \frac{c_{P,end}}{c_{E,0}} \quad 49$$

Rogers and Bommarius [86] showed that the TN can be estimated by the ratio of k_{cat} and $k_{deact.}$, the denaturation constant, if the denaturation follows a first-order kinetic. However, during the kinetic experiments the enzyme denaturation followed a zero-order kinetic, independent of its concentration the active enzyme concentration decreased linearly. As also the product formation rate was found to be constant until complete enzyme deactivation, an apparent TN is estimated using eq. 50.

$$TN_{app.} = \frac{\dot{Q}_P}{k_{deact.}} \quad 50$$

Here $k_{deact.}$ describes the rate of enzyme denaturation and \dot{Q}_P , as before, the product formation rate.

In Figure 7.13 the enzyme denaturation rates during the kinetic investigation, butane to 2-butanol, are shown in respect to the investigated parameter, H₂O₂ feed rate and butane partial pressure. Two trends become visible. With increasing butane partial pressure the denaturation is reduced. A higher butane pressure results in a higher butane concentration and thus increases the chance that an activated enzyme gets in contact with a butane molecule instead of a second and third H₂O₂, which would lead to the catalase or denaturation pathway, respectively (see chapter 7.1.1). The second trend is the increased denaturation with an increased H₂O₂ feed rate, which is to be expected. To put the denaturation in perspective with the achieved hydroxylation \dot{Q}_P , the TN_{app.} was calculated (see Figure 7.14).

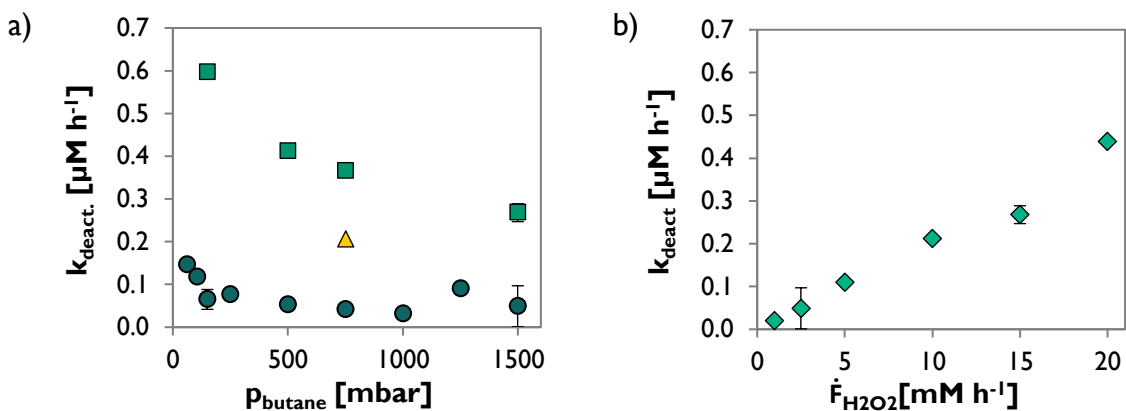


Figure 7.13: Enzyme deactivation rates during the kinetic study for the hydroxylation of butane. For duplicated data points an average was calculated. a) Denaturation in dependency of changing butane partial pressures with H₂O₂ feed rates of 2.5 (●), 10 (△) and 15 mM h⁻¹ (■). b) Denaturation in dependency on H₂O₂ feed rates at constant butane partial pressures of 1500 mbar (◆). Constant reaction conditions: Bubble column with 0.2 L KP_i-buffer (100 mM, pH 7), gassing of butane nitrogen mixtures at 0.33 L min⁻¹ (0.5 Ln min⁻¹), total pressure 1500 mbar, temperature 25 °C, average starting enzyme concentration 0.590 ± 0.033 μM.

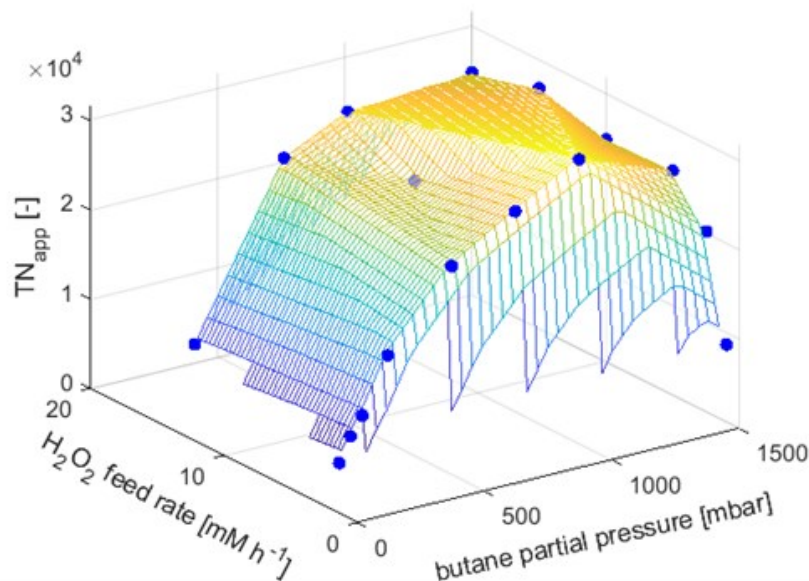


Figure 7.14: TN_{app} in dependency of the applied butane partial pressure and H₂O₂ feed rate. Linear interpolation. Constant reaction conditions: Bubble column with 0.2 L KP_i-buffer (100 mM, pH 7), gassing of butane nitrogen mixtures at 0.33 L min⁻¹ (0.5 Ln min⁻¹), total pressure 1500 mbar, temperature 25 °C, average starting enzyme concentration 0.590 ± 0.033 μM.

The high denaturation rates at low butane partial pressures combined with lower reaction rates result in an overall low TN_{app}. With increasing butane partial pressure a plateau is reached. In contrast to the increasing deactivation rate with increasing H₂O₂

feed rate, the TN first increases with H_2O_2 feed rate and then reaches the mentioned plateau of around 26000. This plateau of TN_{app} implies that the enzyme can only perform a certain amount of catalytic cycles, independent of the applied conditions. This phenomenon was already shown in previous works, with the UPO by Horst et al. [87] and Bormann et al. [88] as well as for the very similar P450 by Brummund et al. [89]. In these cases the enzymes reaches its maximum number of turnovers, the total turnover number TTN, before it is denatured by other factors. Lower TN are a result of additional denaturation, e.g. caused by H_2O_2 , temperature effects or the gassing induced shear stress.

Bormann et al. [88] determined a TTN through extrapolation of the TN for an infinite diluted H_2O_2 supply. Surprisingly the measured TN_{app} at the lowest H_2O_2 feed rate of 1 mM h^{-1} and 1500 mbar butane partial pressure is with 8655 one of the lowest. This can be explained by two factors. For one by the applied method. After one hour of experiment the residual activity is measured to be 96.6 %. Because of the low reaction rate, already small measuring errors for the active enzyme concentration result in huge deviations. Secondly, the used reactor. While the low reaction rate only slightly reduces the active enzyme concentration, the shearing which is induced by the gassing can denature the enzyme nonetheless. At higher H_2O_2 feed rate the loss of active enzyme concentration is likely dominated by the performed reactions.

To evaluate the used method for the determination of TN_{app} one experiment during the kinetic investigation of the butane hydroxylation was carried out until complete enzyme denaturation, at a H_2O_2 feed rate of 20 mM h^{-1} and a butane partial pressure of 1500 mbar. When the TN is calculated with eq. 49 a value of 22905 is measured, while with eq. 50 a TN_{app} of 25966 is achieved. This 13 % deviation can be explained with unnoticed overoxidations, especially during the end of the experiment at high organic substrate concentrations. Another factor might be the change in hydrodynamic conditions. With increasing product concentration pronounced foaming was observed which could increase enzyme denaturation. For the performed comparison the applied method was deemed acceptable.

7.5 Application of UPO for Synthesis

In contrast to the kinetic investigations, in which low enzyme concentration were applied, to rule out mass transport limitations, the following experiments were conducted with higher enzyme concentrations to achieve higher overall \dot{Q}_P and product concentrations. Thereby demonstrating the application of the UPO under process relevant conditions, first in a 0.2 L bubble column and later in a scale up to 2 L with *in situ* product removal by extraction.

7.5.1 0.2 L Bubble Column Reactor

In a first approach similar conditions as during the pre-study experiment were applied, but instead of a step wise increase a constant low H_2O_2 feed rate of 4 mM h^{-1} was used. Since during the application experiments changing enzyme concentrations were utilised, hydrogen peroxide feed rates are additionally given as specific feed rates, here the specific feed rate accounts for $\sim 2 \text{ mM H}_2\text{O}_2 \mu\text{M}_{\text{UPO}}^{-1} \text{ h}^{-1}$. The measured concentrations are shown in Figure 7.15 a). The concentration of 2-butanol increases linear for the first ~ 1.5 hours. The initial rate for the hydroxylation of butane is 2.7 mM h^{-1} . Afterwards the rate slightly decreases and overoxidation is detected. The amount of performed reactions, *i.e.* hydroxylation (butane to 2-butanol) and oxidation (2-butanol to butanone), is almost linearly increasing over the whole experiment, Figure 7.15 b). Similarly, the active enzyme concentration decreases linearly and is virtually zero after 6.5 hours. The slight decrease in 2-butanol concentration at the end of the experiment can be attributed to the dilution caused by the H_2O_2 feed, as the total amount of reactions stagnates. The yield on H_2O_2 is calculated to be around 70 % at the start of the experiment and is decreasing around the time of the first detection of overoxidation to around 60 %. At the end of the experiment H_2O_2 is still fed to the reactor but no active enzyme is present, therefore the yield decreases significantly. Overall a 2-butanol \dot{Q}_P , calculated for 6 h experiment, of 1.98 mM h^{-1} was determined, which when referred to the starting enzyme concentration corresponds to an apparent TOF_{app} of 0.25 s^{-1} . For TN two values are calculated. For one the TN for the performed hydroxylations, $\text{TN}_{\text{hyd.}} = 6004$, and a TN for the total overserved reactions: $\text{TN}_{\text{total}} = 6516$.

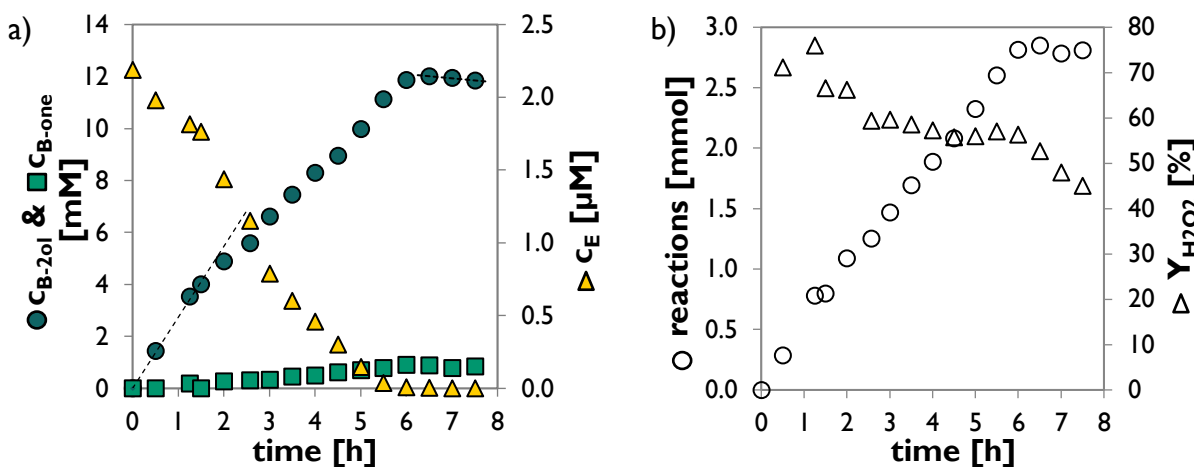


Figure 7.15: rAaeUPO catalysed hydroxylation of butane with a starting enzyme concentration of 2 μM . a) Measured concentrations of 2-butanol (●), butanone (■) and active enzyme (▲). b) Total amount of performed reactions (○) and yield on H_2O_2 (Δ). Reaction conditions: Bubble column with 0.2 L KP_i-buffer (100 mM, pH 7), gassing of pure butane at 0.35 L min⁻¹, temperature 25 °C, overpressure 100 mbar, hydrogen peroxide feed rate 4 mM h⁻¹ (~ 2 mM_{H2O2} $\mu\text{M}_{\text{UPO}}^{-1}$ h⁻¹).

To increase the \dot{Q}_P and product titre the enzyme concentration was increased 5-fold and the specific H_2O_2 feed rate 3-fold to ~6 mM_{H2O2} μM_{UPO} h⁻¹, resulting in a H_2O_2 feed rate of 60 mM h⁻¹. The measured concentrations are shown in Figure 7.16 a).

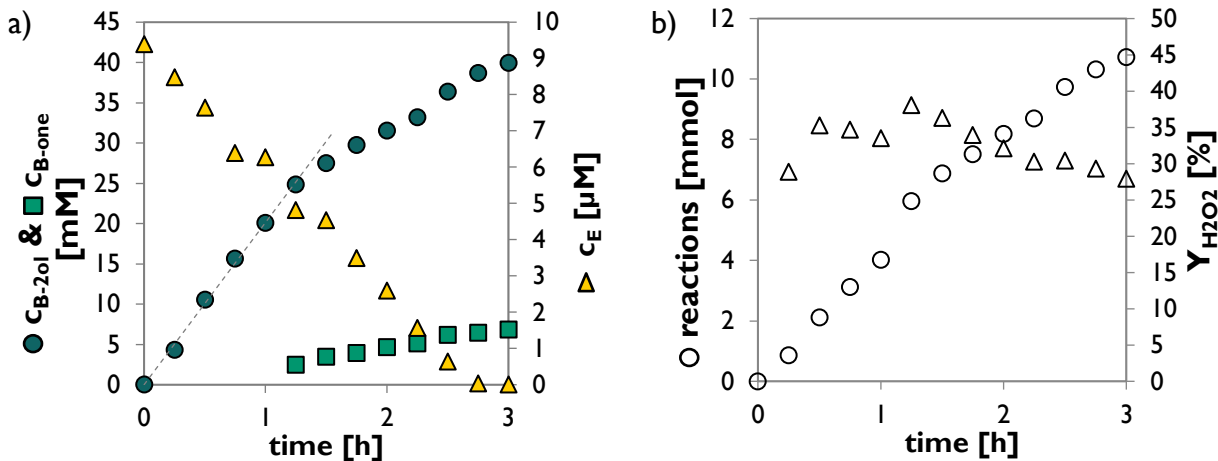


Figure 7.16: rAaeUPO catalysed oxidation of butane with a starting enzyme concentration of 10 μM . a) Measured concentrations of 2-butanol (●), butanone (■) and active enzyme (▲). b) Total amount of performed reactions (○) and yield on H_2O_2 (Δ). Reaction conditions: Bubble column with 0.2 L KP_i-buffer (100 mM, pH 7), gassing of pure butane at 0.35 L min⁻¹, temperature 25 °C, overpressure 100 mbar, hydrogen peroxide feed rate 60 mM h⁻¹ (~ 6.4 mM_{H2O2} $\mu\text{M}_{\text{UPO}}^{-1}$ h⁻¹).

The 2-butanol concentration increases linear at the start of the experiment before slightly slowing down after ~1.2 hours. The initial rate for the hydroxylation of butane is 20.1 mM h⁻¹. In contrast to the previous experiment the rate of the total amount of

performed reactions (Figure 7.16 b) is decreasing as well. Coupled with the steady decrease in yield on H_2O_2 for the second half of the experiment the subsequent oxidation of butanone can be assumed. Overall a 2-butanol \dot{Q}_P of 13.3 mM h^{-1} was determined. This amounts to a $\text{TOF}_{\text{app.}}$ of 0.39 s^{-1} when referred to the starting enzyme concentration. For $\text{TN}_{\text{hyd.}}$ and TN_{total} 4981 and 5710 were calculated, respectively.

Compared to the first experiment a significant higher \dot{Q}_P , ~7 fold, was achieved while the enzyme efficiency, measured in TN, is only slightly reduced (83-88%). However, the pronounced overoxidation reduces the apparent 2-butanol selectivity from 91.5% to 85.4%, or in other words nearly doubles the apparent butanone selectivity (8.5 % to 14.6%). The apparent selectivity is used as no quantification of further overoxidations can be made, nor the butane conversion determined. Nevertheless, the later conditions were considered worthwhile for scale up to preparative 2 L scale.

7.5.2 Scale up with *in situ* Product Removal

To reduce the product concentration in the reaction media and thereby counteract the overoxidation, the scale up was to be joined with an *in situ* product removal (ISPR). For this an extraction column was integrated in experimental setup using an external loop (Figure 3.5, chapter 3.2.2).

Solvent Selection

One of the UPO's strengths, its broad substrate scope, results in a drawback for ISPR by extraction as also many organic solvents can be oxidized by the UPO. For the selection of a suitable solvent the following criteria have to be considered: (I) The solvents capability to extract the desired product from the aqueous reaction media, this means a favourable partition coefficient towards 2-butanol. (II) The impact on the enzyme stability when in direct contact with the solvent. (III) The solvents likelihood to be used as a substrate, or as a simplified indicator, the solubility of the solvent in water. Unfortunately, the first and third criteria counteract each other to a certain degree, due to the hydrophilicity of 2-butanol.

To choose an appropriate solvent a selection of suitable organic solvents were tested regarding their apparent partition coefficient ($P_{\text{app.}}$) and their impact on enzyme stability (Table 7.6).

Table 7.6: Residual enzyme activity and apparent partition coefficient, $c_{2\text{-butanol,org}} / c_{2\text{-butanol,aq}}$, divided by $c_{2\text{-butanol,aq}}$, for cautious (inversion) and intensive mixing. Enzyme activity was determined by ABTS assay in triplicates.

Solvent	Inversion		Intensive mixing	
	Residual activity [%]	$P_{app.}$ [-]	Residual activity [%]	$P_{app.}$ [-]
Rapeseed oil	94	0.05	-	-
Dodecane	112	0.08	-	-
<i>p</i> -xylol	81	0.24	-	-
<i>n</i> -decanol	105	0.55	99	3.2

As no additional power input is applied in the extraction column a low contact area and time are to be expected. To simulate these conditions a simple mixing by inversion (5-times) was applied. Only *p*-xylol and *n*-decanol showed suitable apparent partition coefficients. Because *p*-xylol reduced the relative enzyme concentration already after the first contact and *n*-decanol showed a more than doubled partition coefficient, the later was chosen as solvent.

To estimate the impact of longer contact times the experiment was repeated with a more intense mixing, by vortexing for one minute. Even under these conditions no significant impact on the enzyme stability was observed. The apparent partition coefficient was calculated to 3.2. Additionally, the solubility of *n*-decanol in water (0.25 mM [90]) is significant lower than of butane (\approx 1 mM [31]), which reduces the changes of solvent oxidation.

Scale up

For scale up a bubble column reactor with an initial volume of 2 L was used. As scale up criteria the superficial gas velocity was used, thus the volume flow increases from 0.35 L min⁻¹ to 1.4 L min⁻¹. This corresponds to the reduction of the specific gassing rate from 1.75 VVM to 0.7 VVM. All other parameters were kept constant like in the previously shown experiment (see Figure 7.16). Additionally, a part of the reaction media is continuously withdrawn and pumped via peristaltic pump, at 3 L h⁻¹, in an extraction column. After dropping through a stationary *n*-decanol phase (200 mL), the raffinate is pumped back into the 2 L bubble column. After 2.5 h the organic phase was exchanged. The H₂O₂ concentration was measured online in front of the inlet to the extraction column. Until \sim 95 % enzyme deactivation (\sim 3.25 h) the measured H₂O₂

concentration was below detection limit ($<0.1\text{ mM}$). Figure 7.17 shows the measured concentrations in the organic (top) and aqueous (bottom) phase.

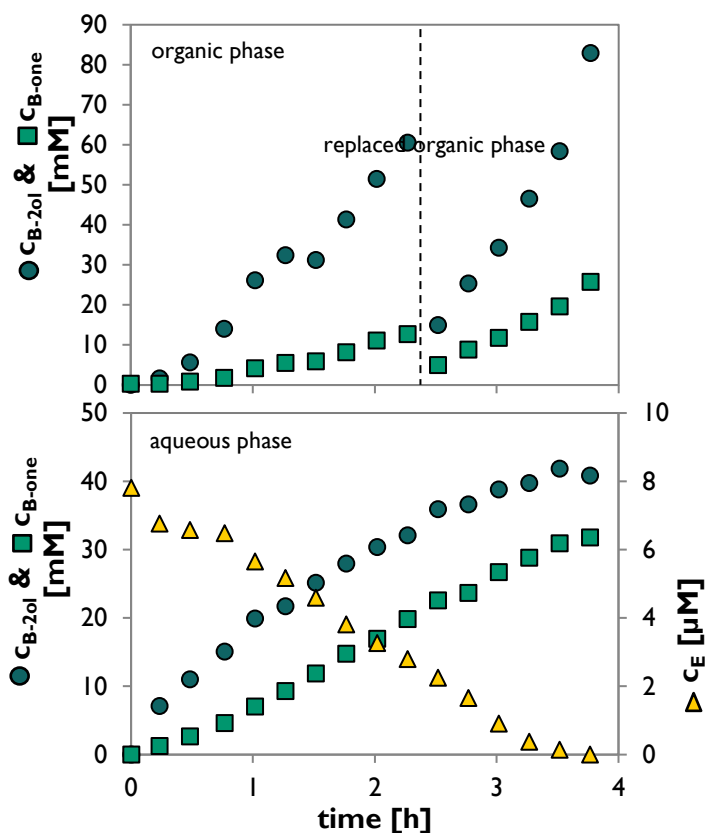


Figure 7.17: rAaeUPO catalysed oxidation of butane in 2 L scale with ISPR. Measured concentrations in organic (upper part) and aqueous phase (lower part) of 2-butanol (●), butanone (■) and active enzyme (▲). Reaction conditions: Bubble column with 2 L KP_i-buffer (100 mM, pH 7), gassing of pure butane at 1.4 L min⁻¹, temperature 25 °C, overpressure 0 mbar, hydrogen peroxide feed rate 60 mM h⁻¹ (~ 7.7 mM_{H2O2} $\mu\text{M}_{UPO}^{-1}\text{ h}^{-1}$).

Similar to the previous experiments the 2-butanol concentration starts to increase linearly. With a little delay the butanone concentration increases considerably as well. The initial rate for the hydroxylation of butane is 28.3 mM h⁻¹. When the sum of all detected reactions, organic and aqueous phase, is plotted over the time (Figure 7.18) it becomes visible that the linear trend is continued for the whole experiment. Only interrupted by the change of the organic solvent at 2.5 h. This also results in a drop of yield on H₂O₂, from an average of 52 % to 46 %. As before, the active enzyme concentration decreases in a linear fashion.

Overall a 2-butanol \dot{Q}_P of 14.3 mM h⁻¹ was determined. Additionally, a butanone \dot{Q}_P of 8.7 mM h⁻¹ is achieved. This amounts to a TOF_{app} of 0.51 s⁻¹ and 0.31 s⁻¹ when referred

to the starting enzyme concentration. For $TN_{hyd.}$ and TN_{total} 11811 and 16290 were calculated, respectively.

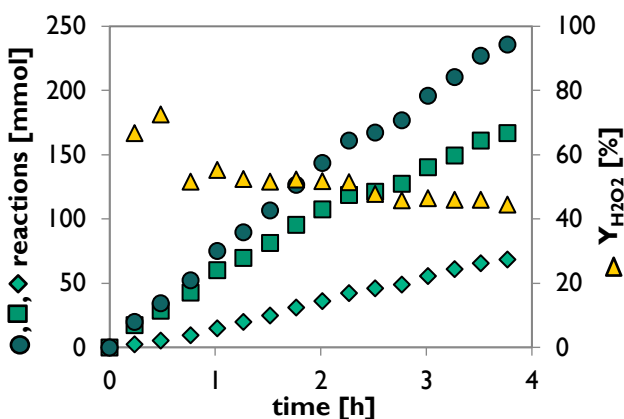


Figure 7.18: rAaeUPO catalysed oxidation of butane in 2 L scale with ISPR. Total amount of performed reactions (●), hydroxylations (butane to 2-butanol, ■), oxidations (2-butanol to butanone, ◆) and yield on H_2O_2 (▲). Reaction conditions: Bubble column with 2 L KP_i-buffer (100 mM, pH 7), gassing of pure butane at 1.4 L min⁻¹, temperature 25 °C, overpressure 0 mbar, hydrogen peroxide feed rate 60 mM h⁻¹ (~ 7.7 mM_{H2O2} µM_{UPO}⁻¹ h⁻¹).

While the aqueous 2-butanol concentration is comparable between the small scale and scale up, the overoxidation increases significantly. Resulting in an apparent 2-butanol selectivity of 62.1 %, about 20 % lower than in the small scale. This indicates a mass transfer limitation, which can be attributed to the reduced specific gassing rate and change in hydrodynamic properties, like less pronounced wall effects in the scale up. Further comparisons of these and previous results will be presented in the next section (Chapter 7.5.3).

The extraction performed well, as 2-butanol and butanone were continuously extracted. The apparent partition coefficients for 2-butanol and butanone at the end of the experiment are 2.35 and 0.9, respectively. This is lower compared to the solvent selection but was expected as no additional power input was applied. Because of the comparable low volume of the organic phase, in total 0.4 L *n*-decanol versus 2 L initial aqueous media, the 2-butanol fraction in the extract is only 27 % of the total 2-butanol. Further optimisations are necessary to improve the 2-butanol extraction performance and thereby reducing the overoxidation. On the instrument side two factors should be addressed. For one the contact time and the intensity of the mixing of the two phases thereby increasing the extraction speed, e.g. by dispersion with a stirrer or pumping

the aqueous phase through a sintered frit. For another the volume or exchange of the organic phase, *i.e.* using a larger extraction column or a continuous extraction. The increased concentration gradient would also increase the extraction speed.

Additionally, the solvent itself can be optimised. For this a detailed screening according to the aforementioned factors has to be conducted.

7.5.3 Comparison of the UPO Application

For a better comparison of the described experiments, Table 7.7 summarizes the achieved TOF and TN, which are recalculated for the individual reactions, *i.e.* hydroxylation of butane to 2-butanol and the oxidation of 2-butanol to butanone. The displayed TOFs describe the average reaction rate over the whole course of the experiment, normalised to the starting enzyme concentration.

Table 7.7: Summary of average TOF and TN for the three application experiments. Indexes: “hyd.” total amount of detected hydroxylations (2-butanol + butanone); “oxi.” total amount of detected oxidations (butanone); “total” all observed reactions (2-butanol + 2x butanone)

Scale [L]	H ₂ O ₂ [mM h ⁻¹]	TOF _{hyd.} [s ⁻¹]	TOF _{oxi.} [s ⁻¹]	TOF _{total} [s ⁻¹]	TN _{hyd.} [-]	TN _{oxi.} [-]	TN _{total} [-]	
0.2	4	0.27	0.02	0.30	6004	511	6516	Figure 7.15
0.2	60	0.46	0.08	0.53	4981	729	5710	Figure 7.16
2	60	0.82	0.31	1.13	11811	4479	16290	Figure 7.17

Comparison of the Three Experiments

The increase in TOF from the first to the second experiment, low and high enzyme concentrations, was discussed previously and is attributed to the higher specific H₂O₂ feed rate. At the same time the TN is only decreased slightly. This is within expectations as a higher H₂O₂ supply boosts the catalase and deactivation pathways of the enzyme. In addition a decreasing yield on H₂O₂ towards the end of the second experiment indicates further oxidations, which were proven during the process curve analysis (chapter 7.3.2). This subsequent reactions decrease the final concentrations of 2-butanol and butanone and thereby affect the TN calculation negatively.

Surprisingly, the average TOF doubles again for the scale up experiment. Ultimately, this is an effect from different enzyme deactivation rates. During both experiments a

constant decrease in active enzyme concentration was measured, $3.41 \mu\text{M h}^{-1}$ and $2.21 \mu\text{M h}^{-1}$ for the small scale and scale up, respectively. Because of this the UPO is longer active in the scale up, doubling the average $\text{TOF}_{\text{hyd.}}$ and $\text{TN}_{\text{hyd.}}$. Again further oxidations of butanone could not be quantified, therefore, the values above have to be considered as apparent.

As all other reaction conditions were kept constant, the explanation for the differences is suspected to originate from the applied scale up criteria. The constant superficial velocity changes the specific gassing rate (VVM). In the small scale the VVM is 2.5-fold higher than in the scale up. This higher specific gas throughput can cause more shear stress, thus increase enzyme deactivation rate. In addition the Reynolds number (Re) is changed during the scale up. While the properties of the media, *i.e.* density ρ and viscosity η , as well as the superficial gas velocity are kept constant, the characteristic length, the inner diameter of the bubble column, doubles (from 4 to 8 cm). Resulting in a doubled Re (see eq. 51).

$$\frac{Re_{2L}}{d_{2L}} = \frac{\rho \cdot v}{\eta} = \frac{Re_{0.2L}}{d_{0.2L}} = \frac{Re_{2L}}{2 \cdot d_{0.2L}} \quad 51$$

It is important to note, that a Re for the gas entering the bubble column is discussed. For investigation of mass transport phenomena the Re is usually calculated for single gas bubbles. The increased Re can lead to an improved mixing, shortening the mixing time in the scale up compared to the small scale. Which is a known phenomenon described in literature. [91] With an improved mixing the dispersion of H_2O_2 is enhanced and local hotspots, e.g. at the feed outlet, are reduced. In the end resulting in lower H_2O_2 driven enzyme denaturation. Lastly, a changed bubble size distributions, caused by the different conditions at the sparger, can affect enzyme denaturation.[61, 62] Further investigations of the above mentioned factors influencing the UPOs stability were outside of the scope of this work but should be performed in the future, see chapter 8.3.

Comparison on Basis of the TN

Compared to the maximum TN_{app} , up to 30000 (see chapter 7.4) which were measured during the kinetic investigation, the achieved TN during the application experiments is comparable low. However, also during the butane kinetic study TNs of or below 10000 were observed, at experiments with low butane partial pressures. At low butane concentrations, caused by low butane partial pressure or mass transport limitation, the probability of an activated enzyme to encounter another H_2O_2 -molecule and thereby enter the catalase/deactivation pathway, increases. Leading to a reduced TN.

An additional factor are the increased run times and product concentrations. Besides the previously mentioned not quantified overoxidations, the hydrodynamic properties inside the bubble column reactor are changing with rising product concentrations. This becomes visible when comparing the media, at the start and after one hour of experiment, see Figure 7.19 a) and b), respectively.

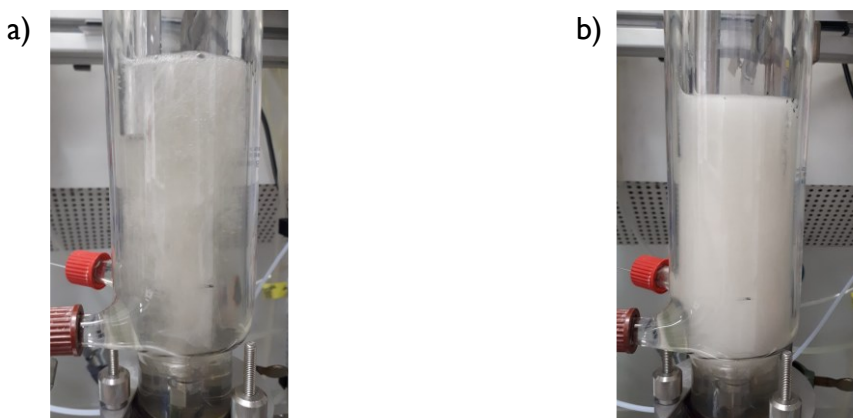


Figure 7.19: Pictures taken during the rAaeUPO catalysed oxidation of butane in the 0.2 L bubble column reactor: a) at the beginning of the experiment. b) after 1 hour of experiment.

Higher product concentrations reduce the surface tension and thereby changing the bubble size distribution and foaming behaviour. While the enzyme denaturation rate is nearly constant over the course of the whole experiment, slightly different rates can be measured at the beginning and end of the experiment, see Table 7.8.

Table 7.8: Enzyme deactivation rates during the initial and end phase as well as the average.

Experiment	Figure	Deactivation rate [$\mu\text{M h}^{-1}$]		
		Initial	End	Average
Small scale	Figure 7.16	3.3	3.9	3.4
Scale up	Figure 7.17	1.8	2.4	2.2

It has to be noted, that also the specific H_2O_2 feed rate increases with decreasing active enzyme concentration. The described change in denaturation rate could also be caused by this. Further investigations, including bubble size distribution measurement at various product concentrations and H_2O_2 caused denaturation in the absence of reactions, need to be performed to quantify these two effects.

Comparison Regarding the Kinetics

Additionally, the anticipated initial reaction rates based on the reactions conditions are calculated. Here the kinetic from chapter 7.3.1 was adapted to a H_2O_2 specific feed rate, to incorporate the change in applied enzymes. In Table 7.9 the measured initial reaction rates for the hydroxylation of butane are compared with calculated predictions. Only the initial rates are compared as the unspecific overoxidation could not be measured.

Table 7.9: Reactions conditions and corresponding TOFs as calculated based on double substrate Michalis-Menten kinetic and actual measurement. Indices: “esti.” Calculated using double substrate kinetic. “init,meas.” Initially measured at the start of the experiment.

Scale [L]	pbutane [mbar]	$C_{E,0}$ [μM]	H_2O_2 [mM h^{-1}]	Spec. H_2O_2 [$\text{mM } \mu\text{M}^{-1} \text{h}^{-1}$]	TOF _{esti.} [s^{-1}]	TOF _{init,meas.} [s^{-1}]	Dif. [%]
0.2	1110	2.2	4	1.8	0.35	0.34	2.9
0.2	1100	9.4	60	6.4	1.18	0.61	48.3
2	1000	7.8	60	7.7	1.41	1.00	29.1

While the initial reaction rate for the experiment with the low enzyme concentration can be simulated with a low error, this is not true for the two experiments with higher starting enzyme concentration. At higher enzyme concentrations the discussed mass transport limitation influences the kinetics, as described in chapter 7.3.1 . Instead eq. 36 (chapter 7.3.1) can be solved for p_{butane} , see eq. 52, which yields the pressure or,

if converted with the Henry's law, the butane concentration which has to be present in the media to reach the measured reaction rate.

$$\frac{k_{m,\text{butane}} \cdot v}{k_{\text{cat}} \cdot c_E \cdot \frac{\dot{F}_{H_2O_2}}{\dot{F}_{H_2O_2} + K_{F,H_2O_2}} - v} = p_{\text{butane}} \quad 52$$

This results for the small scale in a butane concentration of 0.063 mM (57 mbar) and for the scale up in 0.16 mM (146 mbar). The higher butane concentration in the scale up can be attributed to the lower enzyme concentration. While these calculation only attest the mass transport limitation, the methodology can, as briefly discussed in chapter 7.3.3, be used in the future to infer the k_{lA} value for butane according to eq. 53.

$$v = k_{\text{cat}} \cdot c_E \cdot \frac{p_{\text{butane}}}{p_{\text{butane}} + K_{M,\text{butane}}} \cdot \frac{c_{H_2O_2}}{c_{H_2O_2} + K_{M,H_2O_2}} = k_l a \cdot H \cdot (p_{\text{butane}}^* - p_{\text{butane}}) \quad 53$$

7.6 Interim Summary

- The hydroxylation of butane to 2-butanol by the unspecific peroxygenase AaeUPO in two bubble column setups was established and investigated.
- Kinetic parameters were calculated using a modified double substrate Michaelis-Menten kinetic. Experiments were performed in the manner of an initial rate measurement, modified for the applied reaction system.
- Kinetic parameters for subsequent reactions were estimated using progress curve analysis.
- A scale up with *in situ* product removal was performed to show the feasibility in preparative 2 L scale.
- Process optimisations and investigations of the enzyme stability are proposed.

8 Discussion and Outlook

The experimental results of the three investigated reactions systems have been discussed in the corresponding chapters. In this chapter the main results are shortly summarized, compared with existing literature, and discussed in a broader context. In addition, possible future work is proposed. In the end, the alkBGT whole cell system (without the ato system) and the free enzyme (UPO) are compared and a final recommendation for further studies is made.

8.1 Whole Cell Catalysed Oxidation of Butane to Butyric Acid

Summary

The detailed investigation of the mass transfer limited butane oxidation catalysed by the alkBGT enzyme system (heterologously expressed in *E. coli*) was the focus of this chapter. Thereby continuing the research from the predecessor [35] at the institute of Technical Biocatalysis.

An activity test was implemented in a scaled down (from 2 L to 0.2 L) bubble column reactor. This made determination of the cell activity for each fermentation possible, which was normally around 0.4 to 0.45 mM h⁻¹ OD⁻¹. Additionally, the specific glucose feed rate, which is needed to achieve maximum activity, was determined as 45-50 mgGlucose L⁻¹ h⁻¹ OD⁻¹.

By optimising the anti-foam feed rate in the 2 L bubble column reactor, application of a butane content in the feed gas of up to 40 vol.% was made possible. At the same time an increasing \dot{Q}_P with increasing butane content was measured.

Using the method Design of Experiment a process window for the butane hydroxylation was determined. The input parameters were: the butane content in the feed gas, overpressure and the gassing rate. With this multivariable analysis the maximum \dot{Q}_P (11.62 ± 0.76 mM h⁻¹) was determined to be at 500 mbar, 1.5 L min⁻¹ and 35.5 vol.% butane. These are the highest possible conditions regarding the overpressure and the gassing rate. Higher values are prohibited by the design of the

reactor setup.

Lastly the effect of three mass transfer vectors, MgSO₄, n-dodecane and Desmopan® DP9730A, was investigated. An increase in \dot{Q}_P between 5 and 15 % could be observed.

Discussion

The scientific literature regarding the alkBGT system focuses on hydroxylation of longer chain alkanes, fatty acids or esters [92–97]. While the mass transfer of liquid alkanes into the aqueous media can also pose a challenge [98], direct comparison of these systems is unreasonable. The only reasonable comparison can be performed with the work previously (2015–2018) [34, 35] performed at the Institute of Technical Biocatalysis. In this work empirically determined values were used for the maximum bacterial activity and for the glucose demand. In the early phase of that project a specific activity of 0.4 mM OD⁻¹ h⁻¹ was estimated. While this is in good agreement to the activity determined in this work (batch-depending 0.4 to 0.45 mM h⁻¹ OD⁻¹), the activity was determined at a very high glucose feed rate. In subsequent experiments the glucose feed rate was reduced to ~40 mg_{glucose} L⁻¹ h⁻¹ OD⁻¹. According to the experiments performed in this work (chapter 5.2.3), a maximum activity of 0.31 ± 0.04 mM h⁻¹ OD⁻¹ is expected at this glucose feed rate. As normally a significant surplus of biomass is used, this did not influence the overall outcome of the previous works. Still, as shown for the influence of the gassing rate on the \dot{Q}_P in chapter 5.3.2, in some cases a different interpretation of the experimental results is required. Nevertheless, the knowledge about the specific activity, and especially the possibility to verify it for every fermentation is very beneficial. As it allows for future experiments to distinguish between mass transport and biological limitations.

As stated during the analysis of the DoE, direct comparison of the achieved \dot{Q}_P with previously reached \dot{Q}_P at specific conditions is not meaningful. The influence on the system by the optimization of the anti-foam feed rate and the change of the sinter stone was too great for this (see chapter 5.3). For the overall process the comparison of the process window is of greater interest. Especially, as one objective of this work was to broaden the process window and investigate reaction conditions which were prior to this unreachable. In Figure 8.1 the process window established in this work (chapter 5.4.4) is compared to the estimated process window during Sluyters work [35]. The latter was based on single parameters studies. It has to be noted that in the work of

Sluyter also lower gassing rates were applied, for comparison only the data with the same gassing rates are shown.

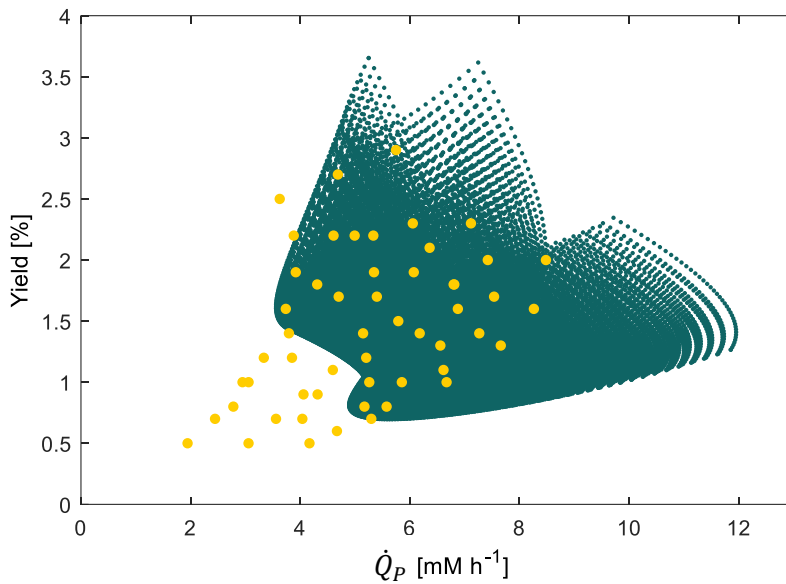


Figure 8.1: Comparison of the process windows for the oxidation of butane by the alkBGT system heterologously expressed in *E. coli*. \dot{Q}_P and yield on butane depending on all possible parameter combinations. For this work in 20 increments for each parameter (●): Gassing rate of 0.7 to 1.5 L min⁻¹, butane content of 14 to 40 vol.% and overpressure of 100 to 500 mbar. G. Sluyters work [35] (○) with fixed parameter values: gassing rates: 0.7, 1 and 1.5 L min⁻¹, butane content: 14, 17, 20, 23, 26, and 28 vol.%, and overpressure, 100, 300 and 500 mbar.

It is shown, that the two process windows overlap for major parts, as is to be expected. Because of the improved anti-foam dosage and the subsequently higher butane content higher \dot{Q}_P were achieved for the otherwise identical process conditions. With an increased \dot{Q}_P at the same reaction conditions the yield also increases. This difference is shown in the upper left part of the diagram, which is the area of low gassing rates, low butane content and low overpressure.

The area where the process windows do not overlap represent the former decreasing effect on the \dot{Q}_P at higher butane contents (see Figure 5.8). In this work higher butane contents were made possible. This leads to the enlargement of the process window shown on the bottom right side of the diagram.

Lastly a factor, that is not specifically visible in the process window has to be mentioned: In Sluyters work [35] the impact of increasing pressure was influenced by the butane content. At a low butane content an increasing overpressure significantly

increased the \dot{Q}_P . In contrast, at higher butane content the \dot{Q}_P only slightly increased with pressure. In fact, higher \dot{Q}_P were achieved at 14 vol.% and 500 mbar (5.7 mM h^{-1}), than at 20 vol.% and 500 mbar (4.7 mM h^{-1}).[35] These conflicting results were not observed in this work. Instead, an increasing pressure resulted in significant increase in \dot{Q}_P for all butane concentrations, see also Figure 5.10 c).

To summarise, the goal to enlarge the process window was achieved by utilising the GMS to investigate until before not feasible process conditions.

Future Work

Further investigations on this topic should focus on improving the mass transport. Based on the results presented in this work, two approaches seem feasible: further investigations of mass transfer vectors or the change of the reactor system.

In chapter 5.5 promising utilisations of mass transport vectors were presented, as an increase in \dot{Q}_P of up to 15 % was achieved in some experiments. A systematic investigation and optimisation was outside of the scope of this work, therefore further work is recommended. As the available literature [30, 99] focuses mainly on idealised pure water-vector systems, the systematic investigation of potentially four-phase systems (liquid-gas-cells-vector) in real reaction media would be an especially interesting field of research. Besides the experimental investigation on the impact of the vectors on the \dot{Q}_P under different reaction conditions, the impact of the vectors on the bubble size distribution should be investigated as well. This can help to better understand the operating principles of the different vectors. Lastly, the effect of reaction temperature, especially the interaction with the vectors, should be investigated. In literature [22] it is reported that higher temperatures increase the k_{LA} but decrease the maximum gas solubility, which yields a constant gas transfer rate. In contrast to the literature, the single parameter temperature investigation by Sluyter et al. [34] found increasing \dot{Q}_P with increasing temperature. As a mass transfer limitation system was observed, the \dot{Q}_P correlates directly to the gas transfer rate. Hence further investigations are advised.

With the completion of the process window investigation the characterisation of the 2 L bubble column reactor is finalised. In the current reactor setup, no higher pressures nor higher gassing rates can be realised. To further increase the mass transport, modifications to the reactor system can be made. Under the premise, that no moving

parts inside the reactor (see chapter 1.3) will be used, a change in aeration system or the use of a pressure stable reactor should be discussed.

So far, a sinter cylinder with an average pore size of 2 μm is used for the dispersion of the gas phase. Bubble size distribution measurements with similar gassing adapters, but other liquid systems, have shown, that with these kind of gassing adapters fine bubble aeration is viable [61, 62]. A systematic investigation of different gassing adapters (e.g. with 0.5 μm), preferable including bubble size distribution measurements, could enable higher gas transfer rates.

Furthermore, a complete change in aeration system is possible. Weber et al. [100] and Ughetti et al. [101] demonstrated for example the use of jet loop aeration during the fermentation of *E. coli*. Jet loop aeration offers gas transfer rates similar or better to those in stirred tank reactors while lower or same volumetric power inputs are applied.[101, 102] A drawback is the comparably high local shear stress in the pump and nozzle outlet. While during *E. coli* cultivation no drawback was found [100, 101], investigations for the impact on resting cells are needed.

Regarding a reactor capable of elevated pressures, the vapour pressure of butane is the limiting factor. At 20°C the vapour pressure of butane is ~2 bar, hence a maximum total pressure in the gas feed of 5 bar (assuming a butane content of 40 vol.%) would be possible. At higher pressures the butane would partially condensate in the tubing. In fact, also the application of liquid butane is possible. Staudt et al. [4] performed the hydroxylation of butane by a P450 at temperatures between -5 and 8°C. At these conditions the butane was present in liquid state. Similarly, the oxidation of longer chain alkanes by the alkBGT system [94, 98] is performed with an organic liquid phase. The liquid phase is thereby used as a substrate reservoir. In a pressure resistant reactor, the same principle could be applied for a whole cell catalysed butane oxidation. Additionally, the liquid butane might work as a mass transfer vector in respect to the oxygen transfer.

8.2 Utilisation of Butane as Energy- and Carbon-Source

The results presented in chapter 6 were already extensively discussed in the corresponding chapter (6.3.1). Suggestions for further work were proposed and discussed as well. Therefore, in the following only the summary of the chapter is given.

Summary

With the characterisation of the 2 L bubble column set-up complete, the investigated microorganism was changed. The goal was to perform the hydroxylation of butane without the need of supplying glucose as energy source. At the same time the butane should be used as energy- and carbon source. For this the ato system was added to the whole cell catalyst, which allows the *E. coli* cells to metabolise butyric acid as well. The new strain was again provided by Evonik Creavis. To examine the ato system and its cooperation with the alkBGT system, cultivations on butyric acid and butanol were performed, respectively. For both substrates a substrate inhibition was detected and a maximum apparent growth rate of 0.13 h^{-1} was determined. The maximum apparent growth rate was reached at concentrations of 17 mM and 12 mM, for butanol and butyric acid respectively.

When butane as single energy- and carbon source was used, no growth could be detected. Only in a dual substrate cultivation, with either butanol, butyric acid or a combination of these as co-substrate, butane was fixated. Equivalents of up to ~32 % of the initially applied liquid substrate (butanol and or butyric acid) were fixated during the experimental runtime.

The primary goal to perform the hydroxylation of butane without the demand for glucose was successfully shown. For the utilisation of butane as single energy- and carbon-source further research is needed, see also chapter 6.3.1.

8.3 Butane hydroxylation by Unspecific Peroxygenase

Summary

Starting from a cooperation with the DECHEMA's Research Institute and the TU Delft this work investigated the butane hydroxylation catalysed by a soluble enzyme, the unspecific peroxygenase (*AaeUPO*).

The feasibility of the reaction was demonstrated in a 0.2 L bubble column reactor and a stepwise increased H₂O₂ feed rate. Using a modified double substrate Michaelis-Menten-equation the kinetic parameters for the hydroxylation of butane to 2-butanol, the oxidation of 2-butanol to butanone and further overoxidation of the butanone were determined. As hydrogen peroxide concentration could not be measured inline, the feed rate was used in the Michaelis-Menten equation and steady state conditions were assumed. Table 8.1 summarises the important parameters for the different substrates.

Table 8.1: Summary of kinetic parameters regarding the organic substrate

Substrate	k _{cat, i} [s ⁻¹]	K _M [mM]
Butane	32 ± 24	0.072 ± 0.030
2-butanol	15.2 ± 2.9	2.74 ± 0.79
Butanone	7.9 ± 2.1	1.07 ± 0.93

Besides the kinetic, the turnover number for the hydroxylation of butane was investigated. The results indicate a plateau at which the TTN of ~26000 can be achieved.

While the kinetic investigations were performed at low enzyme concentrations, also higher enzyme concentrations were applied to study the overall process performance. In the 0.2 L scale an average and maximal butane hydroxylation rate of 15.6 mM h⁻¹ ($\dot{Q}_{P,avg,hyd.}$) and 20.1 mM h⁻¹ ($\dot{Q}_{P,max,hyd.}$) were measured. The applied conditions were used for a scale up to the 2 L scale, using the superficial gas velocity as scale up criteria. To counteract overoxidation of the 2-butanol to butanone a ISPR by liquid-liquid extraction was applied. An average and maximal butane hydroxylation rate of 23.0 mM h⁻¹ ($\dot{Q}_{P,avg,hyd.}$) and 28.3 mM h⁻¹ ($\dot{Q}_{P,max,hyd.}$) were measured.

Discussion

The experiments themselves were discussed in the corresponding chapters. Also, the assumptions made for the determination of the kinetic parameters were critically reviewed. In the following, the comparison to other UPO-systems will be discussed. Afterwards other alkane/butane hydroxylating enzyme systems are addressed.

In the years after the discovery of the UPO in 2004 by Ullrich [78] several reaction systems were investigated. In recent research, systems with impressive TN and k_{cat} were published. Depending on the system, a TN of several thousand are reported. [13, 80] For the hydroxylation of ethylbenzene even TNs of 400,000 [87] or above [103] are reported. At the same time, depending on the system, $k_{\text{cat}} \text{ [s}^{-1}\text{]}$ of several hundred are reported [81, 104], e.g. for the hydroxylation of ethylbenzene 410 s^{-1} [104]. Compared to these reports the herein found catalytic performance, TN of $<30,000$ and k_{cat} of $32 \pm 24 \text{ s}^{-1}$, is rather low. According to Wang et al. [82] and Peter [105] the cause for large differences in the catalytic performance of the UPO are the bond dissociation energies (BDE). These authors found a distinct nonlinear correlation between the rate limiting reaction step, the oxidation of the substrate, and the BDE of the oxidised bond. At low BDEs the reaction is not impacted by the BDE. But starting from BDEs of $\approx 90 \text{ kcal mol}^{-1}$, the reaction rate decreases drastically. For ethane, with a BDE of $\approx 101 \text{ kcal mol}^{-1}$ [106], Peter [105] postulates that it is the shortest alkane to be possibly hydroxylated. For reference the BDE of the C-H bonds of the two central butane carbon atoms is $\approx 98 \text{ kcal mol}^{-1}$ [107]. The BDE for the outer carbon atoms is slightly higher, which favours the reaction towards 2-butanol. Additionally, Bormann [8] discusses, that besides the reaction velocity the BDE also impacts the TN. This correlation must be kept in mind when comparing the benzylic hydroxylation of ethylbenzene (BDE $\approx 87 \text{ kcal mol}^{-1}$ [108]) and the hydroxylation of butane.

The only publication that can directly be compared to this work is the previously mentioned work of Peter et al. [84]. Unfortunately, no kinetic data is published. Only a TN of 1207 can be deduced, which is significantly lower than the herein reported values. Still two results of Peter et al.'s work are noteworthy and are confirmed in this work. For one the high (100 %) regioselectivity towards 2-butanol. Also, in the here presented work no 1-butanol was detected. Secondly, Peter reports an enantiomeric excess (ee) of $30.9 \pm 4.7 \%$ towards the (S) enantiomer. During the UPO application

experiments (chapter 7.5) two samples were externally analysed and an ee of 23.6 and 35 % was measured, which is well in line with the values of Peter et al.

In the introduction (chapter 1.1) enzyme systems, which are capable to oxyfunctionalise butane or short chain alkanes in general, are named. While none of these were tested in a preparative scale, for some kinetic data in analytical scale exist. In the following a selection of these are summarized and discussed for comparison to the above presented data of the UPO.

Some investigations originate from the analysis of pathways of butane degrading microorganism. One example is the kinetic investigation of the NADH depending soluble butane monooxygenase (sBMO) of the wild type (WT) *Thauera butanivorans* by Cooley et al. [109]. They report a k_{cat} of 0.6 s^{-1} and a K_m of $0.24 \mu\text{M}$ for the hydroxylation of butane. It should be noted that the reported K_m value is estimated via a competing reaction. Also, a selectivity of 80 % towards 1-butanol is observed.

Other groups focused directly on enzymes for the alkane hydroxylation. Glieder et al. applied a directed evolution approach [110] to the WT P450 BM-3 from *Bacillus megaterium* (P450_{BM3}). Besides other substrates also the hydroxylation of butane to 2-butanol was examined. The initial (2 s) consumption rate of NADPH was measured and a k_{cat} estimated: An increase from 0.28 s^{-1} to 30 s^{-1} was achieved, from the WT to the fifth generation (variant P450_{BM3,139-3}). In later publications by the working group of Arnolds the best mutant P450_{BM3,139-3} was further engineered and investigated by Peters [111]. In this work propane and octane were used as a substrate. Besides the consumption of NADPH also the product formation was measured (over 15 s). Only 9/22 % (propane/octane) of the consumed NADPH result in product formation. Resulting in specific reaction rates ($\approx k_{cat}$) of 0.2 s^{-1} and 8 s^{-1} for propane and octane, respectively. Additionally, total turnover numbers of 500/1000 (propane/octane) are reported. Based on the first publication (Glieder et al. [110]) the performance of the P450_{BM3,139-3} regarding the hydroxylation of butane should be in between. After a total of eight steps of genetic engineering, including several directed evolutions approaches and amino acid substitutions [112], a new P450 propane monooxygenase (P450_{PMO}) was established by the working group of Arnolds. Fasan et al. [113] generated two variants exhibiting high propane hydroxylation rates of 7.6 s^{-1} and 6.2 s^{-1} at TNs of 35600 respectively 45800. The product ration between 2-propanol and 1-propanol is

reported to be 9:1. Regarding other alkanes no product formation rates, only TNs are reported. For butane the total turnovers of the P450_{PMO} are reduced by more than 50 % to 15400. Activity, expressed in TN, towards all other tested alkanes (C2 to 10) is reduced by more than 90 %. [112]

Bell et al. applied genetic engineering via active site amino acid substitution on the P450_{cam} from *Pseudomonas putida*. This increased the product formation (\approx TOF or k_{cat}) from 0.007 s^{-1} to 12.6 s^{-1} . It must be noted that in these experiments a temperature of 30°C was applied, while all other described results were gained at 25°C . Again, no data regarding the stability is reported.

A major drawback of these reported systems is the use of expensive NADPH as cofactor and the uncoupling. The latter refers to a phenomenon in which the activated active centre unproductively decays and forms hydrogen peroxide, which can damage the enzyme. While high coupling efficiencies (>90 %) are reported [112], the use of catalase would be necessary in larger scale. Therefore, including a cofactor regeneration system, three enzymes would be needed to generate a bulk chemical, questioning overall feasibility.

In the recent research of Chen et al. [114] an artificial P450_{BM3} peroxygenase system was established. In this system a “dual functional small molecule” is used, which allows the conversion of small chain alkanes while using H₂O₂ instead of NADPH. Additional genetic engineering led to variants with a TN of up to ~ 2200 and a selectivity towards 2-butanol of $\sim 96\%$. Of most interest are product formation rates (\approx TOF or k_{cat}) of up to 18 s^{-1} (1 minute experiment at 25°C and 60 mM H₂O₂).[114]

When comparing the results of this work to these summarised results the huge potential of the UPOs becomes visible. The herein reported UPOs performance, regarding TN and product formation rate/ k_{cat} , is even in a preparative scale comparable or better than of various engineered P450 in analytical scale. Two factors make this especially noteworthy. For one as seen in the last example, product formation rates were investigated at a huge surplus (60 mM) of co-substrate (H₂O₂). In the herein presented work significant lower feed rates of H₂O₂ were applied and still comparable product formation rates were achieved. More importantly, the UPO used in this work is a non-optimised enzyme. The working group of Arnolds applied eight

steps of genetic engineering to achieve 100 times increase in TN for the P450_{PMO}, which is in the same order of magnitude of the herein reported UPO.

Future work

Besides the potential of genetic engineering, as demonstrated above for the P450, screening for other native UPO variants is a promising approach for further works. As described during the introduction of the UPO (chapter 7.1.1) the herein applied rAaeUPO variant is only the first to be expressed in significant amounts [115]. The variety of other UPOs should be investigated. In the context of the UPOs, this also includes the two groups of UPOs, which are differentiated by the length of the corresponding sequence (see chapter 7.1) After this screening, genetic engineering can be applied to further increase the enzymes performance. Special emphasis in screening and genetic engineering should also be placed on the enantioselectivity.

Parallel to providing other UPO variants, the process development should be promoted. Only if an enzyme performs under process relevant conditions, industrial application becomes viable. As discussed during the kinetic characterisation (chapter 7.3) the inline measurement of H₂O₂ could improve the determination of the kinetic parameters. The two major points for improvements are the enzyme stability and the overoxidation. Both points were discussed previously (chapter 7.4 and 7.5.2) and are summarized below. The main decrease in stability, besides the naturally limited number of turnovers, are most likely caused by gassing effects and the H₂O₂ feed. For a better understanding, systematic stability investigations coupled with bubble size distribution measurements are proposed. On the other hand a more dedicated ISPR would counteract the overoxidation. As described in chapter 7.5.2, e.g. a higher energy input to improve the dispersion of the aqueous phase in the extractant could be applied.

Further investigations of the UPO system will be pursued in a cooperation of the working groups of D. Holtmann and A. Liese. For this, screening for further variants as well as process development will be addressed in the upcoming DFG funded projected “Enzyme and reaction engineering of unspecific peroxygenase driven hydroxylation of butane (BUPOx)”.

8.4 Comparison

In this chapter the two systems which were investigated up to the 2 L scale are to be compared and discussed in respect to further potentials and scale up. I.e. the whole cell system with the alkBGT system and the UPO as free enzyme. The discussion will be focussing on three main parameters: the productivity, the butane yield and process stability. A summary of the corresponding results is given in Table 8.2.

Table 8.2: Summary and comparison of the alkBGT system (in *E. coli*) and the UPO (as free enzyme)

System	Whole cell alkBGT	Free enzyme UPO
Product	butyric acid	2-butanol (+butanone)
Co-substrate	oxygen & glucose	H_2O_2
Max. productivity*	12 mM h^{-1}	23 mM h^{-1}
Yield on butane*	1 – 4 %	1.5 %
Operation mode	“continuous”	“fed batch”
Process stability	$>19 \text{ h}^{**}$	$\text{TN}_{\max} = 23000 / 16000^{***}$
Challenges	mass transfer	stability & ISPR

* Based on total hydroxylations of butane in 2 L scale. ** Data not shown, see[35]: 19 h of reaction without decrease in \dot{Q}_P (2 L scale). *** measured in 0.2 L / 2 L scale

Productivity

When comparing the systems only in terms of \dot{Q}_P , it becomes clear that the isolated UPO (23 mM h^{-1}) is nearly twice as fast as the whole cell system (12 mM h^{-1}). The main limitation for the latter system is the mass transport. While pure butane can be used for the UPO, a mixture of air/oxygen and butane must be utilised for the whole cells. This leads to lower butane partial pressure and thereby to lower mass transport. Additionally, the salt concentration is higher in the whole cell system (see chapter 3.3.2). This reduces the maximum gas solubility and thereby the mass transport. Independently of the reactor scale or configuration, the maximum possible reaction rate will be higher for the UPO system.

Yield on butane

For both systems a comparably low yield on butane, the amount of product(s) per supplied butane, was measured. I.e. 1 to 4 % for the alkBGT system and 1.5 % in the UPO scale up experiment. This is mainly due to the low height of the reactor. In a scaled up bubble column, the residence time of the gas would be significantly increased. This

would lead to higher gas conversion. Nevertheless, a gas recycling system would be required for both systems in a scale up. In the case of the UPO a simple recycling of the off-gas is possible. After condensation of the entrained water the pure butane could be compressed and lead back into the reactor. By keeping the total pressure in the bubble column constant, the additional feed of butane could be regulated.

Recycling of the butane in the whole cell system requires more dedicated measures. The off-gas contains CO₂ from the cell metabolism and an undefined ration of butane and oxygen. Using gas measurement and a purge stream, the off-gas could be lead back into the reactor. Alternatively, as also suggested by Sluyter [35], the off-gas could be first compressed and then cooled until butane condensates. This condensate can then be evaporated and mixed with fresh air into the feed gas.

In consequence, with both systems a high yield (up to 100 %) is achievable.

Stability

Regarding the stability of the process, the whole cell system is favourable. In all experiments a constant product formation rate was measured. Even after >19 h of experiment no drop in \dot{Q}_P was measured, data shown in Slyuters works [35]. Further experiments could show at which butyric acid concentration or after which time the \dot{Q}_P decreases. Based on the currently available results, a continuous mode of operation should be possible. Either as continuous bubble column with cell retention or with an *ISPR*.

The UPO system on the other hand is limited by its TN_{max}, see also chapter 7.4. Additionally, the reaction conditions might deactivate the enzyme further. By genetic engineering the TN_{max} could be improved, and process optimisation could reduce the stress on the enzymes. Nevertheless, the enzymes will always be better protected in the whole cell system, which can also repair or reproduce the enzymes.

Conclusion

Both systems, the whole cell and the free enzyme, offer advantages and disadvantages. These are in accordance to the textbook statements and can be summarised as: Whole cell are in general more stable but need more supporting chemicals (glucose, oxygen) which can negatively impact the \dot{Q}_P . Free enzyme on the other hand only need their reactants, which enables high \dot{Q}_P but are more exposed to reaction conditions.

Lastly, it must be mentioned that the comparison is in parts unreasonable as different products are compared. The whole cell system is a model system producing an over oxidised product. While the UPO system performs the desired oxyfunctionalisation of butane as a single oxidation (or more specific hydroxylation). Overall, further process engineering should focus on the UPO system.

On the other hand, the potential of the whole cell system should not be neglected. With further research on butane as single carbon and energy source, back at the level of biochemistry and genetic engineering, the conversion of butane to a broad range of products can be made possible.

9 Summary

In this thesis three biocatalytic systems, which perform the selective oxyfunctionalisation of butane, were investigated in bubble column reactor setups. To supply the two used bubble column reactors (reaction volume of ~ 0.2 L and 2 L) with butane, first a gas mixing station (GMS) was constructed. This GMS allows for an arbitrary mixing of butane with air or nitrogen. The first investigated system was a whole cell approach, in which a modified *E. coli* strain, containing the AlkBGT system, was utilised. This model system performs the hydroxylation and subsequent over oxidation of butane to butyric acid. To clearly differentiate between mass transport and biological limitations an activity test for the applied bacteria was established. All experiments performed with this system were mass transport limited. To investigate the possible process window a Design of Experiment (Response Surface Methodology) was conducted. The input factors were gassing rate, over pressure, and butane content in the feed gas. The main responses were the volumetric productivity (\dot{Q}_P) and yield on butane. While the maximum possible values for over pressure and gassing rate were applied no clear optimum inside the design space could be determined. Nevertheless, the model can be used to navigate the design space to predict the responses. The maximum \dot{Q}_P is 12 mM h $^{-1}$. Through the application of mass transport vectors the mass transport and thereby \dot{Q}_P could be improved by up to 15 %.

The second system combines the AlkBGT enzyme system with the Ato system, the latter allowing the metabolism of butyric acid. The growth on butane, butanol and butyric acid was studied. For the growth on butanol and butyric acid a maximum apparent growth rate of 0.13 h $^{-1}$ and a substrate inhibition (K_I of 17 and 12 mM, respectively) was found. While no growth on pure butane could be detected, a dual substrate cultivation, butane with butyric acid and/or butanol, showed the fixation of butane by higher growth than a control without butane.

In the third system an unspecific peroxygenase (UPO) was applied as soluble enzyme. Here the application of this enzyme outside of analytical scale was demonstrated in 0.2 L scale. Kinetic parameters for the hydroxylation of butane to 2-butanol were determined under process relevant conditions. A first estimation of unwanted subsequent reactions were performed as well. This process was scaled up to 2 L scale, including an *in situ* product removal.

10 References

- [1] L. Soussan, N. Pen, M.-P. Belleville, J. S. Marcano, and D. Paolucci-Jeanjean, “Alkane biohydroxylation: Interests, constraints and future developments,” *Journal of biotechnology*, vol. 222, 2016, doi: 10.1016/j.jbiotec.2016.02.007.
- [2] E. Roduner, W. Kaim, B. Sarkar, V. B. Urlacher, J. Pleiss, R. Gläser, W.-D. Einicke, G. A. Sprenger, U. Beifuß, E. Klemm, C. Liebner, H. Hieronymus, S.-F. Hsu, B. Plietker, and S. Laschat, “Selective Catalytic Oxidation of C-H Bonds with Molecular Oxygen,” *ChemCatChem*, vol. 5, no. 1, 2013, doi: 10.1002/cctc.201200266.
- [3] W. Storhas, *Bioreaktoren und periphere Einrichtungen: Ein Leitfaden für die Hochschulausbildung, für Hersteller und Anwender*. Berlin: Springer, 2000.
- [4] S. Staudt, C. A. Müller, J. Marienhagen, C. Böing, S. Buchholz, U. Schwaneberg, and H. Gröger, “Biocatalytic hydroxylation of n-butane with in situ cofactor regeneration at low temperature and under normal pressure,” *Beilstein journal of organic chemistry*, vol. 8, 2012, doi: 10.3762/bjoc.8.20.
- [5] S. Chakrabarty, Y. Wang, J. C. Perkins, and A. R. H. Narayan, “Scalable biocatalytic C-H oxyfunctionalization reactions,” *Chemical Society reviews*, vol. 49, no. 22, 2020, doi: 10.1039/d0cs00440e.
- [6] J. Münch, P. Püllmann, W. Zhang, and M. J. Weissenborn, “Enzymatic Hydroxylations of sp³-Carbons,” *ACS Catal.*, vol. 11, no. 15, 2021, doi: 10.1021/acscatal.1c00759.
- [7] J. Dong, E. Fernández-Fueyo, F. Hollmann, C. E. Paul, M. Pesic, S. Schmidt, Y. Wang, S. Younes, and W. Zhang, “Biocatalytic Oxidation Reactions: A Chemist's Perspective,” *Angewandte Chemie (International ed. in English)*, vol. 57, no. 30, 2018, doi: 10.1002/anie.201800343.
- [8] S. Bormann, “Process engineering and heterologous enzyme production for hydrogen peroxide driven biocatalysis,” Dissertation, DECHEMA-Forschungsinstitut, Universität Kaiserslautern, 2021. [Online]. Available: www.shaker.de/shop/978-3-8440-7968-5
- [9] P. Tufvesson, J. Lima-Ramos, M. Nordblad, and J. M. Woodley, “Guidelines and Cost Analysis for Catalyst Production in Biocatalytic Processes,” *Org. Process Res. Dev.*, vol. 15, no. 1, 2011, doi: 10.1021/op1002165.

- [10] D. Balcells, E. Clot, and O. Eisenstein, “C-H bond activation in transition metal species from a computational perspective,” *Chemical reviews*, vol. 110, no. 2, 2010, doi: 10.1021/cr900315k.
- [11] M. Bordeaux, A. Galarneau, and J. Drone, “Catalytic, mild, and selective oxyfunctionalization of linear alkanes: current challenges,” *Angewandte Chemie (International ed. in English)*, vol. 51, no. 43, 2012, doi: 10.1002/anie.201203280.
- [12] A. Gunay and K. H. Theopold, “C-H bond activations by metal oxo compounds,” *Chemical reviews*, vol. 110, no. 2, 2010, doi: 10.1021/cr900269x.
- [13] S. Bormann, A. Gomez Baraibar, Y. Ni, D. Holtmann, and F. Hollmann, “Specific oxyfunctionalisations catalysed by peroxygenases: opportunities, challenges and solutions,” *Catal. Sci. Technol.*, vol. 5, no. 4, 2015, doi: 10.1039/c4cy01477d.
- [14] J. Wang, “Strömungsmodell der Gas-Flüssigreaktoren nach der Filmtheorie,” *Heat and Mass Transfer*, vol. 30, no. 4, 1995, doi: 10.1007/BF01602769.
- [15] W. K. Lewis and W. G. Whitman, “Principles of Gas Absorption,” *Ind. Eng. Chem.*, vol. 16, no. 12, 1924, doi: 10.1021/ie50180a002.
- [16] R. HIGBIE, “The Rate of Absorption of a Pure Gas into a Still Liquid during Short Periods of Exposure,” *Trans. AIChE*, vol. 31, pp. 365–389, 1935. [Online]. Available: <https://ci.nii.ac.jp/naid/10003391803/>
- [17] P. V. Danckwerts, “Gas absorption accompanied by chemical reaction,” *AIChE J.*, vol. 1, no. 4, 1955, doi: 10.1002/aic.690010412.
- [18] F. Garcia-Ochoa and E. Gomez, “Bioreactor scale-up and oxygen transfer rate in microbial processes: an overview,” *Biotechnology advances*, vol. 27, no. 2, 2009, doi: 10.1016/j.biotechadv.2008.10.006.
- [19] W. Henry, “Experiments on the quantity of gases absorbed by water, at different temperatures, and under different pressures,” *Proc. R. Soc. Lond.*, vol. 1, 1832, doi: 10.1098/rspl.1800.0063.
- [20] H. Chmiel, R. Takors, and D. Weuster-Botz, Eds., *Bioprozesstechnik*, 4th ed. Berlin, Heidelberg: Springer Spektrum, 2018.
- [21] M. Teramoto, S. Tai, K. Nishii, and H. Teranishi, “Effects of pressure on liquid-phase mass transfer coefficients,” *The Chemical Engineering Journal*, vol. 8, no. 3, 1974, doi: 10.1016/0300-9467(74)85027-6.

- [22] J. Vogelaar, A. Klapwijk, J. B. van Lier, and W. H. Rulkens, “Temperature effects on the oxygen transfer rate between 20 and 55°C,” *Water Research*, vol. 34, no. 3, 2000, doi: 10.1016/S0043-1354(99)00217-1.
- [23] A. Prins and K. van't Riet, “Proteins and surface effects in fermentation: foam, antifoam and mass transfer,” *Trends in Biotechnology*, vol. 5, no. 11, 1987, doi: 10.1016/0167-7799(87)90080-1.
- [24] Y. Kawase and M. Moo-Young, “The effect of antifoam agents on mass transfer in bioreactors,” *Bioprocess Engineering*, vol. 5, no. 4, 1990, doi: 10.1007/BF00369581.
- [25] K. Kim, J. Lee, K. Seo, M.-G. Kim, K.-S. Ha, and C. Kim, “Enhancement of methane–water volumetric mass transfer coefficient by inhibiting bubble coalescence with electrolyte,” *Journal of Industrial and Engineering Chemistry*, vol. 33, no. 68, 2016, doi: 10.1016/j.jiec.2015.10.018.
- [26] H. Zhu, B. H. Shanks, and T. J. Heindel, “Effect of Electrolytes on CO–Water Mass Transfer,” *Ind. Eng. Chem. Res.*, vol. 48, no. 6, 2009, doi: 10.1021/ie8012924.
- [27] E. Dumont and H. Delmas, “Mass transfer enhancement of gas absorption in oil-in-water systems: a review,” *Chemical Engineering and Processing: Process Intensification*, vol. 42, no. 6, 2003, doi: 10.1016/S0255-2701(02)00067-3.
- [28] G. Quijano, M. Hernandez, S. Villaverde, F. Thalasso, and R. Muñoz, “A step-forward in the characterization and potential applications of solid and liquid oxygen transfer vectors,” *Applied microbiology and biotechnology*, vol. 85, no. 3, 2010, doi: 10.1007/s00253-009-2146-x.
- [29] K. A. Stone, M. V. Hilliard, Q. P. He, and J. Wang, “A mini review on bioreactor configurations and gas transfer enhancements for biochemical methane conversion,” *Biochemical Engineering Journal*, vol. 128, November, 2017, doi: 10.1016/j.bej.2017.09.003.
- [30] D. Ho, K. Kim, T. Earmme, and C. Kim, “Enhancing gas–liquid volumetric mass transfer coefficient,” *Journal of Industrial and Engineering Chemistry*, vol. 87, 2020, doi: 10.1016/j.jiec.2020.03.009.
- [31] IFA, *GESTIS-Stoffdatenbank: Butan*. [Online]. Available: <https://gestis.dguv.de/data?name=010030> (accessed: May 14 2021).
- [32] Directive 1999/92/EC of the European Parliament and of the Council of 26 February of 16 December 1999 on minimum requirements for improving the

- safety and health protection of workers potentially at risk from explosive atmospheres (15th individual Directive within the meaning of Article 16(1) of Directive 89/391/EEC).* Accessed: Sep. 14 2021. [Online]. Available: <http://data.europa.eu/eli/dir/1999/92/oj>
- [33] *Directive 2014/34/EU of the European Parliament and of the Council of 26 February 2014 on the harmonisation of the laws of the Member States relating to equipment and protective systems intended for use in potentially explosive atmospheres.* Accessed: Sep. 14 2021. [Online]. Available: <http://data.europa.eu/eli/dir/2014/34/oj>
- [34] G. Sluyter, J. Kleber, F. Perz, B. Grund, S. Leuchs, S. Sieberz, P. Bubenheim, O. Thum, and A. Liese, “Fermentative oxidation of butane in bubble column reactors,” *Biochemical Engineering Journal*, vol. 155, no. 11, 2020, doi: 10.1016/j.bej.2020.107486.
- [35] G. Sluyter, “Entwicklung und Charakterisierung einer fermentativen Oxidation von Butan im Blasensäulenreaktor,” TUHH Universitätsbibliothek, 2019, doi: 10.15480/882.2384.
- [36] F. Perz, S. Bormann, R. Ulber, M. Alcalde, P. Bubenheim, F. Hollmann, D. Holtmann, and A. Liese, “Enzymatic Oxidation of Butane to 2-Butanol in a Bubble Column,” *ChemCatChem*, vol. 12, no. 14, 2020, doi: 10.1002/cctc.202000431.
- [37] John Wiley & Sons, Inc., *Wiley Article Sharing Policy*. [Online]. Available: <https://authorservices.wiley.com/author-resources/Journal-Authors/Promotion/article-sharing-policy.html> (accessed: Sep. 14 2021).
- [38] P. Molina-Espeja, E. Garcia-Ruiz, D. Gonzalez-Perez, R. Ullrich, M. Hofrichter, and M. Alcalde, “Directed evolution of unspecific peroxygenase from Agrocybe aegerita,” *Applied and environmental microbiology*, vol. 80, no. 11, 2014, doi: 10.1128/AEM.00490-14.
- [39] P. Molina-Espeja, S. Ma, D. M. Mate, R. Ludwig, and M. Alcalde, “Tandem-yeast expression system for engineering and producing unspecific peroxygenase,” *Enzyme and microbial technology*, 73-74, 2015, doi: 10.1016/j.enzmictec.2015.03.004.
- [40] M. H. Pahl and D. Franke, “Schaum und Schaumzerstörung - ein Überblick,” *Chemie Ingenieur Technik*, vol. 67, no. 3, 1995, doi: 10.1002/cite.330670306.

- [41] C. E. Zobell, "ACTION OF MICROÖRGANISMS ON HYDROCARBONS," *Bacteriol Rev*, vol. 10, 1-2, 1946, doi: 10.1128/br.10.1-2.1-49.1946.
- [42] L. D. Bushnell and H. F. Haas, "The Utilization of Certain Hydrocarbons by Microorganisms," *J Bacteriol*, vol. 41, no. 5, 1941, doi: 10.1128/jb.41.5.653-673.1941.
- [43] H.-G. Hennemann, S. Schaffer, M. Wessel, M. Pötter, J. P. Pfeffer, T. Haas, J. Corthals, E.-M. Eckl, S. Röder, W. Kroutil, and A. Skerra, "Method for aerobic production of alanine," EP 2 834 347 B1.
- [44] J. P. Pfeffer, T. Haas, O. Thum, F. Erhardt, E. M. Wittmann, C. Gehring, S. Hafkemeyer, and T. Hüller, "Biological alkane oxidation," US 10,053,713 B2.
- [45] J. P. Pfeffer, T. Haas, O. Thum, E. M. Wittmann, C. Gehring, S. Hafkemeyer, and T. Hüller, "Use of an alkB alkane 1-monooxygenase for the oxidation of propane and butane," EP 2 788 493 B1.
- [46] M. Pötter, A. Schmid, B. Bühler, H.-G. Hennemann, M. K. Julsing, S. Schaffer, T. Haas, M. Schrewe, S. Cornelissen, M. Roos, and H. Häger, "Biocatalytic oxidation process with alkL gene product," EP2560987B1.
- [47] O. Thum, P. Engel, C. Gehring, S. Schaffer, and M. Wessel, "Methods of producing rhamnolipids," EP 3 148 335 B1.
- [48] J. N. Baptist, R. K. Gholson, and M. J. Coon, "Hydrocarbon oxidation by a bacterial enzyme system," *Biochimica et Biophysica Acta*, vol. 69, 1963, doi: 10.1016/0006-3002(63)91223-X.
- [49] J. A. Peterson, D. Basu, and M. J. Coon, "Enzymatic ω -Oxidation," *Journal of Biological Chemistry*, vol. 241, no. 21, 1966, doi: 10.1016/S0021-9258(18)99684-5.
- [50] J. B. van Beilen, S. Panke, S. Lucchini, A. G. Franchini, M. Röthlisberger, and B. Witholt, "Analysis of *Pseudomonas putida* alkane-degradation gene clusters and flanking insertion sequences: evolution and regulation of the alk genes," *Microbiology (Reading, England)*, vol. 147, Pt 6, 2001, doi: 10.1099/00221287-147-6-1621.
- [51] I. E. Staijen, J. B. van Beilen, and B. Witholt, "Expression, stability and performance of the three-component alkane mono-oxygenase of *Pseudomonas oleovorans* in *Escherichia coli*," *European journal of biochemistry*, vol. 267, no. 7, 2000, doi: 10.1046/j.1432-1327.2000.01196.x.

- [52] J. B. van Beilen, “Alkane oxidation by *Pseudomonas oleovorans*: genes and proteins,” Dissertation, 1994. Accessed: Sep. 14 2021. [Online]. Available: <https://research.rug.nl/en/publications/alkane-oxidation-by-pseudomonas-oleovorans-genes-and-proteins>
- [53] C. Gehring, M. Wessel, S. Schaffer, and O. Thum, “The Power of Biocatalysis: A One-Pot Total Synthesis of Rhamnolipids from Butane as the Sole Carbon and Energy Source,” *ChemistryOpen*, vol. 5, no. 6, 2016, doi: 10.1002/open.201600127.
- [54] E. Fletcher, T. Pilizota, P. R. Davies, A. McVey, and C. E. French, “Characterization of the effects of n-butanol on the cell envelope of *E. coli*,” *Applied microbiology and biotechnology*, vol. 100, no. 22, 2016, doi: 10.1007/s00253-016-7771-6.
- [55] S. Mohagheghian and B. Elbing, “Characterization of Bubble Size Distributions within a Bubble Column,” *Fluids*, vol. 3, no. 1, 2018, doi: 10.3390/fluids3010013.
- [56] S. Shu, D. Vidal, F. Bertrand, and J. Chaouki, “Multiscale multiphase phenomena in bubble column reactors: A review,” *Renewable Energy*, vol. 141, no. 6, 2019, doi: 10.1016/j.renene.2019.04.020.
- [57] W. F. Guthrie, “NIST/SEMATECH e-Handbook of Statistical Methods (NIST Handbook 151),” 2020.
- [58] A. I. Khuri and S. Mukhopadhyay, “Response surface methodology,” *WIREs Comp Stat*, vol. 2, no. 2, 2010, doi: 10.1002/wics.73.
- [59] J. B. van Beilen, M. G. Wubbolts, and B. Witholt, “Genetics of alkane oxidation by *Pseudomonas oleovorans*,” *Biodegradation*, vol. 5, 3-4, 1994, doi: 10.1007/BF00696457.
- [60] A. Morão, C. I. Maia, M. M. R. Fonseca, J. M. T. Vasconcelos, and S. S. Alves, “Effect of antifoam addition on gas-liquid mass transfer in stirred fermenters,” *Bioprocess Engineering*, vol. 20, no. 2, 1999, doi: 10.1007/s004490050576.
- [61] B. Thomas, “Anwendung von Feinblasentechnologie in der Biokatalyse,” TUHH Universitätsbibliothek, 2021, doi: 10.15480/882.3438.
- [62] D. Ohde, B. Thomas, S. Matthes, S. Tanaka, P. Bubenheim, K. Terasaka, M. Schlüter, and A. Liese, “Microbubble enhanced mass transfer efficiency of CO 2 capture utilizing aqueous triethanolamine for enzymatic resorcinol carboxylation,” *RSC Adv.*, vol. 11, no. 7, 2021, doi: 10.1039/D0RA08690H.

- [63]A. R. Nair, "Incapacitating the bottleneck in Biocatalytic Oxyfunctionalization of Butane with the help of Mass Transfer Vectors," Institute of Technical Biocatalysis, Technical University of Hamburg, 2020.
- [64]ROTH AG, *Freiwillige Sicherheitsinformation in Anlehnung an das Sicherheitsdatenblattformat gemäß Verordnung (EG) Nr.1907/2006 (REACH): Magnesiumhydroxid.*
- [65]S. Sinha, D. Mishra, A. Agrawal, and K. K. Sahu, "Aqueous process intensification through enhanced oxygen mass transfer using oxygen vector: An application to cleaner leaching," *Journal of Cleaner Production*, vol. 176, no. 1, 2018, doi: 10.1016/j.jclepro.2017.12.122.
- [66]J. L. Rols, J. S. Condoret, C. Fonade, and G. Goma, "Mechanism of enhanced oxygen transfer in fermentation using emulsified oxygen-vectors," *Biotechnology and bioengineering*, vol. 35, no. 4, 1990, doi: 10.1002/bit.260350410.
- [67]G. Quijano, S. Revah, M. Gutiérrez-Rojas, L. B. Flores-Cotera, and F. Thalasso, "Oxygen transfer in three-phase airlift and stirred tank reactors using silicone oil as transfer vector," *Process Biochemistry*, vol. 44, no. 6, 2009, doi: 10.1016/j.procbio.2009.01.015.
- [68] P. Garbers, "Butane to Biomass: Characterization and Optimization of a Butane Fermentation," Hamburg University of Technology, 2020.
- [69]J. Tomei and R. Helliwell, "Food versus fuel? Going beyond biofuels," *Land Use Policy*, vol. 56, no. 1, 2016, doi: 10.1016/j.landusepol.2015.11.015.
- [70]C. Dellomonaco, C. Rivera, P. Campbell, and R. Gonzalez, "Engineered respiro-fermentative metabolism for the production of biofuels and biochemicals from fatty acid-rich feedstocks," *Applied and environmental microbiology*, vol. 76, no. 15, 2010, doi: 10.1128/AEM.00046-10.
- [71] G. Pauli, P. Overath, "ato Operon: a Highly Inducible System for Acetoacetate and Butyrate Degradation in Escherichia coli", *FEBS J.*, vol. 29, no.3 1972, doi: j.1432-1033.1972.tb02021.x.
- [72]J. Monod, "The Growth of Bacterial Cultures," *Annu. Rev. Microbiol.*, vol. 3, no. 1, 1949, doi: 10.1146/annurev.mi.03.100149.002103.
- [73]J. F. Andrews, "A mathematical model for the continuous culture of microorganisms utilizing inhibitory substrates," *Biotechnol. Bioeng.*, vol. 10, no. 6, 1968, doi: 10.1002/bit.260100602.

- [74] V. Bernal, S. Castaño-Cerezo, and M. Cánovas, “Acetate metabolism regulation in *Escherichia coli*: carbon overflow, pathogenicity, and beyond,” *Applied microbiology and biotechnology*, vol. 100, no. 21, 2016, doi: 10.1007/s00253-016-7832-x.
- [75] Y. Wang, D. Lan, R. Durrani, and F. Hollmann, “Peroxygenases en route to becoming dream catalysts. What are the opportunities and challenges?,” *Current opinion in chemical biology*, vol. 37, 2017, doi: 10.1016/j.cbpa.2016.10.007.
- [76] M. Hofrichter and R. Ullrich, “Heme-thiolate haloperoxidases: versatile biocatalysts with biotechnological and environmental significance,” *Applied microbiology and biotechnology*, vol. 71, no. 3, 2006, doi: 10.1007/s00253-006-0417-3.
- [77] V. B. Urlacher and M. Girhard, “Cytochrome P450 monooxygenases: an update on perspectives for synthetic application,” *Trends in Biotechnology*, vol. 30, no. 1, 2012, doi: 10.1016/j.tibtech.2011.06.012.
- [78] R. Ullrich, J. Nüske, K. Scheibner, J. Spantzel, and M. Hofrichter, “Novel haloperoxidase from the agaric basidiomycete *Agrocybe aegerita* oxidizes aryl alcohols and aldehydes,” *Applied and environmental microbiology*, vol. 70, no. 8, 2004, doi: 10.1128/AEM.70.8.4575–4581.2004.
- [79] A. Kinner, K. Rosenthal, and S. Lütz, “Identification and Expression of New Unspecific Peroxygenases - Recent Advances, Challenges and Opportunities,” *Frontiers in bioengineering and biotechnology*, vol. 9, 2021, doi: 10.3389/fbioe.2021.705630.
- [80] M. Hobisch, D. Holtmann, P. Gomez de Santos, M. Alcalde, F. Hollmann, and S. Kara, “Recent developments in the use of peroxygenases - Exploring their high potential in selective oxyfunctionalisations,” *Biotechnology advances*, 2020, doi: 10.1016/j.biotechadv.2020.107615.
- [81] M. Hofrichter and R. Ullrich, “Oxidations catalyzed by fungal peroxygenases,” *Current opinion in chemical biology*, vol. 19, 2014, doi: 10.1016/j.cbpa.2014.01.015.
- [82] X. Wang, S. Peter, M. Kinne, M. Hofrichter, and J. T. Groves, “Detection and kinetic characterization of a highly reactive heme-thiolate peroxygenase compound I,” *Journal of the American Chemical Society*, vol. 134, no. 31, 2012, doi: 10.1021/ja3049223.

- [83] A. Karich, K. Scheibner, R. Ullrich, and M. Hofrichter, “Exploring the catalase activity of unspecific peroxygenases and the mechanism of peroxide-dependent heme destruction,” *Journal of Molecular Catalysis B: Enzymatic*, vol. 134, 2016, doi: 10.1016/j.molcatb.2016.10.014.
- [84] S. Peter, M. Kinne, X. Wang, R. Ullrich, G. Kayser, J. T. Groves, and M. Hofrichter, “Selective hydroxylation of alkanes by an extracellular fungal peroxygenase,” *The FEBS journal*, vol. 278, no. 19, 2011, doi: 10.1111/j.1742-4658.2011.08285.x.
- [85] L. Michaelis and M. L. Menten, “Die Kinetik der Invertinwirkung,” *Biochemische Zeitschrift*, vol. 1913, no. 49, pp. 333–369.
- [86] T. A. Rogers and A. S. Bommarius, “Utilizing Simple Biochemical Measurements to Predict Lifetime Output of Biocatalysts in Continuous Isothermal Processes,” *Chemical engineering science*, vol. 65, no. 6, 2010, doi: 10.1016/j.ces.2009.12.005.
- [87] A.E.W. Horst, S. Bormann, J. Meyer, M. Steinhagen, R. Ludwig, A. Drews, M. Ansorge-Schumacher, and D. Holtmann, “Electro-enzymatic hydroxylation of ethylbenzene by the evolved unspecific peroxygenase of Agrocybe aegerita,” *Journal of Molecular Catalysis B: Enzymatic*, vol. 133, no. 5770, 2016, doi: 10.1016/j.molcatb.2016.12.008.
- [88] S. Bormann, D. Hertweck, S. Schneider, J. Z. Bloh, R. Ulber, A. C. Spiess, and D. Holtmann, “Modeling and simulation-based design of electroenzymatic batch processes catalyzed by unspecific peroxygenase from A. aegerita,” *Biotechnology and bioengineering*, vol. 118, no. 1, 2021, doi: 10.1002/bit.27545.
- [89] J. Brummund, M. Müller, T. Schmitges, I. Kaluzna, D. Mink, L. Hilterhaus, and A. Liese, “Process development for oxidations of hydrophobic compounds applying cytochrome P450 monooxygenases in-vitro,” *Journal of biotechnology*, vol. 233, 2016, doi: 10.1016/j.jbiotec.2016.07.002.
- [90] Dechema, *CHEMSAFE PTB-BAM*.
- [91] K. Wadaugson, S. Limtrakul, T. Vatanatham, and P. A. Ramachandran, “Mixing Characteristics of Gas and Liquid Phases in Bubble Column Reactors from Virtual Tracer Simulation,” *Ind. Eng. Chem. Res.*, vol. 57, no. 42, 2018, doi: 10.1021/acs.iecr.8b03708.

- [92] T. P. Call, M. K. Akhtar, F. Baganz, and C. Grant, “Modulating the import of medium-chain alkanes in *E. coli* through tuned expression of FadL,” *Journal of biological engineering*, vol. 10, 2016, doi: 10.1186/s13036-016-0026-3.
- [93] Q. He, G. N. Bennett, K.-Y. San, and H. Wu, “Biosynthesis of Medium-Chain ω -Hydroxy Fatty Acids by AlkBGT of *Pseudomonas putida* GPo1 With Native FadL in Engineered *Escherichia coli*,” *Frontiers in bioengineering and biotechnology*, vol. 7, 2019, doi: 10.3389/fbioe.2019.00273.
- [94] J. F. Kolmar, O. Thum, and F. Baganz, “Customized microscale approach for optimizing two-phase bio-oxidations of alkanes with high reproducibility,” *Microbial cell factories*, vol. 16, no. 1, 2017, doi: 10.1186/s12934-017-0788-4.
- [95] M. Schrewe, M. K. Julsing, K. Lange, E. Czarnotta, A. Schmid, and B. Bühler, “Reaction and catalyst engineering to exploit kinetically controlled whole-cell multistep biocatalysis for terminal FAME oxyfunctionalization,” *Biotechnology and bioengineering*, vol. 111, no. 9, 2014, doi: 10.1002/bit.25248.
- [96] Y. M. van Nuland, G. Eggink, and R. A. Weusthuis, “Application of AlkBGT and AlkL from *Pseudomonas putida* GPo1 for Selective Alkyl Ester ω -Oxyfunctionalization in *Escherichia coli*,” *Applied and environmental microbiology*, vol. 82, no. 13, 2016, doi: 10.1128/AEM.00822-16.
- [97] Y. M. van Nuland, F. A. de Vogel, G. Eggink, and R. A. Weusthuis, “Expansion of the ω -oxidation system AlkBGT of *Pseudomonas putida* GPo1 with AlkJ and AlkH results in exclusive mono-esterified dicarboxylic acid production in *E. coli*,” *Microbial biotechnology*, vol. 10, no. 3, 2017, doi: 10.1111/1751-7915.12607.
- [98] J. F. Kolmar, O. Thum, and F. Baganz, “Improving Product Specificity of Whole-Cell Alkane Oxidation in Nonconventional Media: A Multivariate Analysis Approach,” *Biotechnology journal*, vol. 14, no. 10, 2019, doi: 10.1002/biot.201800581.
- [99] S. Zhang, D. Wang, P.-P. Fan, and L.-P. Sun, “Enhancement of gas-to-liquid oxygen transfer in the presence of fine solid particles for air-exposed multiphase system,” *Chemical Engineering Research and Design*, vol. 100, 2015, doi: 10.1016/j.cherd.2015.04.024.
- [100] S. Weber, S. Schaepe, S. Freyer, M.-H. Kopf, and C. Dietzsch, “Jet aeration as alternative to overcome mass transfer limitation of stirred bioreactors,” *Engineering in life sciences*, vol. 18, no. 4, 2018, doi: 10.1002/elsc.201700169.

- [101] M. Ughetti, D. Jussen, and P. Riedlberger, "The ejector loop reactor: Application for microbial fermentation and comparison with a stirred-tank bioreactor," *Engineering in life sciences*, vol. 18, no. 5, 2018, doi: 10.1002/elsc.201700141.
- [102] M. Moresi, G. Bartolo Gianturco, and E. Sebastiani, "The ejector-loop fermenter: Description and performance of the apparatus," *Biotechnology and bioengineering*, vol. 25, no. 12, 1983, doi: 10.1002/bit.260251207.
- [103] Y. Ni, E. Fernández-Fueyo, A. Gomez Baraibar, R. Ullrich, M. Hofrichter, H. Yanase, M. Alcalde, W. J. H. van Berkel, and F. Hollmann, "Peroxygenase-Catalyzed Oxyfunctionalization Reactions Promoted by the Complete Oxidation of Methanol," *Angewandte Chemie (International ed. in English)*, vol. 55, no. 2, 2016, doi: 10.1002/anie.201507881.
- [104] M. Kluge, R. Ullrich, K. Scheibner, and M. Hofrichter, "Stereoselective benzylic hydroxylation of alkylbenzenes and epoxidation of styrene derivatives catalyzed by the peroxygenase of Agrocybe aegerita," *Green Chem*, vol. 14, no. 2, 2012, doi: 10.1039/C1GC16173C.
- [105] S. Peter, "Oxyfunctionalization of alkanes, alkenes and alkynes by unspecific peroxygenase (EC 1.11.2.1)," Dresden, Technische Universität Dresden, Diss., 2013, Saechsische Landesbibliothek- Staats- und Universitaetsbibliothek Dresden; Technische Universität Dresden; IHI Zittau - Zentrale Einrichtung der TU Dresden, Dresden, Zittau, 2013.
- [106] S. J. Blanksby and G. B. Ellison, "Bond dissociation energies of organic molecules," *Accounts of chemical research*, vol. 36, no. 4, 2003, doi: 10.1021/ar020230d.
- [107] JJS Technical Services, *Butane (C₄H₁₀)*. [Online]. Available: <https://www.jjstech.com/butanec4h10.html> (accessed: August 2021).
- [108] H. R. Lucas, L. Li, A. A. N. Sarjeant, M. A. Vance, E. I. Solomon, and K. D. Karlin, "Toluene and ethylbenzene aliphatic C-H bond oxidations initiated by a dicopper(II)-mu-1,2-peroxo complex," *Journal of the American Chemical Society*, vol. 131, no. 9, 2009, doi: 10.1021/ja807081d.
- [109] R. B. Cooley, B. L. Dubbels, L. A. Sayavedra-Soto, P. J. Bottomley, and D. J. Arp, "Kinetic characterization of the soluble butane monooxygenase from *Thauera butanivorans*, formerly 'Pseudomonas butanovora'," *Microbiology (Reading, England)*, vol. 155, Pt 6, 2009, doi: 10.1099/mic.0.028175-0.

- [110] A. Glieder, E. T. Farinas, and F. H. Arnold, “Laboratory evolution of a soluble, self-sufficient, highly active alkane hydroxylase,” *Nature biotechnology*, vol. 20, no. 11, 2002, doi: 10.1038/nbt744.
- [111] M. W. Peters, P. Meinholt, A. Glieder, and F. H. Arnold, “Regio- and enantioselective alkane hydroxylation with engineered cytochromes P450 BM-3,” *Journal of the American Chemical Society*, vol. 125, no. 44, 2003, doi: 10.1021/ja0303790.
- [112] R. Fasan, Y. T. Mehareenna, C. D. Snow, T. L. Poulos, and F. H. Arnold, “Evolutionary history of a specialized p450 propane monooxygenase,” *Journal of molecular biology*, vol. 383, no. 5, 2008, doi: 10.1016/j.jmb.2008.06.060.
- [113] R. Fasan, M. M. Chen, N. C. Crook, and F. H. Arnold, “Engineered alkane-hydroxylating cytochrome P450(BM3) exhibiting nativelike catalytic properties,” *Angewandte Chemie (International ed. in English)*, vol. 46, no. 44, 2007, doi: 10.1002/anie.200702616.
- [114] J. Chen, F. Kong, N. Ma, P. Zhao, C. Liu, X. Wang, and Z. Cong, “Peroxide-Driven Hydroxylation of Small Alkanes Catalyzed by an Artificial P450BM3 Peroxygenase System,” *ACS Catal.*, vol. 9, no. 8, 2019, doi: 10.1021/acscatal.9b02507.
- [115] F. Tonin, F. Tieves, S. Willot, A. van Troost, R. van Oosten, S. Breestraat, S. van Pelt, M. Alcalde, and F. Hollmann, “Pilot-Scale Production of Peroxygenase from Agrocybe aegerita,” *Organic process research & development*, vol. 25, no. 6, 2021, doi: 10.1021/acs.oprd.1c00116.

11 Appendix

11.1 Composition of Stocks

11.1.1 HCD media salt mix

The HCD media is a complex media that was used for the fermentation of the whole cell biocatalysts in the 2 L Fermenter. Salt stocks were prepared for 2 L reactor volume.

Table A.1: Composition of HCD salt mix

Substance	Formula	Concentration [g L ⁻¹]
Ammonium sulfate	(NH ₄) ₂ SO ₄	1.8
Dipotassium hydrogen phosphate	K ₂ HPO ₄	19.1
Potassium dihydrogen phosphate	KH ₂ PO ₄	12.5
Sodium citrate	C ₆ H ₅ Na ₃ O ₇ · 2 H ₂ O	2.3
Yeast extract	-	6.7

11.1.2 Trace elements solution

The trace elements solution was prepared in a volumetric flask with deionized water, sterile filtrated and aliquoted in 50 mL Falcons.

Table A.2: Composition of trace elements stock solution

Substance	Formula	Concentration [g L ⁻¹]
Hydrochloric acid (37 %)	HCl	36.50
Manganese dichloride	MnCl ₂ · 4 H ₂ O	1.91
Zinc sulfate	ZnSO ₄ · 7 H ₂ O	1.87
Triplex® III	Na-EDTA · 2 H ₂ O	0.84
Boric acid	H ₃ BO ₃	0.30
Sodium molybdate	Na ₂ MoO ₄ · 2 H ₂ O	0.25
Calcium chloride	CaCl ₂ · 2 H ₂ O	4.70
Iron(II) sulfate	FeSO ₄ · 7 H ₂ O	17.80
Copper(II) chloride	CuCl ₂ · 2 H ₂ O	0.15

11.1.3 HCD Feed

The HCD feed is a concentrated glucose solution containing additional magnesium sulfate and ammonium chloride. The glucose stock was normally prepared in a 500 mL laboratory flask and autoclaved. The two salts stocks were separately prepared in water, sterile filtrated and aliquoted in 50 mL Falcons. Directly before use the salts solutions were added to the glucose.

Table A. 3: Composition of HCD feed solution

Substance	Formula	Concentration [mL L ⁻¹]
Glucose stock (500 g kg ⁻¹)	C ₆ H ₁₂ O ₆	850
Magnesium sulfate (200 g L ⁻¹)	MgSO ₄ · 7 H ₂ O	50
Ammonium chloride (220 g L ⁻¹)	NH ₄ Cl	100

11.1.4 M9 media

The M9 minimal media was used in all bubble column experiments with whole cell biocatalysts where no bacterial growth was desired. The salt preparation was prepared for 0.25 and 2 L reactor volume.

Table A.4: Composition for M9 minimal media

Substance	Formula	Concentration [g L ⁻¹]
Disodium hydrogen phosphate	Na ₂ HPO ₄	6.8
Potassium dihydrogen phosphate	KH ₂ PO ₄	3.0
Sodium chloride	NaCl	0.5
Ammonium chloride	NH ₄ Cl	2.0

The M9+ media was used in all experiments with the alkBGT/ato whole cell system where bacterial growth was desired. For this, the above described media (after autoclaving) was supplemented with the following:

Table A.5: Addition to the M9 minimal media for the M9+

Substance	Formula	Concentration [ml L ⁻¹]
Magnesium sulfate (200 g L ⁻¹)	MgSO ₄ · 7 H ₂ O	2.45
Ammonium chloride (220 g L ⁻¹)	NH ₄ Cl	9.09
Trace elements US3-stock	-	15
DCPK	-	0.25
IPTG (1 M)	-	1
Kanamycin (50 g L ⁻¹)	-	1
Ampecilin (100 g L ⁻¹)	-	1

11.2 Design of Experiment

11.2.1 Experimental Conditions and Results

Table A.6: Summary of the experimental conditions and results for the Design of Experiment.

Butane [vol.%]	Over pressure [mbar]	Gassing [L min ⁻¹]	Gassing [Ln min ⁻¹]	\dot{Q}_P [mM h ⁻¹]	Yield [%]	avg. DO [%]	avg. OD ₆₀₀ [-]	Activity [mM OD ⁻¹ h ⁻¹]
27	300	0.7	0.91	6.07	1.84	59.0	13.3	0.46
14	500	0.7	1.05	7.31	3.71	85.3	17.2	0.43
40	100	0.7	0.77	6.32	1.53	14.6	15.9	0.40
14	100	0.7	0.77	4.99	3.45	55.6	16.0	0.31
40	100	1.5	1.65	7.13	0.81	21.6	19.4	0.37
27	300	1.1	1.43	5.3	1.02	66.5	12.6	0.42
27	300	1.1	1.43	5.01	0.97	56.6	12.5	0.39
27	300	1.1	1.43	5.55	1.07	71.5	14.0	0.40
40	500	1.5	2.25	11.47	1.24	31.0	25.3	0.45
40	300	1.1	1.43	5.67	0.74	47.7	13.1	0.43
14	500	1.5	2.25	9.72	2.3	84.7	23.7	0.41
40	500	0.7	1.05	7.8	1.39	30.7	23.4	0.33
27	300	1.1	1.43	5.9	1.14	59.3	12.9	0.46
27	100	1.09	1.20	5.31	1.22	51.2	13.0	0.41
14	100	1.55	1.71	4.86	1.52	66.3	14.2	0.34
27	300	1.5	1.95	8.52	1.21	48.9	22.1	0.39
14	300	0.92	1.20	4.67	2.08	-	12.2	0.38
27	500	1.1	1.65	9.2	1.51	62.6	23.3	0.39
27	300	1.1	1.43	5.46	1.06	63.6	13.6	0.40

11.2.2 DoE Modell: Volumetric Productivity

Summary of the examination of the Response \dot{Q}_P .

Table A. 7: ANOVA, Fit Statistic and Final Equation for the Response: \dot{Q}_P . As parameters the butane content in [%], the gassing rate in [L min^{-1}] and the over pressure in [mbar] must be used. The result is in [mM h^{-1}].

Source	Sum of Squares	df	Mean Square	F-value	p-value	
Model	63.30	8	7.91	37.28	< 0.0001	significant
A-Butane	5.14	1	5.14	24.20	0.0006	
B-Gassing	7.65	1	7.65	36.02	0.0001	
C-Pressure	29.56	1	29.56	139.26	< 0.0001	
AB	1.01	1	1.01	4.75	0.0543	
BC	4.27	1	4.27	20.13	0.0012	
A^2	1.70	1	1.70	7.99	0.0180	
B^2	4.63	1	4.63	21.81	0.0009	
C^2	4.62	1	4.62	21.76	0.0009	
Residual	2.12	10	0.2122			
Lack of Fit	1.69	6	0.2823	2.64	0.1837	not significant
Pure Error	0.4285	4	0.1071			
Cor Total	65.43	18				

Std. Dev.	0.4607	R²	0.9676
Mean	6.65	Adjusted R²	0.9416
C.V. %	6.93	Predicted R²	0.8620
		Adeq Precision	24.2238

STY	=
+13.67302	
+0.243040	* Butane
-20.74480	* Gassing
-0.020632	* Pressure
+0.067050	* Butane * Gassing
+0.009013	* Gassing * Pressure
-0.004840	* Butane ²
+8.35689	* Gassing ²
+0.000032	* Pressure ²

11.2.3 DoE Modell: Yield

Summary of the examination of the Response Yield.

Table A. 8: ANOVA, Fit Statistic and Final Equation for the Response: Yield. As parameters the butane content in [%], the gassing rate in [L min⁻¹] and the over pressure in [mbar] must be used. The equation gives the decadic logarithm of the actual value. The actual value has the unit [%].

Source	Sum of Squares	df	Mean Square	F-value	p-value	
Model	0.6430	7	0.0919	145.67	< 0.0001	significant
A-Butane	0.2756	1	0.2756	437.16	< 0.0001	
B-Gassing	0.1246	1	0.1246	197.67	< 0.0001	
C-Pressure	0.0213	1	0.0213	33.82	0.0001	
AB	0.0090	1	0.0090	14.31	0.0030	
BC	0.0192	1	0.0192	30.53	0.0002	
B ²	0.0550	1	0.0550	87.26	< 0.0001	
C ²	0.0235	1	0.0235	37.23	< 0.0001	
Residual	0.0069	11	0.0006			
Lack of Fit	0.0042	7	0.0006	0.8951	0.5801	not significant
Pure Error	0.0027	4	0.0007			
Cor Total	0.6499	18				

Std. Dev.	0.0251	R²	0.9893
Mean	0.1520	Adjusted R²	0.9825
C.V. %	16.52	Predicted R²	0.9657
Adeq Precision			42.6837

Log₁₀(Yield)	=
+2.18279	
-0.019777	* Butane
-2.42809	* Gassing
-0.001726	* Pressure
+0.006312	* Butane * Gassing
+0.000605	* Gassing * Pressure
+0.819113	* Gassing ²
+2.15261E-06	* Pressure ²

11.3 Matlab scripts

All in this work applied scripts were written and executed in MATLAB® R2020b. The

11.3.1 Butane single substrate kinetic

This script was used to determine kinetic parameters for the UPO catalysed butane hydroxylation at a constant hydrogen peroxide feed rate.

```
function [fitresult, gof] = UPOfit1()
%Data
pi = [0;60;105;150;250;500;750;1000;1250;1500]; % mbar
TOF = [0;24;31;39;47;46;57;53;55;53]./60; % TOF in 1/min -> in 1/s
[xData, yData] = prepareCurveData( pi, TOF );
% Set up fittype and options.
ft = fittype( 'kcat* x / (km + x)', 'independent', 'x', 'dependent', 'y' );
opts = fitoptions( 'Method', 'NonlinearLeastSquares' );
opts.Display = 'Off';
opts.StartPoint = [0.186229921362058 0.0929533073641942];
% Fit model to data.
[fitresult, gof] = fit( xData, yData, ft, opts );
% Plot fit with data.
figure( 'Name', 'untitled fit 1' );
h = plot( fitresult, xData, yData);
```

11.3.2 Two-substrate kinetic

This script was used to determine kinetic parameters for the double substrate kinetic of UPO catalysed butane hydroxylation.

```
function [fitresult, gof] = createFit(Butane, H2O2, TOF_s)
% Butane = partial pressure of butane [mbar]
% H2O2 = molar feed rate of H2O2 [mM/h]
% TOF = Turnover frequency [1/s] (Q_P/c_enzyme)
%% Fit:
[xData, yData, zData] = prepareSurfaceData( Butan, H2O2, TOF_s );
% Set up fittype and options.
ft = fittype( 'kcat.* (Butan ./ (km_Butane + Butan)).* (H2O2 ./ (H2O2 + km_H2O2))', ...
    'independent', {'Butan', 'H2O2'}, 'dependent', 'z' );
opts = fitoptions( 'Method', 'NonlinearLeastSquares' );
opts.Display = 'Off';
opts.StartPoint = [0.111202755293787 0.780252068321138 0.389738836961253];

% Fit model to data.
[fitresult, gof] = fit( [xData, yData], zData, ft, opts );

% Plot fit with data.
figure( 'Name', 'untitled fit 1' );
h = plot( fitresult, [xData, yData], zData );
```

11.3.3 Process curve analysis

For the process curve analysis in total three scripts are used. The main script (UPO_Butanol_lsqcurve) calls one function (Conc_Curve_Model_UPO_oxi), which in turn calls the function for the ordinary differential equation (UPODGL_lsq).

Main script: UPO_Butanol_lsqcurve

```

%%
%Strucute of the experimental results
%Werte(1) = 'B_ol_5mM_2_5mMh.mat' Butanol 5 mM und 2.5 mM H2O2
%Werte(2) = 'B_ol_10mM_2_5mMh.mat' Butanol 10 mM und 2.5 mM H2O2
%Werte(3) = 'B_ol_10mM_50mMh.mat' Butanol 10 mM und 5.0 mM H2O2
%Werte(4) = 'B_ol_10mM_100mMh.mat' Butanol 10 mM und 10 mM H2O2
%Werte(i).Butanol = Butanol concentration [mM]
%Werte(i).Butanone = Butanone concentration [mM]
%Werte(i).Time = Time [h]
load('WerteIN2.mat')
% Delete Fitst Data of Experiment 4: no H2O2 Feed (pipe was empty at start)
Werte = WerteIN;
Werte(4).Butanol(1:3) = [];
Werte(4).Butanone(1:3) = [];
Werte(4).Time(1:3) = [];
Werte(4).Enzym(1:3) = [];
%%
global c_measured0 N_spec N_experiments N_max_exp N_data_points N_params
%N_spec=1; %We have 3 species - will be used for the ode45-given matrix
N_params=6; %Number of kinetic parameters to fit.
param_names={'kcat_ol','km_Butanol','km_H2O2','kcat_one','km_Butanone','km_H2O2_one'}; %the fit result will be printed using these names.
units={'1/s','mM','mM/uM/h','1/s','mM','mM/uM/h'};
global kdeak
global Feedh2o2
global kdeacktivierung
global enzym_t0
global Feedh2o2_all
kdeacktivierung = [0.094 0.062 0.141 0.2224]/3600; % from uM/h to uM/s
enzym_t0 = [0.566 0.534 0.603 0.5416]; % uM !!! Bei V4
estimated Starting concentration at t = 15min
Feedh2o2_all = [2.5 2.5 5 10]; % mM/h
N_experiments = 4;
%%
Pre-processing
%disp('Starting preprocessing...Aka: Turning excel data into one vector');
%Order the data in a nice way so lsqcurvefit can compare two matrizes
V1 = [Werte(1).Butanol Werte(1).Butanone];
V2 = [Werte(2).Butanol Werte(2).Butanone];
V3 = [Werte(3).Butanol Werte(3).Butanone];
V4 = [Werte(4).Butanol Werte(4).Butanone];
C_cleared= [V1; V2; V3; V4];
t_measured_vector =[ Werte(1).Time; Werte(2).Time; Werte(3).Time;
Werte(4).Time];
t_measured_vector = t_measured_vector*3600; %Werte.Time sind in [h]
Berechnung aber für [s]
c_measured0_ol = [Werte(1).Butanol(1); Werte(2).Butanol(1);
Werte(3).Butanol(1); Werte(4).Butanol(1)];
c_measured0_one= [Werte(1).Butanone(1); Werte(2).Butanone(1);
Werte(3).Butanone(1); Werte(4).Butanone(1)];

```

```

c_measured0 = [c_measured0_01 c_measured0_one enzym_t0'];
for i = 1:N_experiments
t_measured{i} = Werte(i).Time*3600; %Werte.Time sind in
[h] Berechnung aber für [s]
end
%% Now to the fitting:
disp('Starting fitting')
options = optimoptions('lsqcurvefit','Display','iter',...
    'MaxFunctionEvaluations',1e4,'FunctionTolerance',1e-16);
params0= rand(1,N_params); %[40000 25 20 40000 25 20];
params_lb=zeros(1,N_params); %lower bounds for parameters
params_ub=zeros(1,N_params)+1000000; %[100000 100000 100000 100000 100000
100000]; %upper bounds for parameters
[params_fit,~,residual,exitflag,~,~,jacobian]=...
    lsqcurvefit(@Conc_Curve_Model_UPO_oxi,params0,',...
        t_measured,C_cleared,params_lb,params_ub,options);
%% Post processing
disp('Starting post-processing...')
CInt=nlparci(params_fit, residual, 'jacobian', jacobian);
CInt=abs((CInt(:,1)-CInt(:,2))/2);
disp('done post processing')
%% printing results
fprintf('Parameters:\n\t\t Calculated\t Confi.Int\n')
formatSpec ='%s\t %6.2f \t\t %6.2f \t%s\n';
for i=1:N_params
    fprintf(formatSpec,param_names{i},params_fit(i),CInt(i),units{i})
end
disp('done printing... baka')
%% Calculate using the found parameters
C_simulation=cell(N_experiments,1);
tout=cell(N_experiments,1);
figure
for i=1:N_experiments
    kdeak = kdeacktivierung(i);
    Feedh2o2 = Feedh2o2_all(i);
    [WerteOUT(i).Time,Ctemp]=ode45(@UPODGL_lsq,[t_measured{i}(1)
1.1*t_measured{i}(end)],...
    [params_fit, c_measured0(i,:)]);
    WerteOUT(i).Butanol = Ctemp(:,N_params+1);
    WerteOUT(i).Butanone = Ctemp(:,N_params+2);
    WerteOUT(i).Enzyme = Ctemp(:,N_params+3);
end

```

Function 1: Conc_Curve_Model_UPO_oxi

```

function [C_to_compare] = Conc_Curve_Model_UPO_oxi(params,t_measured)
%CONC_CURVE_MODEL VERSION 3.1 is called by the main script curve_fit.
% It takes kinetic parameters and calls an ode-solver to calculate the
% concentration curves of different species. If you change the number of
% parameters make sure to also change the column-indecies that contain the
% relevant concentrations. Otherwise you will compare product-concentration
% curve with substrate-concentrations or parameters.
global c_measured0 N_data_points N_experiments N_max_exp N_spec N_params
global Feedh2o2_all kdeak Feedh2o2 kdeacktivierung
%N_data_points is a vector with the number of data points for each
%experiment in each index.
%N_measurements: number of experiments
C_to_compare=[];

```

```

for i=1:N_experiments
    kdeak = kdeacktivierung(i);
    Feedh2o2 = Feedh2o2_all(i);
    [~,Ctemp]=ode45(@UPODGL_lsq,t_measured{i},[params,
c_measured0(i,:)]);
    C_calced_temp=Ctemp(:,N_params+1:N_params+2);
    C_to_compare = [C_to_compare;C_calced_temp];
end
end

```

Ordinary differential equation: UPODGL_lsq

```

function dx=UPODGL_lsq(t,x)
global Feedh2o2
global kdeak
global N_params
dx=zeros(size(x));
kcat_ol           = x(1);
km_butanol        = x(2);
km_H2O2           = x(3);
kcat_one          = x(4);
km_butanone       = x(5);
km_H2O2_one       = x(6);
c_butanol         = x(N_params+1);
c_butanone        = x(N_params+2);
c_enzyme          = x(N_params+3);
H2O2spez = Feedh2o2/c_enzyme;
v_ol= kcat_ol * (c_enzyme/1000) * (c_butanol /(c_butanol+km_butanol))
*(H2O2spez/(H2O2spez+km_H2O2));
% 1/min; μM/100= mM [mM]/([mM]+[mM]) * ([mM/h])/([mM/h]+[mM/h])
v_one = kcat_one * (c_enzyme/1000) * (c_butanone /(c_butanone+km_butanone))
*(H2O2spez/(H2O2spez+km_H2O2_one));
dx(N_params+1)=-v_ol;
dx(N_params+2)=+v_ol-v_one;
dx(N_params+3)=-kdeak;

```

end

11.4 Laboratory Protocols

11.4.1 Fermentation

HCD Production of alkB induced <i>E.coli</i>			
Experimental Background: 2x PTFE Rushton Turbine and 1x diagonally cross PTFE at the bottom; 2µm big stainless steel sinther cylinder in vertical position; Antifoam feed of 80 µl/h; 2 L initial medium and a initial dilutionrate of D=0,004;			
Preparation & 1 st Pre Culture			
Number of Experiment:	PC#	Date:	<input checked="" type="checkbox"/>
1. Dissolve one prior prepared HCD-Salt mix for 2 Liter in 2 Liter Millipore Water			
2. Measure 120 ml from the HCD Salt Solution into a 250 ml Schott bottle to autoclave			
3. Fill fermenter with the rest prepared HZD-Salt Solution and MARK THE LIQUID LEVEL; Calibrate the pH probe and fix into the fermenter with DO-probe and gassing adapter. Connect everything and autoclave with everything else needed over night to the next day.			
4. Prepare Glukose Feed in 0,5L bottle			
Bezeichnung	Stoff	Konz. [ml/l]	Pro 0,5L Ansatz [ml]
HZD-Feed-Glukosestock	Glukose 500 [g·kg ⁻¹]	850	425
Magnesiumsulfat-Stock	MgSO ₄ ·7H ₂ O (200 [g/kg])	50	25
Ammoniumchlorid-Stock	NH ₄ Cl	100	50
5. preculture (2 x cryostock ring -->1 L shakingflask with 100 ml medium)			
HCD Production of alkB induce	Content	Conz. [ml/l]	Per 100 ml [ml]
HZD-Salt Stock	Lösung	1 Liter	100
NH4Fe-Citrat	NH4Fe-Citrat	17	1.7
HZD-Feed Mix	Glukose+NH4Cl+MgCl	30	3
Trace Elements US3-Stock	US3-Stock	3	0.3
Antibiotika	Kanamycin (50g/l)	1	0.1
6. Inoculate with two cryorings at 37°C let shake Start: 08 : 00 Uhr			
7. Stopp shaking Ende: 16 : 45 Uhr			
8. Fill 2x 25ml syringe under the cleanbench with cell suspension and inoculate at step 4			
HCD Fermentation			
Number of Experiment:	HZD#	Date:	
9. At the next morning connect the HCD Fermenter to the control unit.			
10. Prepare all Components but the HZD-Salt Sol. Into the feeding bottle under the cleanbench			
Media	Content	Conz. [ml/l]	Per 2 L [ml]
HZD-Salt Solution from 1. already in the Fermenter		940	1880
NH4Fe-Citrat	NH4Fe-Citrat	17	34
HZD-Feed	Lösung von oben	30	60
Trace Elements US3-Stock	US3-Stock	15	30
Antibiotika	Kanamycin (50g/L)	1	2
11. Fill up the HZD-Salt Solution in the fermenter to the level-mark with Millipore water. Connect the feeding bottle to the fermenter and transfer the other components.			
12. Change the feeding bottle so that the HZD-Feed is ready to be feeded through the cap			
13. Temperatur auf 37°C, pH-Schlauch füllen, pH _{soil} auf 6,8; DO=100%, Begasung auf 4 [L·min ⁻¹], D = _____ [h ⁻¹] und + h ⁻¹ mit h stepweise increase ; Antischäum feed auf µl·h ⁻¹			
14. Beimpfen des Fermenter auf eine Start OD ₆₀₀ von 0,____ Start: 17 : 00 Uhr			
15. HZD-Feed startet nach ____ h umstieg auf D _{INT} = _____ und +0,001 h ⁻¹ nach ____ h			
16. Nach ____ h wird die Temperatur auf 30°C gesenkt mit einer ____ °C/h Rampe			
17. 4 h vor Feedende → Induktion mit 0,025 vol.% DCPK (25 µl·L ⁻¹) um: 11 : 00 Uhr			
18. Wenn Feedzeit vorbei Temp auf 2°C und Fermentation beenden und Zellen abzentrifugieren			
Comments:			

Figure A. 1: Protocol for the production of the alkBGT strain

11.4.2 Bubble column experiments

Oxidation of Butane in Bubble Column Reactors			
Number of Experiment:	Buto#	Date:	
Experimental background: Versuch der Butanoxidation mit E. coli W3110 2L Medium in der Bläsensäule; Zellen aus H2D# mit Ziel-OD = >25, bzw. >90% Punkt prediction, Konstant T=30°C, Begassing = 5 l/min, End 37 vol-%, p = 500 mbar > 2,25 bar/mm; (sofern schaffbar) Nach 1 Tag abgegeb. 3,5 vol-% Butane (0,072 mol/l); Bedingungen sonst konstant			
1. Wash bubble column with 1% Corisol solution over night via cleaning pump tank → 2. Let the Corisol solution drain off completely back into the cleaning pump tank → 3. Wash of Corisol residue with water via the spray head of the bubble column 4. Flush gassing adapter with water (syringe) and with air (0,2 l/min) to remove corisol 5. When no foam is visible (2 min washing) stop the steril. water feed 6. Keep on gassing with air at 1,0 l/min until the experiment starts → 7. Add antibiotics and M9 salt mix Media Content Conz. [mM] total [ml] M9-Media Buffer salts - 2000 Antibiotika Kanamycin [50g/l] 1 2 8. Heat up the media to +C and set pH-Kont = 6,8 and calibrate DO-Probe at 103 hPa 9. Prepare 50 ml syringe with glucose solution (500 g/kg) and tubing connectors with needle 10. To resuspend the cells from H2D# → thaw the Falcon tube in warm water → 11. Let the cell block drop into 50 ml syringes and flush into bubble column until (OD-kont.) → 12. Turn on the glucose (ml/h) and the antifoam (μl/h) feed → 13. Wait for 5 minutes as adaption time for the cells and take ZERO SAMPLE → 14. Flush the system with nitrogen via MFC at desired gassing rate → 15. Switch from nitrogen to butane and start gassing with _____ l/min of _____ % Butane/Air Mix → 16. Take samples due to the timetable from the bubble column and the wash bottle → 17. Mix 500 μl of ethylacetate 50μl of 3M HCl and 500μl of sample in an eppi and vortex for 2 min 18. Centrifuge the eppi tube for 3 minutes at 13000 rpm 19. Fill 200 μl of the upper organic phase carefully in an GC vial with insert 20. Analyze in CS with GS_ButoK and name data file according to experiment type and number			
Biomass Concentration and Glucose Feed Calculation			
Experiment#	Buto#	Date:	00.01.1900
Wet Biomass	OD _{600nm} during resuspension	[g] H2D#	Initial Feedrate [mg/g _{dw} · h ⁻¹] [500g/kg]
glu feedrate:	[ml/h]	↑ MW OD _{600nm}	↑ [ml · min ⁻¹] mit _____ g/kg Glucose

Oxidation of Butane in Bubble Column Reactors			
Experiment#	Buto#	Date:	00.01.1900
Sample#	Bubble Column	Comments	Peakarea
[]	[h:mm:m]	[sL ⁻¹]	[mAU]
Zero sample	00:00		
1			
2			
3			
4			
5			
6			
7			
8			
9			
10			
11			
12			
13			
14			
15			
16			
17			
18			
19			
20			
21			
22			
23			
24			
25			
26			
27			
28			
29			
30			
31			
32			
33			
34			

Figure A. 2: Protocol for the butane oxidation in a bubble column reactor

11.4.3 Cultivation of the alkBGT/ato strain

Kultivierungsversuche im Schüttelkolben/Blasensäulenreaktor				
Vorbereitung				
M9 Medium				
1. Einwage in 15 mL Falcon				
Bezeichnung	Stoff	Konzentration [mmol/l]	Konzentration [g/l]	Einwaage _{soll} [g/250ml]
Stock M9	Na ₂ HPO ₄	47.8	6.8	1.7
	KH ₂ PO ₄	22.0	3.0	0.8
	NaCl	8.6	0.5	0.1
	NH ₄ Cl	37.4	2.0	0.5
2. Beschriften mit "M9 Medium für Zellanzucht 300 ml" & Datum				
Nutzung				
3. Stock in 305 mL Millipure Wasser lösen (etwas Puffer gegen Verdampfung beim Autoklavieren)				
4. Autoklavieren				
5. Unter Cleanbench mit folgenden Stoffen versetzen und Mischen				
Bezeichnung	Stoff	Konz. [g/l]	Pro 0,3L Ansatz [ml]	
Magnesiumsulfat-Stock	MgSO ₄ *7H ₂ O (200 g/kg)	0.49	0.735	
Ammoniumchlorid-Stock	NH ₄ Cl (220 g/kg)	2	2.727	3x 0,909
Strace elements	US3 Stock	15 mL/L	4.5	5 * 0,900
Induktor	DCPK	250 µL/L	0.075	
	IPTG	1 M	0.300	
Antibiotika	Kanamycin (50g/L)	-	0.300	
	Ampecilin (100 g/L)	-	0.300	
Durchführung Kolben				
1. OD von Stammkultur/Vorkultur bestimmen, Berechnen wie viel Inokulum benötigt wird, die 1,5-fache Menge in ein Falcon füllen -> zentrifugieren (10 min, 5000 rpm, 4°C)				
2. Während zentrifugation: Vorbereitetes Medium in 300 mL Kolben (je 50 mL) geben und Substrat (abhängig vom Experiment) zugeben				
3. Überstand im zentrifugierten Falcon abgießen und unter der Sterilbank M9 Medium (~10 mL) hinzugeben. Zellen resuspendieren, OD bestimmen -> Kolben mit benötigter Menge für Ziel OD inokkulieren				
4. 0,650 mL Probe aus jedem Kolben nehmen und die Kolben in den Inkubator stellen				
5. OD Bestimmen				
6. Reste des Mediums in Kolben geben, Inokulieren und als Negativ Kontrolle mit in den Inkubator stellen				

Durchführung BS				
1. Vorbereitetes Medium in 300 mL in Blasensäule füllen und Temperatur einstellen.				
2. OD von Stammkultur/Vorkultur bestimmen, Berechnen wie viel Inokulum benötigt wird, die entsprechende Menge in ein Falcon füllen -> zentrifugieren (10 min, 5000 rpm, 4°C)				
3. Überstand im zentrifugierten Falcon abgießen und Zellen resuspendieren (Medium aus Blasensäule). Zellsuspension in Blasensäule geben. Substrat hinzugeben.				
4. t0 Probe nehmen				
5. 50 mL in 300 mL Kolben füllen und im Inkubator kultivieren				
6. Butanzufuhr starten				

Figure A. 3: Protocol for the cultivation of the alkBGT/ato strain

11.5 Chromatograms

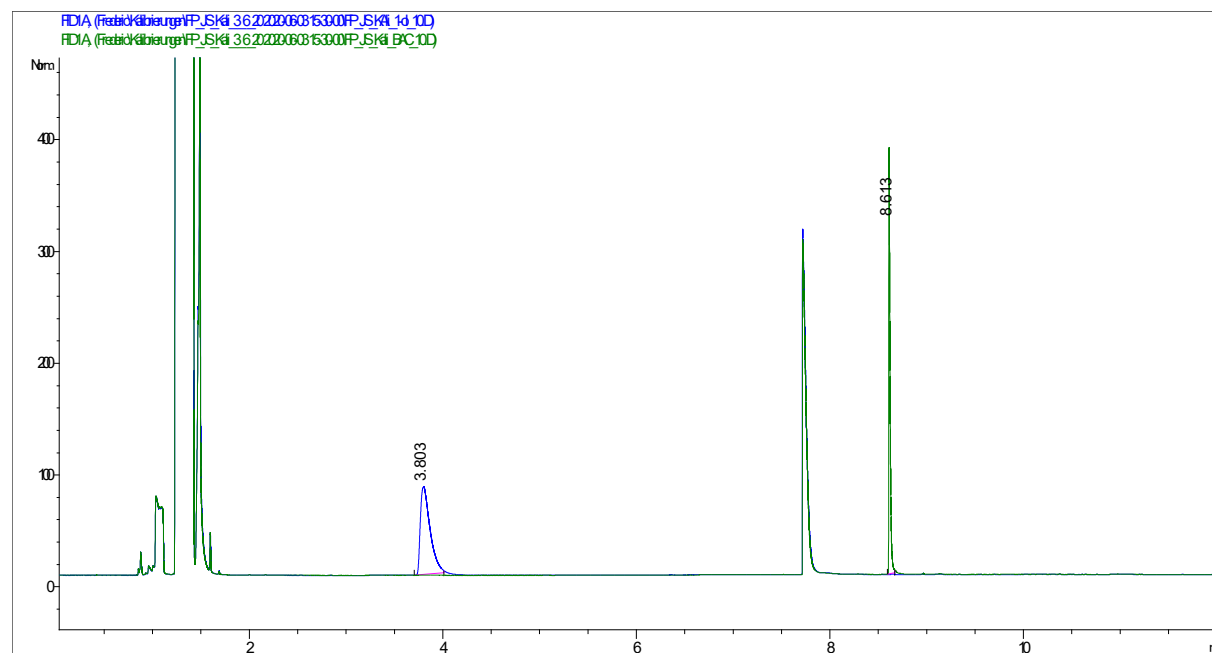


Figure A. 4: Exemplary chromatograms of the GC analysis of 1-butanol (blue, retention time 3.8 min) and butyric acid (green, retention time 8.6 min). Exemplified for a concentration of 10 mM. Unmarked peaks are caused by the solvent.

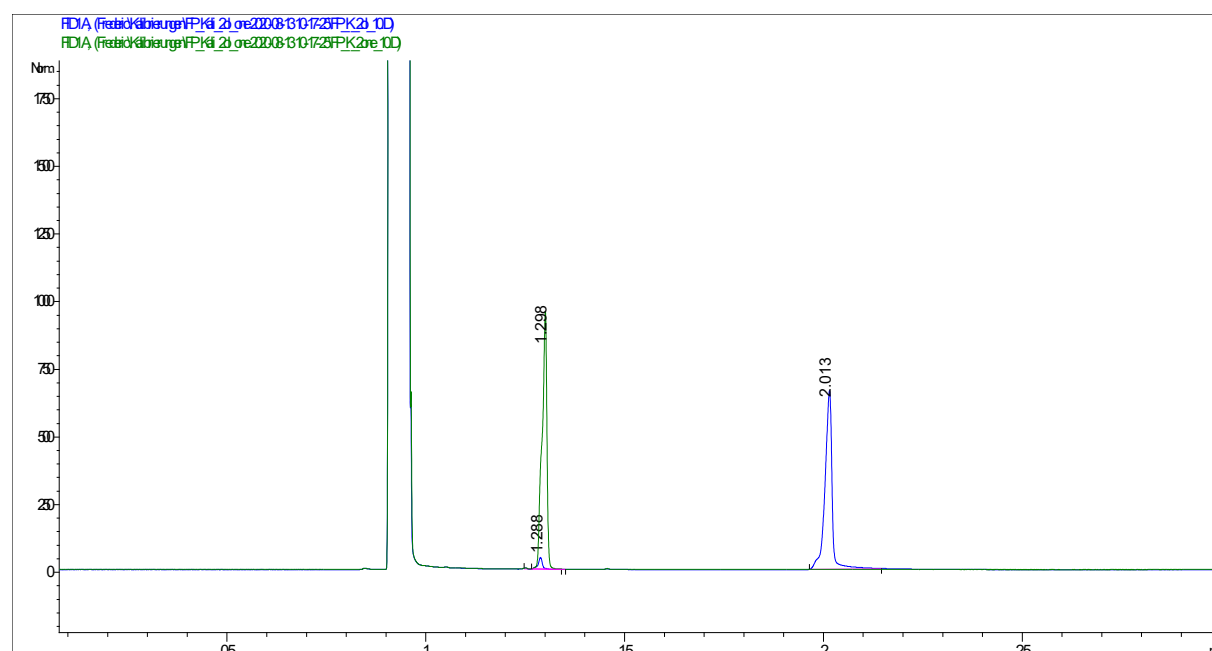


Figure A. 5: Exemplary chromatograms of the GC analysis of 2-butanol (blue, retention time 1.3 min) and butanone (green, retention time 2.0 min). Exemplified for a concentration of 10 mM. Unmarked peaks are caused by the solvent.

11.6 Engineering drawing

Top and bottom plate for small bubble column

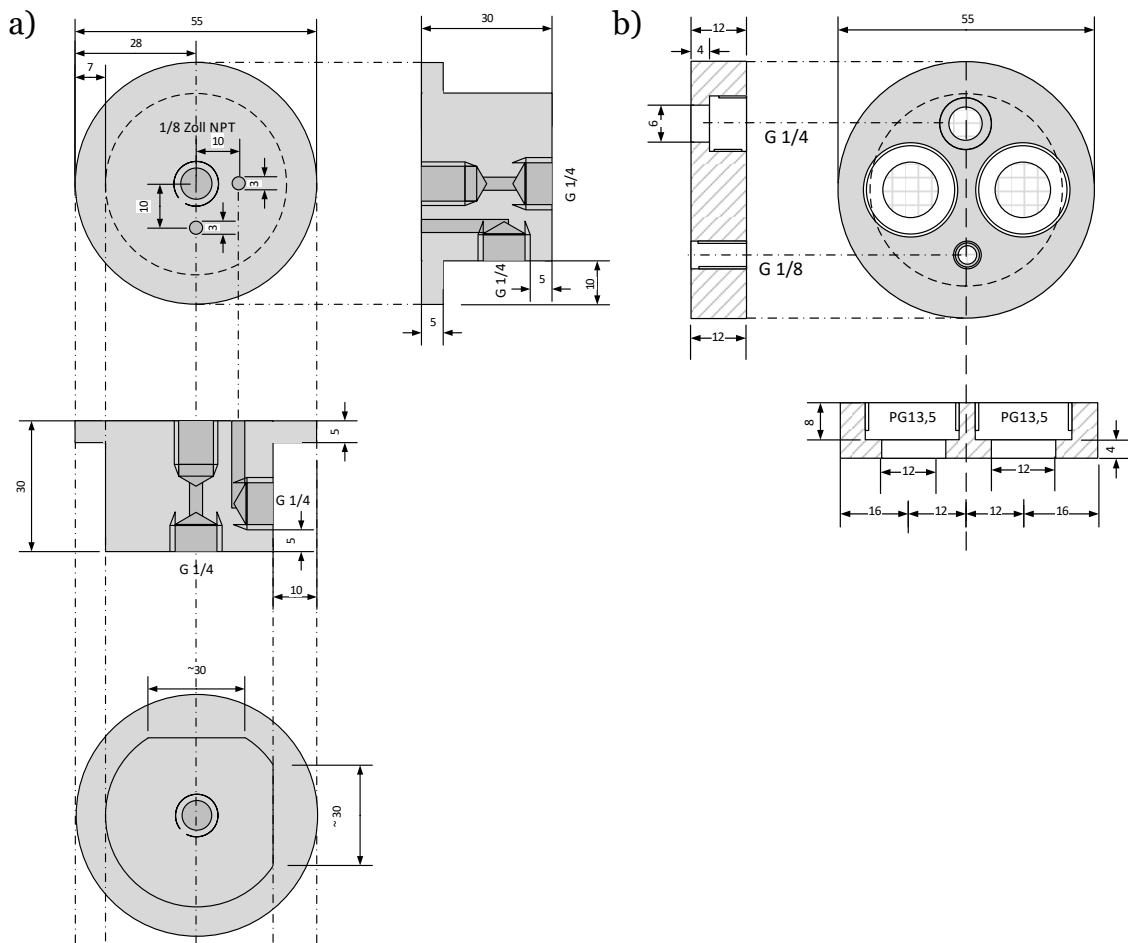


Figure A.6: Design drawing for the top (a) and bottom (b) plate of the 0.2 L bubble column reactor. Dimensions in millimetre.